

University of Central Florida

STARS

Electronic Theses and Dissertations

2006

Polymer-derived Si-al-c-n Ceramics:oxidation, Hot-corrosion, And Structural Evolution

Yiguang Wang

University of Central Florida



Part of the [Materials Science and Engineering Commons](#)

Find similar works at: <https://stars.library.ucf.edu/etd>

University of Central Florida Libraries <http://library.ucf.edu>

This Doctoral Dissertation (Open Access) is brought to you for free and open access by STARS. It has been accepted for inclusion in Electronic Theses and Dissertations by an authorized administrator of STARS. For more information, please contact STARS@ucf.edu.

STARS Citation

Wang, Yiguang, "Polymer-derived Si-al-c-n Ceramics:oxidation, Hot-corrosion, And Structural Evolution" (2006). *Electronic Theses and Dissertations*. 762.

<https://stars.library.ucf.edu/etd/762>

POLYMER-DERIVED Si-Al-C-N CERAMICS:
OXIDATION, HOT-CORROSION AND STRUCTURAL EVOLUTION

by:

YIGUANG WANG

Bachelor, Tianjin University, China 1994

Master, Tianjin University, China 1997

A dissertation submitted in partial fulfillment of the requirements
for the degree of Doctor of Philosophy
in the Department of Mechanical, Materials and Aerospace Engineering
in the College of Engineering and Computer Science
at the University of Central Florida
Orlando, Florida

Spring Term
2006

© 2006 Yiguang Wang

ABSTRACT

Polymer-derived ceramics are a new class of materials synthesized by thermal decomposition of polymer precursors. Previous studies have shown that the materials exhibit excellent thermo-mechanical properties and can be stable at temperatures up to 2000°C. Furthermore, the novel polymer-to-ceramics process enables the manipulation of the ceramic structures at the atomic/nano level by designing the chemistry of polymer precursors and controlling the pyrolysis conditions, thereby, the properties of ceramics. In this dissertation, oxidation/hot-corrosion behavior and the structural evolution of Si-Al-C-N ceramics have been studied.

The structural evolution and crystallization behavior of the SiCN and SiAlCN ceramics are investigated using FT-IR, XRD, and NMR. The results revealed that aluminum could greatly affect the structural evolution and crystallization behavior of polymer-derived ceramics, resulting to better stability.

The oxidation kinetics of the SiCN and SiAlCN ceramics in air is determined by directly measuring the thickness of the oxide scale with SEM as a function of oxidation time. The results revealed that while the oxidation of the SiCN ceramics follows parabolic kinetics in all of the ranges of testing temperatures, oxidation of the SiAlCN ceramics is complicated: their oxidation rates are similar to that of SiCN ceramics at the earlier stage, but they decrease to very low levels after a certain time. The oxidation rate of the SiAlCN ceramics is more than an order of magnitude lower than any other silicon based ceramics previously reported. The transportation behavior of oxygen through the oxide scales is studied by ^{18}O diffusion. The results indicate that oxidation is controlled by molecular oxygen diffusing through the oxides for both SiCN and

SiAlCN ceramics; however, the oxygen diffusion rate in the oxides on SiAlCN ceramics is remarkably retarded. The structures of the oxides are characterized by XRD and NMR. A structural model is advanced to account for the aluminum effect on the oxygen diffusion in the oxide.

The oxidation and hot-corrosion kinetics of the SiCN and SiAlCN ceramics in water vapor are determined by measuring their weight changes as a function of annealing time. The kinetic constants, k_p and k_l , are obtained by fitting the weight-change data with a parabolic model. The results reveal that the SiAlCN ceramics have a much better corrosion resistance than the SiCN and CVD SiC/Si₃N₄. After annealing at 1400°C for 300 hours, the SiAlCN-20 still retains more than 70% of its original strength, while the SiCN only retains about 20% of its original strength. The improvement in oxidation/hot-corrosion resistance of the SiAlCN ceramics is attributed to the low activity of the SiO₂ in the Al₂O₃-containing silica. In summary, I have developed a new class of high-temperature materials, Si-Al-C-N ceramics. It is demonstrated that these new materials have excellent oxidation and corrosion resistance and thermal stability. Together with their easy processability, the materials will find many high temperature applications such as environmental barrier coatings, ceramic matrix composites, and MEMS for harsh environments.

ACKNOWLEDGMENTS

I greatly appreciate the help of Professor Linan An, my advisor. He encouraged me and gave me great advice during my study and research at UCF. He provided direction for my research so that I can get the results as soon as possible.

I would also like to thank Professor Vimal Desai, Professor Young-ho Sohn, Professor Kevin R. Coffey, and Professor Lei Zhai for their assistance with analyzing of the results of my experiments. I also appreciate Mr. Weixing Xu and Dr. Weifeng Fei for their support in preparing samples and maintaining apparatus.

I also wish to express my sincere gratitude to all of the staff of the MCF: Mr. Mikhail Klimov, Mr. Zia Rahman, and Mr. Kirk Scammon for their assistance with my experiments; Chongmin Wang and Sarah Burton, the scientists in Pacific Northwest National Laboratory, for their kind help with TEM and NMR experiments and analysis.

I would especially like to thank my wife, Xue Zhao, for her immense love, support, and constant encouragement.

TABLE OF CONTENTS

LIST OF FIGURES.....	ix
LIST OF TABLES.....	xiii
LIST OF ACRONYMS/ABBREVIATIONS.....	xiv
CHAPTER ONE: INTRODUCTION.....	1
1.1 Overview.....	1
1.2 Outline of dissertation.....	3
CHAPTER TWO: LITERATURE REVIEW.....	4
2.1 Polymer derived ceramics.....	4
2.1.1 <i>Polymer precursors</i>	5
2.1.2 <i>Process of fabricating bulk ceramics</i>	18
2.1.3 <i>Pyrolysis of PDC and their structural evolution at high temperatures</i>	21
2.1.4 <i>The properties of PDCs</i>	31
2.2 Oxidation behavior of silicon-based materials.....	34
2.2.1 <i>Oxidation behavior of pure silicon</i>	34
2.2.2 <i>Oxidation behavior of SiC and Si₃N₄</i>	36
2.2.3 <i>Oxidation behavior of additive-containing materials</i>	41
2.2.4 <i>Oxidation behavior of sialon</i>	44
2.2.5 <i>Oxidation of polymer derived ceramics</i>	44
2.3 Wet oxidation behavior of silicon-based materials.....	46
2.3.1 <i>Oxidation of silicon-based materials in wet environments</i>	46
2.3.2 <i>Corrosion of silicon-based materials in wet environment</i>	47

CHAPTER THREE: CHARACTERIZATION OF POLYMER DERIVED CERAMICS	50
3.1 Experimental procedure	50
3.1.1 Processing of fully dense monolithic ceramics	50
3.1.2 Structural characterization	53
3.2 Results and discussion	55
3.2.1 Structural evolution	55
3.2.2 The crystallization behavior of Si-Al-C-N ceramics	62
3.3 Summary	67
CHAPTER FOUR: OXIDATION BEHAVIOR OF POLYMER DERIVED SiCN AND SiAlCN CERAMICS	68
4.1 Experimental procedures	68
4.1.1 Oxidation experiments for SiCN and SiAlCN bulk ceramics	68
4.1.2 Characterization of oxide structure	70
4.1.3 $^{18}\text{O}_2$ diffusion in the oxide produced by oxidation of SiCN and SiAlCN ceramics	70
4.2 Oxidation at the temperatures lower than 1200°C	73
4.2.1. Results	73
4.2.2. Discussion	80
4.3 Oxidation at the temperature of 1400°C	85
4.4 $^{18}\text{O}_2$ tracer diffusion	90
4.5 Summary	100
CHAPTER FIVE: WET OXIDATION AND HOT-CORROSION OF SiCN AND SiAlCN CERAMICS	101
5.1 Experimental procedure	101

5.2 Wet oxidation at the temperature of 1100°C.....	106
5.3 Wet oxidation at the temperature of 1400°C.....	110
5.4 NaCl corrosion at 1200°C.....	116
5.5 Summary.....	117
CHAPTER SIX: CONCLUSION.....	118
LIST OF REFERENCES.....	120

LIST OF FIGURES

Figure 1: Schematic illustration of the powder processing route and pyrolysis of polymer precursor.	19
Figure 2: The schematic behavior of the viscosity as a function of temperature for fusible and infusible polysilazanes ⁹³	23
Figure 3: Composition diagram for Si–C–N system. Tie line represents “stoichiometric” ternary compositions so that all carbon and nitrogen atoms are bonded to silicon ¹⁰⁶	28
Figure 4: Thermodynamic stability range of Si ₃ N ₄ and SiC relative to temperature and nitrogen pressure ¹⁰⁷	29
Figure 5: Optical micrographs of specimens prepared by the powder and the pressure casting routes ¹¹⁷	31
Figure 6: Change of the strain rate in Si/(B)/C/N vs. time showing three different stages ¹¹⁹	32
Figure 7: Specific electrical resistance of Si/C/N ceramics derived from PHMS (NCP2000) and Si/B/C/N ceramics. From comparison some typical values for insulators, semiconductors and conductors are also shown ¹²⁵	34
Figure 8: Process involved in Silicon oxidation ¹²⁸	35
Figure 9: Re-oxidation curve for Si ₃ N ₄ with MgO additives ¹⁶⁴	42
Figure 10: Two extreme cases for morphology of oxide overgrowth on pore surface. (a) growth rate is faster than supply rate of oxygen from atmosphere into pore, leading to pore clogging near surface. (b) growth rate is slower than oxygen supply rate, leading to uniform oxidation through specimen ¹⁰⁶	43
Figure 11: Some k _p values of silicon-based ceramics.....	45

Figure 12: Structure of (a) Ceraset TM and (b) Aluminum isopropoxide.....	51
Figure 13: The Schematic Sintering Procedure for SiCN and SiAlCN ceramics.....	51
Figure 14: FTIR spectra of Ceraset as obtained (a), CER-10AIs mixed at room temperature (b) and CER-10AIs heat-treated at 150 °C (c).....	56
Figure 15: Solid-state NMR spectra of SiAlCN-10 heat-treated at different temperatures: (a) ²⁹ Si NMR, (b) ²⁷ Al NMR.....	57
Figure 16: The Schematic Structure of SiAlCN ceramics.....	60
Figure 17: ²⁹ Si solid-state NMR spectra of the ceramics obtained at 1000 °C from pure Ceraset (SiCN), CER-5AIs (SiAlCN-5), CER-10AIs (SiAlCN-10), and CER-20AIs (SiAlCN-20).61	61
Figure 18: XRD of SiCN, SiAlCN-5, SiAlCN-10, and SiAlCN-20 at (a) 1400°C, (b) 1500°C, and (c) 1600°C.....	63
Figure 19: TEM results of SiAlCN-10 heat-treated at 1400°C. (a) The morphology of the SiAlCN-10 sample; (b) diffraction pattern for region 1; (c) diffraction pattern for region 2; (d) HRTEM for region 2, showing some crystallines.....	64
Figure 20: The idealized Si-N layers in α -, and β -Si ₃ N ₄ structure ^{207, 208}	65
Figure 21: Schematic diagram of annealing apparatus for ¹⁸ O tracer diffusion.....	71
Figure 22: SEM micrograph showing the morphology of the cross-section of the SiAlCN-5 oxidized at 1100 °C for 20 hours.....	73
Figure 23: XRD patterns of SiAlCN-10 (top) and SiCN (bottom) oxidized at 1200 °C for 200 hours.....	74
Figure 24: Plots of the square of the oxide scale thickness as a function of annealing times for the SiCN, SiAlCN-5 and SiAlCN-10 at temperatures (a) 900, (b) 1000, (c) 1100 and (d) 1200 °C.....	76

Figure 25: Plot of log parabolic rate constants as a function of reciprocal of temperature for SiCN, SiAlCN-5 and SiAlCN-10. The rate constants of SiAlCN-5 and SiAlCN-10 for temperatures higher than 1000 °C were calculated using initial stage data.....	78
Figure 26: ²⁹ Si NMR spectra of the SiCN and SiAlCNs oxidized at (a) 900 °C x 50 hours, (b) 1200 °C x 20 hours and (c) 1200 °C x 200 hours.....	79
Figure 27: Two-dimensional schematic showing the proposed structure of silica oxide scale, in which aluminum atoms sit in the center of the 6-membered rings of Si-O to block the diffusion of oxygen.	84
Figure 28: SEM morphology of cross-section of oxide scale for SiAlCN-10 ceramics oxidized at 1400°C for 20 hours.....	85
Figure 29: The Square of oxide scale thickness as a function of oxidation time.....	86
Figure 30: Comparison of oxidation rate constants for different silicon-based ceramics (SC: single crystal).....	87
Figure 31: XRD patterns of the SiCN, SiAlCN-10, SiAlCN-20 and SiAlCN-30 oxidized at 1400°C for 200 hours.....	88
Figure 32: SIMS profiles of ¹⁶ O and ¹⁸ O in the oxide scales formed on (a) the SiCN, (b) and (c) the SiAlCN after annealing in ¹⁸ O enriched gas.	94
Figure 33: Comparison between the experimental ¹⁸ O concentration-penetration profiles obtained from the SiAlCN after annealing in ¹⁸ O enriched gas at 1100 °C for 3 hours and that calculated using equation (4-8).....	96
Figure 34: Arrhenius plot for the oxygen network-diffusion in pure silica and Al-doped silica..	96
Figure 35: A schematic diagram of the two-dimensional structures of (a) pure silica, (b) silica with impurities (conventional model) and (c) Al-doped silica (currently proposed).	98

Figure 36: Schematic diagram of the apparatus for wet oxidation.	102
Figure 37: Weight change as a function of annealing time for the SiAlCN-20 and SiCN as indicated.....	106
Figure 38: SEM images showing the surface (a) and cross-section (b) of the SiCN and the surface (c) and cross-section (d) of SiAlCN-20 after annealing for 100 hours.	108
Figure 39: XRD patterns showing phase compositions in the oxide scales formed on SiCN and SiAlCN-20, respectively, after annealing for 200 hours.....	109
Figure 40: Weight change as a function of oxidation time at the temperature of 1400°C with 50% water-50%O ₂ at the rate of 4.4cm/s.	111
Figure 41: The corrosion surface of SiAlCN and SiCN at 1400°C with 50%H ₂ O-50%O ₂ at the flowing rate of 4.4cm/s for 300hours.....	112
Figure 42 : Fracture strength of SiCN and SiAlCN ceramics as a function of corrosion time...	113
Figure 43: The XRD pattern of SiAlCN and SiCN ceramics after oxidized at 1400°C with 50%H ₂ O-50%O ₂ at the flowing rate of 4.4cm/s for 300 hours.....	113
Figure 44: Activity of silica in Al ₂ O ₃ -SiO ₂ system ²⁴⁴ . The points of SiAlCN (SA) ceramics are also shown in the figure.	115
Figure 45: SEM morphologies of the surfaces of (a) SiCN, (b) SiAlCN-5, and (c) SiAlCN-10. The specimens were first immersed in de-ionized water saturated with NaCl at 100°C and then annealed at 1200°C for 50 hours in air.....	116

LIST OF TABLES

Table 1: The Composition of Si(Al)CN Samples	53
Table 2: The lattice constants of Si ₃ N ₄ calculated from XRD pattern.....	66
Table 3: Parabolic rate constants and activation energies for the SiCN ceramics and SiAlCN ceramics at the initial oxidation stage.....	77
Table 4: Parabolic rate constants and activation energies for the SiCN ceramics and SiAlCN ceramics after the initial oxidation stage	77
Table 5: The lattice constants of cristobalite formed on different materials.	89
Table 6: D ₀ and Q values for ¹⁸ O diffusion in SiCN and SiAlCN-10 ceramics	97
Table 7 Parabolic rate constants (k _p) and linear rate constants (k _l) for silicon based materials	107
Table 8: Comparison of k _l values of silicon-based ceramics at the condition of 50% water vapor-50%O ₂ at 1400°C with the flowing rate of 4.4cm/s.....	111
Table 9: The lattice constants for cristobalite crystalline calculated from XRD results (Figure 43).	114

LIST OF ACRONYMS/ABBREVIATIONS

PDC	Polymer Derived Ceramics
SEM	Scanning electron microscopy
TEM	Transmission electron microscopy
HRTEM	High resolution transmission electron microscopy
SIMS	Secondary ion mass spectrometry
XRD	X-ray diffraction
NMR	Nuclear magnetic resonance
FT-IR	Fourier Transform-Infrared
Me	Methyl
MS	Mass spectroscopy
TTMS	Tetrakis(trimethylsilyl)silane
PS	Polysilane
PCS	Polycarbosilane
PDMS	Poly(dimethylsilane)
PSZ	Polysilazanes
PHPSZ	Perhydropolysilazane
PECS	Precision Etching Coating System
BOE	Buffered Oxide Etchants
CVD	Chemical Vapor Deposition
TGA	Thermogravimetry Analysis

CHAPTER ONE: INTRODUCTION

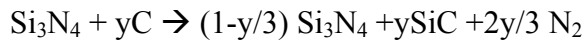
1.1 Overview

Non-oxide silicon-based ceramics, such as SiC and Si₃N₄, have attracted great interest for high temperature applications due to their excellent strength, hardness, and corrosion resistance at elevated temperatures¹. Traditionally, SiC/Si₃N₄ ceramics are synthesized by sintering their powders. However, due to the intrinsically low diffusivity of these covalent ceramics, the high temperature, high pressure, as well as oxide sintering aids, such as Al₂O₃ and Y₂O₃, are normally required to obtain ceramics with high density. The sintering aids react with silicon oxide to form liquid phases at sintering temperature to improve mass transportation and thus the densification. However, the liquid phases lead to the decrease in high-temperature mechanical properties of the materials, thus limit their applications.

In past decades, many alternative processing techniques have been pursued to overcome such problems. One of them is to synthesize silicon-based ceramics by thermal decomposition of polymeric precursors, named polymer-to-ceramics (PDCs)^{2, 3}. The basic steps involved in PDC processing are: (i) synthesis of polymer precursors, (ii) cross-linking the polymer to form pre-ceramic network, and (iii) pyrolysis of the cured precursor to form ceramics. The materials as obtained are predominantly amorphous in nature. Depends on precursors and processing conditions, materials in Si-C-N and Si-C-N-M (M represents forth element such as B, Al etc) can be synthesized^{4, 5, 6}. Compared with conventional processes, PDCs can be synthesized at a temperature as low as 1000°C free of any oxide additives. Therefore, better high temperature

mechanical properties can be foreseen. Furthermore, the chemical-to-ceramics route provides opportunities for fabrication of fibers preparation, coatings, and MEMS at simple and cost-efficient manners, which the powder-route can not perform.

Polymer precursors, as well as cross-linked precursor materials, possess amorphous networks which transfer to amorphous silicon carbonitride ceramics at around 1000°C in inert atmosphere. However, upon further heat treatment, the non-stoichiometric amorphous Si-C-N ceramics decompose, giving rise to the thermally stable phases, named Si₃N₄ and SiC by following the reactions:



Consequently, the thermal stability of polymer-derived ceramics should be considered when they are applied at elevated temperatures. Compared with binary Si-C or Si-N amorphous ceramics that are derived from carbon-free or nitrogen-free silicon-based polymer precursors, Si-C-N ceramics have higher thermal stability. Recently, even better stable quaternary Si-B-C-N ceramics were derived from boron-modified polysilazanes. It can be stable up to 2000°C without obvious weight loss and the crystallization temperature is as high as 1700°C⁷. The improved thermal stability was explained by the formation of BNC_x phase, which retards the decomposition of Si-N units. One aim of this dissertation is to investigate the thermal stability of Si-Al-C-N ceramic system in which the boron is substituted by its higher homologue aluminum.

As potential structural materials for high temperature applications, silicon-based ceramics must embody excellent resistance to oxidation and corrosion in the oxygen/water containing environments. Silicon based materials suffer severe material degradation when exposed to water vapor at high temperatures owing to the formation of volatile Si(OH)_x through reaction of silica

and water vapor. Environmental barrier coating (EBC) is currently applied to provide protection for the silicon-based materials^{8,9}. However, EBC is not applicable for many applications such as MEMS and heat-exchangers. The improvement of the inherent resistance to water vapor and oxidation for these materials is required. In the present work, oxidation and hot-corrosion properties of polymer-derived SiCN and SiAlCN ceramics are studied to illustrate the effect of aluminum-doping effects.

1.2 Outline of dissertation

The work in this dissertation is organized as follows:

Chapter 2 provides the background information following this chapter. The ensued part is the characterization of polymer-derived ceramics, including fabrication processes, structural evolution, and crystallization behavior of polymer-derived ceramics. The fourth chapter focuses on the oxidation behavior of polymer-derived ceramics. Chapter 5 is the results and discussion for wet corrosion and hot-corrosion in a sodium chloride environment of polymer-derived ceramics. A general conclusion is given in Chapter 6.

CHAPTER TWO: LITERATURE REVIEW

Silicon-based non-oxide ceramics attract extensive attention due to their high hardness, strength, creep resistance, and refractoriness. They are considered as next generation high temperature structural materials. However, their intrinsic low diffusivity associated with covalent-bond makes it difficult to obtain this class of materials through the traditional sinter process of green powder compacts and thereby limits the various applications of these ceramics. The precursor-conversion route provides an alternative for processing these materials. By this technique, silicon-based non-oxide ceramics can be fabricated free of any additives at temperatures as low as 1000°C. Hence, the mechanical properties such as strength and creep resistance at elevated temperatures will greatly be improved. Previous studies suggested that the microstructures of PDCs can be controlled over a wide span of possibilities. Micro-structural manipulation can be achieved by chemically modifying the precursors and by the use of distinct processing conditions during the course of polymer-to-ceramic conversion. Previous studies on polymer-derived ceramics are summarized in the following section. In the second and third section of this chapter, the review on the oxidation and corrosion of silicon-based ceramics will be advanced respectively.

2.1 Polymer derived ceramics

Historically, the first efforts in silazane chemistry were simply directed toward the preparation and characterization of silazane and polysilazanes^{10,11,12,13,14}. The earliest attempt to

form Si-N bonds using chlorosilanes was reported in the nineteenth century^{10,11}. Since the first preparation of silazanes by Stock and Somieski in 1921, a number of works was devoted to synthesize PSZs . The earliest report on the pyrolysis of silicones to obtain silicon-based materials was by Weyer¹⁵. As quoted by Rice¹⁶, a comprehensive approach to obtain ceramics from polymer precursors was preformed at the British Ceramic Research Association under the guidance of Popper in the early 1960's. Despite some attempts to prepare silicon(carbo)nitrides and relative materials in the 1960s, the general potential of preceramic compounds in the area of ceramics was not recognized until the pioneer work of Verbeek^{17, 18} and Yajima^{19, 20}, who prepared precursor-derived Si₃N₄ and SiC ceramic fibers. Since then the route of synthesizing Si/C/N ceramics from polymer precursors has attracted increasing attention, and a variety of new organometallic polymers have been developed as precursors for different non-oxide ceramics. Today, the interest in silazanes primarily derives from their applications as silylating agents in synthetic chemistry and as single source precursors for the preparation of ceramic materials by vapor, liquid, and solid phase pyrolysis.

2.1.1 Polymer precursors

In order to obtain any kind of ceramic materials from organometallic compounds, the starting precursors, themselves, have to be synthesized. Large volumes of Gmelin's handbook²¹ and chapters in other monographs^{22, 23}, as well as some review articles^{24, 25, 26}, are devoted to related topics. Furthermore, a large and increasing number of original papers and proceeding contributions are published each year. It is the objective of this section to give a brief

summarization of the formation and modification of ceramic precursors such as polycarbosilanes, polysilazanes, and polycarbosilazanes.

Wynne and Rice²⁷ have set forth a series of general empirical rules that should be considered for the design of a proper ceramic precursor, and Seyferth²⁸ also stated various requirements for this purpose. Briot *et al.* stated a compromise of properties, that an ideal preceramic polymer should possess, which are sometimes incompatible:

1. Molecular weight should be sufficiently high to prevent any volatilization of oligomers
2. A polymeric structure should contain cages or rings to decrease the volatile fragments resulting from backbone cleavage
3. Desired viscoelastic properties (fusibility, malleability, or solubility) to apply the polymer in the desired shape before the pyrolytic process
4. Presence of latent reactivity (functional substituent) to obtain thermosetting or curing properties
5. Low organic group content to increase ceramic yield and avoid the production of undesired free carbon excess

It is evident that variations in functional substituent and different polymer precursor microstructures will strongly effect the final ceramic compositions and structures. Thus, a number of studies are devoted to the synthesis of preceramic precursors and the subsequent precursors obtained upon judicious cross-linking. In this section, the polymer precursors of SiC/Si₃N₄ will be discussed first, followed by the precursors of Si-C-N, and finally, Si-(E)-C-N precursors will be mentioned.

2.1.1.1 Polymer precursors of SiC

A common approach for synthesizing of SiC precursors is through the synthesis of polysilanes (PSs), which can be further converted to polycarbosilanes (PCSs) by thermolysis. After the pioneering work of Verbeek and Yajima²⁹, whose synthesis strategy has allowed the production of commercial SiC-based fibers (Nicalon³⁰ and Tyranno³¹), a number of reports have described the preparation of PSs³², PCSs³³, and SiC-based materials on the pyrolysis of cured PCS.

The extended Yajima work is based on the following transformations:

dichlorosilane → polysilane (PS) → polycarbosilane (PCS) → SiC material

The second step of above transformations is considered to be critical in terms of yield and reaction conditions. It is necessary in the conversion of PS to PCS because the PS obtained from the first step generally is not a conventional ceramic precursor. In an earlier publication, a PCS was obtained from $(\text{Me}_2\text{-Si})_6$ autoclaved at 400°C in Argon³⁴. This precursor is suitable for the fabrication of fibers. The main drawbacks of this method are the cost of dodecamethylcyclohexasilane and the use of an autoclave. Later, Yajima proposed a simpler and more economical route to synthesize a commercially available PCS: heating polydimethylsilane (PDMS), obtained from Me_2SiCl_2 and Na in xylene, under pressure. The yield of the precursor is up to 60%. Yajima noted that the properties of the SiC fibers were intimately related to those of the precursor itself. The PCS should contain as many Si-H bonds as possible and its molecular weight should be relatively high. To avoid the use of an autoclave, alternative PCS precursors were obtained from PDMS at about 350°C under atmospheric pressure, with either the initiator or catalyst polyborodiphenylsiloxane (PBDPSO)³⁵. The yields were lower than those for the

precursors produced with autoclave, but the pyrolysis residue is higher. Furthermore, the initial results showed that the mechanical properties of the obtained fibers were somewhat inferior to those from precursors produced with pressure³⁶.

Further work focused on lowering the oxygen and free carbon content in the fiber and, more generally, on improving the mechanical properties at higher temperatures. Lipowitz³⁷ obtained a near pure, nanocrystalline SiC fiber with less than 0.1% oxygen by melt-spinning various precursors, cross-linking them and then heating them at 1600°C. A dense structure and high tensile strength were preserved by using a non-specified additive. In addition, the curing of Yajima PCSs by γ -ray or electron irradiation followed by heat treatment at 1200°C-2000°C results in a “High Nicalon” SiC fibers with 0.4% oxygen^{38, 39} and improved thermal properties⁴⁰.

Yakima made several attempts to synthesize effective silicon carbide ceramic precursors, especially for fibrous materials from precursors other than PDMS. Among these alternative organosilicon polymers, only polycarbosilanes are considered here. Several routes have been explored to obtain such polymers including the following:

1. Ring-opening polymerization reactions^{41, 42}
2. Polycondensation of chloromethylchlorosilanes^{43, 44}
3. Copolymer with 1,3-disilapentanes⁴⁵
4. Polycondensation of chlorosilanes with methylene halides^{46, 47}
5. Polycondensation of chlorosilanes with acetylides⁴⁸
6. Hydrosilylation reactions^{49, 50}
7. Polycondensation of chlorosilanes with unsaturated hydrocarbons⁵¹
8. Dehydropolycondensation of hydrogenosilanes⁵²

Intense investigations to develop the precursor to SiC fibers and relative compounds started about thirty years ago. Birot gave a nice summarization of these studies. The main points are listed below:

1. PS or PCS prepared by linear precursors result in very low yields unless an appropriate treatment was used to produce a subsequence cross-linking. Indeed, without branching, back-biting reactions generate cyclic or linear, low-boiling oligomers which are distilled. A reasonable ceramic yield can only be obtained after sufficient cross-linking that increases the softening temperature and decreases the solubility.
2. PCS precursors obtained by thermolysis of PS usually possess ill-defined complex structures.
3. The formation of hydrogen is closely connected with the presence of Si-H bonds responsible for the branching, either by thermal or catalyzed hydrosilylation or dehydrocondensation reactions.
4. Either air or electron beam is used to cure the precursors. Si-H bonds play a major role in cross-linking reactions regardless of the method used. Although they are totally unreactive, C-H and Si-C bonds still participate to some extent in the process.
5. The presence of pendent methyl groups in the polymer generally leads to a major loss of carbon as methane. Thus, pyrolysis of materials having the same chemical composition and different structures, such as $-(\text{MeHSiVH}_2)_n$ - or $-(\text{H}_2\text{SiCH}_2\text{CH}_2)_n$ -, leads to a material richer in free carbon in the latter case because of the absence of methyl groups which are partially converted into methane in the former case. However, when the pendent constituents are vinyl or phenyl groups, the pyrolysis

leads to free-carbon-rich materials due to the preliminary polymerization of vinyl moieties in the former case and subsequent formation of carbon during the mineralization step. These considerations illustrate the influence of the structure of the precursor on the composition of the resulting inorganic material.

6. From the perspective of making fibers, the best precursors are those that present alternating silicon and carbon atoms in the main chain. The formation of branching nodes prefiguring the SiC structure should also be beneficial.

2.1.1.2 Polymer Precursors of Si₃N₄

As for Si₃N₄ based materials, the possibilities of polysilazanes (PSZs) used for making silicon nitride⁵³ were known early. However, the first intensive investigations oriented toward the preparation of the inorganic materials came from Verbeek⁵⁴. Most of routes to such ceramics involve PSZs^{55, 56, 57} as the basic preceramic polymer precursors. Several schemes to fabricate the PSZ precursors for Si₃N₄ are briefly stated in this section:

1. Ammonolysis of tetrachlorosilane

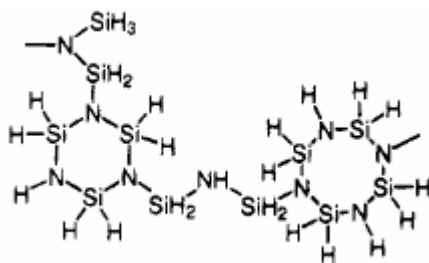
Silicon tetrachloride and ammonia are known to react under various conditions to give a silicon diimide, “Si(NH)₂”, leading to Si₃N₄ after heating up to 1250°C⁵⁸.



Though the process has been used to prepare the Si₃N₄ fibers⁵⁹, ammonolysis of tetrachlorosilane is more particularly useful in the CVD process⁶⁰. In any case, this route is not suitable for obtaining fusible or soluble preceramic polymers.

2. Perhydropolysilazanes (PHPSZ)s

Aylett⁶¹ emphasized that PSZs without carbon substituents had poor storage stability. Since these compounds contain SiH-NH linkages, they lose hydrogen so readily that they can undergo cross-linking in storage. The stable complexes obtained from polychlorosilanes and tertiary amines brought out beneficial effects in various polycondensation reactions⁶². Taking advantage of this property, Isoda *et al.*⁶³ succeeded in the preparation of a spinnable precursor by using the complex, H₂SiCl₂2py. The tentatively proposed oligomeric structure is formed of rings linked by linear segments.



(2-2)

The introduction of pyridine offers several advantages such as stabilization of the dichlorosilane, increase in the molecular weight, and beneficial introduction of a very small percentage of carbon in the ceramics.

The direct synthesis of tris(dimethylamino)silane from silicon and dimethylamine (shown below) followed by a reaction with amines or ammonia constitutes an alternative to the PHPSZ route to silicon nitride which does not require the use of a chlorosilane⁶⁴.



3. Pyrolysis/nitridation of organosilicon polymers under ammonia

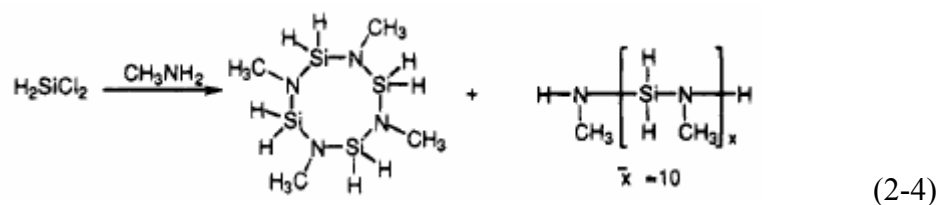
Pyrolysis of cross-linked PCSs, PSs, and PSZs under ammonia or hydrazine constitutes a general route to highly pure Si₃N₄^{65, 66}. This method has been used for the conversion of both bulk precursors and oxygen-cured PCS fibers⁶⁷. Partial replacement of carbon is possible when

using a gas carrier containing ammonia, thus enabling the preparation of ceramics with controlled composition⁶⁸.

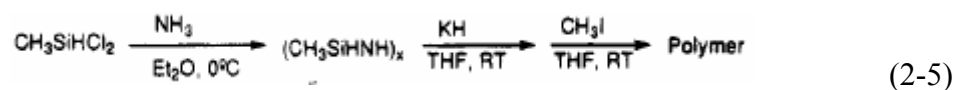
2.1.1.3 Polymer Precursors of Si-C-N

The pure amorphous Si_3N_4 is expected to readily crystallize above 1200°C - 1300°C , which is detrimental to the thermal stability and performance of ceramic fibers. Isoda *et al.*⁶⁹ reported that stoichiometric Si_3N_4 fibers exhibited a catastrophic drop in their mechanical properties above 1300°C . In order to delay Si_3N_4 crystallization, the presence of a suitable second refractory phase in the material is desirable. Accordingly, considerable effort has been put forth during the last few years to prepare ternary Si/C/N systems, and a wide range of PSZ oligomers bearing various adjacent hydrocarbon groups on silicon and nitrogen have been investigated as ceramic precursors. In the same way, polymers containing hydrocarbon groups in the main backbone have led to useful precursors.

Sevferth and Wiseman⁷⁰ use the scheme of the aminolysis of dichlorosilane with methylamine in the hope of obtaining non-cross-linked precursors with better processability than those obtained from the ammonolysis of dichlorosilane, but the char yield is low (38%).



Based on the work of Fink⁷¹, Sevferth and Wiseman have found that the use of strong bases led to a polymeric silylamide of type. Next, this material was quenched with MeI and pyrolyzed to provide ceramics in high yields.

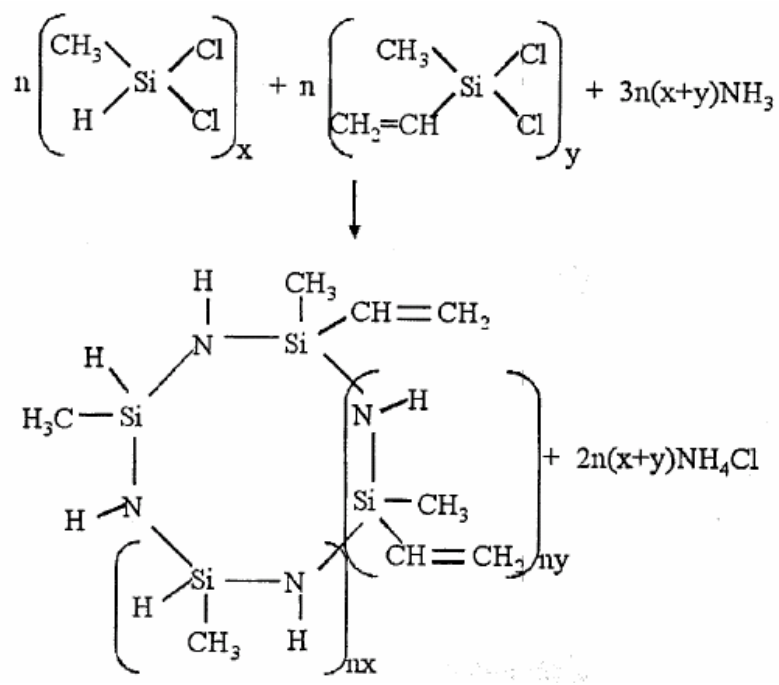


Ammonolysis of chlorosilanes results in copious amounts of ammonium chloride which is difficult to remove. This byproduct is undesirable since it contributes to the introduction of chlorine in the precursors while it acts as a catalyst in the splitting of Si-N bonds. To overcome this problem, the previously known Si-Cl/Si-N disproportionation involving hexamethyldisilazane (HMDZ), leading mainly to trimethylchlorosilane instead of hydrogen chloride as a byproduct, was extended to the synthesis of a wide range of precursors^{72, 73}.

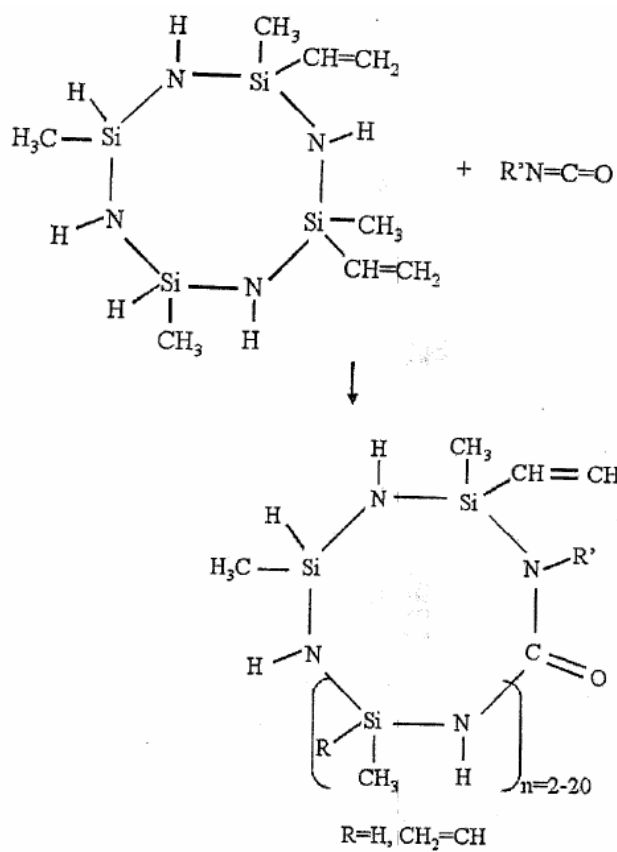
Polysilazanes with a tailorable viscosity have been prepared by reacting poly(methylvinyl)silazanes, obtained from co-ammonolysis of dichloromethyl- and dichloromethylvinylsilane, with mono- and multifunctional isocyanates^{74, 75, 76}. A commercial product, Polyureamethylvinylsilazane (PUMVS), was used based on this synthesis in present work.

The PUMVS precursor was patented by Schwark⁷⁷ at Hercules Inc. and was commercially developed by Dupont Lanxide as CerasetTM, which now is owned by Kion Corporation.

The precursor is prepared in two steps. The first is co-ammonolysis of methylvinylchlorosilane and methylchlorosilane. Methylchlorosilane gives off silyl group Si-H and the methylvinylchlorosilane gives off vinyl group, making it possible that the precursor cross-links thermally. The co-ammonolysis results in a cyclic oligomer called methylvinylsilazane as shown in Eq. (2-6):



(2-6)



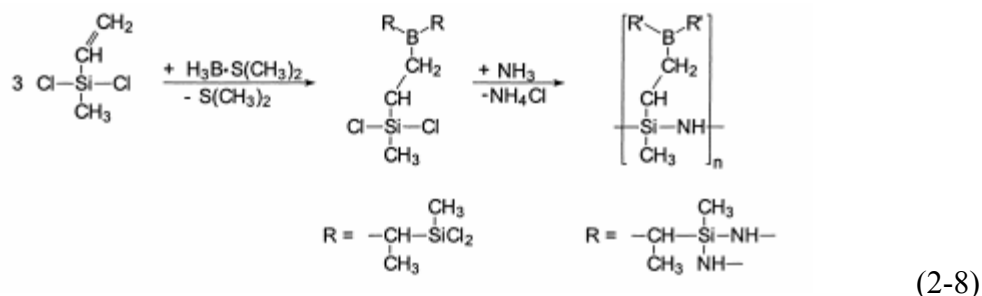
(2-7)

The cyclic methylvinylsilazane is then modified with a small amount of isocyanate to increase the molecular weight of oligomers. This helps to reduce the volatility of oligomer. The isocyanate is introduced into the ring structure to form PUMVS. The reaction is schematically shown in Eq. (2-7).

2.1.1.4 Polymer Precursors of Si-(E)-C-N

Multinary ceramics and composite materials are of interest due to their enhanced properties. For example, the addition of boron nitride leads to a better thermoshock resistance of hot-pressed silicon nitride ceramics⁷⁸. Precursor derived ceramics may have a tendency to show better high temperature properties going from binary to ternary phases⁷⁹.

Precursor derived Si/B/C/N ceramics have a number of advantages over the Si/C/N system including their thermal stabilities, oxidation resistance, and higher crystallization temperatures and ceramics yield. Ralf Riedel and his co-workers have synthesized a Si/B/C/N precursor, from which the ceramic materials derived, are stable against decomposition up to 2000°C and start to crystallize above 1700°C. The reactions are shown in Eq. (2-8):



The polymer was isolated in 80% yield. It consists of a white solid power that is soluble in THF and toluene. FTIR and NMR examinations of the product indicate a trigonal planar co-

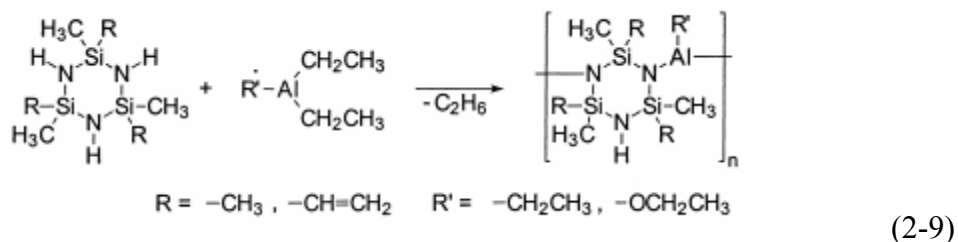
ordination for boron. It was concluded that cyclic oligosilazane, which is two-dimensionally cross-linked via Si-C-C-B-C and Si-C-B-C bridges, is formed.

Besides boron, other elements have been introduced into silazanes, in order to obtain quaternary precursors of Si-E-C-N ceramics. A method similar to the above-described preparation of Si/B/C/N precursors by the treatment of polysilazanes with tris(dialkylamino)borane $B(NR_2)_3$ has been utilized to obtain phosphorous containing silazanes. Tris(dimethylamino)phosphane $P[N(CH_3)_2]_3$ was mixed with mesitylen and polyhydridomethylsilazane derived from dichloromethylsilane and dichlorodimethylsilane. Thermal cross-linking applying 400°C for 4 hours gave a colorless solid which was pyrolyzed at 1000°C . A very low phosphorous content of 0.5 wt.% was found. This value decreased further to 0.4wt% and 0.0 wt.% upon heating to 1400°C and 1500°C for 50 hours respectively. It was also found that Si/P/C/N ceramics tend to crystallize faster than Si/C/N materials, which is opposite to the behavior of analogous Si/B/C/N systems.

Another promising element candidate is aluminum because AlN, Al_2O_3 , SiAlONs and other Al-containing materials show interesting properties such as high strength, high hardness or resistance to thermal shock and oxidation. Polysilazane-derived ceramic materials in the Si/Al/O/N system have been found to show suppressed grain growth compared to aluminum-free analogues⁸⁰. Recently, high-strength alkali-resistant Si/Al/C/O-fibers have been produced from a polyaluminocarbosilane⁸¹. Oxygen-free precursors for Si/Al/C/N-materials have been synthesized by the pyrolysis of polyaluminosilazanes with varied Si:Al ratios, at varied pyrolysis conditions^{82,83, 84, 85}.

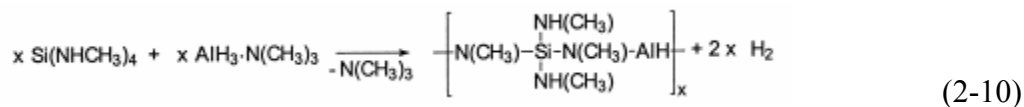
Single-source precursors have been obtained from the reaction of ethylaluminum compounds with 1,3,5-trimethyl-1,3,5-trivinylcyclotrisilazane. The polymers are formed by a

known condensation process which occurs between the N-H groups of the silazane and the organoaluminum reagent to form Al-N bonds and evolve ethane⁸⁶. The same reaction type takes place when HMCTS and triethylaluminum (TEA) are mixed at room temperature either neat or with both compounds dissolved in dry hexane (Eq. 2-9):



The Si:Al ratios were varied from 1 to 5 for R=methyl and from 1 to 9 for R=vinyl. The air sensitive products were examined by thermogravimetric analysis, FTIR, ²⁹Si, ¹³C, and ²⁷Al MAS NMR spectroscopy. The polymers were pyrolyzed and crystallized at temperatures up to 1900°C to give SiC/AlN-composite materials.

Aluminum-doped silazane polymers were also obtained analogous to the above described reactions of borane with tetrakis(methylamino)silane. The alane Lewis-base adduct AlH₃N(CH₃)₃ dissolved in toluene was mixed with Si(NHCH₃)₄ at -78°C. Hydrogen evolution indicates a dehydrocoupling reaction to give a colorless solid polymer containing 12.4 wt.% aluminum (Eq. 2-10):



2.1.2 Process of fabricating bulk ceramics

Polymer to ceramic route is proven to be a successful method to fabricate low dimension materials such as fibers, coatings, powders, and MEMS. Attempts to produce bulk ceramics by pyrolysis of liquid or cross-linked polysilazanes were not successful because the evolution of oligomers during pyrolysis resulted in considerable pores or cracks of the pyrolyzed bodies^{87, 88}. A glassy solid polyvinylsilazane obtained by cross-linking of liquid oligomers was pyrolyzed up to 1400°C in Argon. SEM investigations revealed the presence of extensive cracks and pores which were found to be due to the generation of stress induced by the volume decrease during pyrolysis. However, the pyrolyzed porous bodies had locally dense regions and maintained their shapes without bloating after pyrolysis, even at higher heating rates. This suggests the possibility of obtaining dense Si/C/N bulk ceramics through the pyrolysis of polysilazanes. However, to reduce the porosity and to avoid cracking, an optimized processing is needed.

Currently, three main methods are developed to fabricate dense and crack-free ceramics through polymer-to-ceramic route: the warm-press powder route, the active/inactive filler route, and the pressure-assistance route.

In 1991, Riedel *et al.* developed a new process which produces dense Si/C/N bulk ceramics. This method (Figure 1) involves cross-linking of polysilazanes into infusible solids, milling the cross-linked silazanes into fine powders followed by shaping green bodies, and pyrolyzing the compacts around 1000°C. The unique feature of this novel process is the direct transformation from highly cross-linked polymer networks to dense monolithic Si/C/N bodies by pyrolysis without sintering aids. This route from polymers to ceramics promises to become a new process compared with the traditional liquid sintering of ceramic powders.

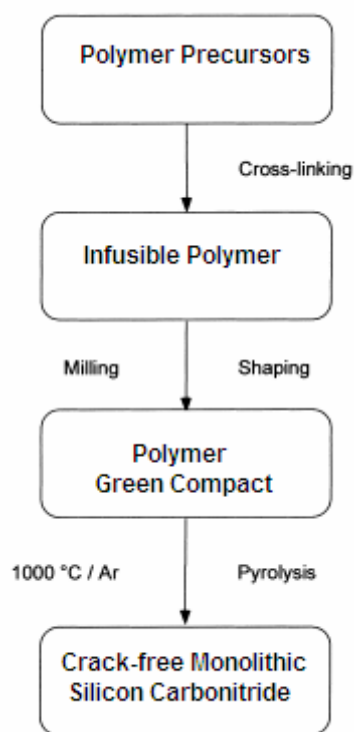


Figure 1: Schematic illustration of the powder processing route and pyrolysis of polymer precursor.

The key steps to this process are the cross-linking process and the compaction process. The high degree of cross-linking is required in order to get a high-dense final product. However, the plasticity of the cross-linked polymer is also critical. An optimal temperature is needed.

Dense and crack-free pre-ceramic powder compacts of the cross-linked polysilazanes are required for obtaining crack-free dense bulk ceramics after pyrolysis. Early attempts to prepare polymer compacts for bulk pyrolysis used isostatic or uniaxial cold pressing leading to densities of the compacts of 84%. The final bulk density of the Si/C/N ceramics after pyrolysis at 1000°C was 93%.

Warm-pressing methods have recently been used by Seitz and Bill to compact cross-linked polyvinylsilazane powders for bulk pyrolysis⁸⁹. The pressing temperature should be in the range of the softening point of the cross-linked polysilazanes since plastic forming can be realized under these conditions. A pressing temperature of 250°C was used to compact the polyvinylsilazane powders (28 mm) under an acting pressure of 47.75 MPa. Dense green bodies with porosity of 7.5% were obtained by this compaction technique. After pyrolysis, Si/C/N ceramics with a relative density of 97% were obtained.

Instead of using a pure single source, active or passive powders (fillers) may be added to the precursor. The active fillers may react with the silazane, its decomposition products, or active atmospheres during pyrolysis to form carbide, nitride, carbonitride, oxide phases, which in turn can reduce the shrinkage and the amount of volatile side products. A similar effect may be gained by passive fillers which do not react with the silazane matrix, but decrease shrinkage and formation of volatiles due to a reduction of the total polymer amount^{90, 91}.

Loading of polymers with various metallic fillers was conducted to produce bulk amorphous ceramics. In this process, liquid or solid polymer precursors were mixed with active filler powders, followed by shaping and pyrolysis. Suitable active fillers are elements or compounds forming carbide, nitride or oxide, such as Al, B, Si, Ti, CrSi₂, and MoSi₂ which exhibit a high specific volume increase upon reaction. By this process, zero shrinkage after pyrolysis could be achieved allowing a near net shape forming of ceramic composite materials. However, the pyrolyzed bodies were not fully densified with an appreciable amount of residual open porosity. This process was previously applied to polysiloxane precursors to produce oxygen-containing ceramic composites such as Si/O/C-TiC, Si/O/C-TiN, and Si/O/C-SiC. However, it may also be applicable to process polysilanes or polysilazanes to produce non-oxide

ceramic composites. Some studies on ceramic conversion via the filler strategy have been summarized recently by Greil.

Recently, a novel pressure-assistance pyrolysis process has been developed by Linan An and co-workers to synthesize fully dense bulk polymer-derived ceramics without pore and crack⁹². In this process, the cross-linked polymer precursor is pyrolyzed in the hot-isostatic press furnace (HIP) at low ramping rate in order to release the gaseous by-products without breaking the structure. The applied isostatic pressure prevented the formation of pore and cracks during pyrolysis.

2.1.3 Pyrolysis of PDC and their structural evolution at high temperatures

The pyrolysis of polymer precursor results in the loss of some organic molecules, survived by the hybrid ceramic structure. The availability of a wide variety of polysilazane precursors with selected physical and chemical properties offers multiple ways to perform polymer-to-ceramic conversion and allows the formation of different geometries of Si-based ceramics such as fibers, coatings, films, and bulk materials. Depending on the processing conditions, the structure of the ceramics can either be amorphous, nanocrystalline, or crystalline. Their compositions vary from binary (Si/N) and ternary (Si/C/N) ceramics to quaternary systems (Si/E/C/N), where E refers as to an additional element such as B, Al, Ti, P, or Zr. The starting precursor is normally in oligomeric form with a mixture of different molecular weight oligomers. The processing of precursor to ceramic conversion can be classified as a solid, liquid, or vapor

process depending on the physical and chemical properties of the selected precursors such as solubility, rheology, infusibility, and the behavior of cross-linking and pyrolysis.

For chemical vapor deposition (CVD) to prepare ceramic coatings and films or chemical vapor infiltration (CVI) to produce composites, silazanes with high volatility are used. A vapor phase of the precursor can be generated either by evaporating the molecules above their boiling point at a certain pressure or by using a carrier gas bubbling through the liquid precursor below its boiling point. It is necessary that the precursors do not cross-link or decompose upon heating to the required temperature.

For the spinning of fibers or the fabrication of coatings, films, or laminates, liquid precursors are desired, but fusible solid or soluble polymers can also be applied. For infiltration of porous materials or as binders for ceramic compaction, precursors with low viscosity and a high ceramic yield are required. The liquid polysilazanes can also be used to produce fine ceramic powders or films through liquid processes such as spray pyrolysis and spray coatings.

For the synthesis of ceramic powders or bulk ceramics, highly cross-linked and infusible precursors are suitable. The different degree of cross-linking and viscosity can be tailored in the precursors using proper reactant groups or simply annealed at different temperatures. Figure 2 shows the schematic behavior of the viscosity as a function of temperature for fusible and infusible polysilazanes⁹³.

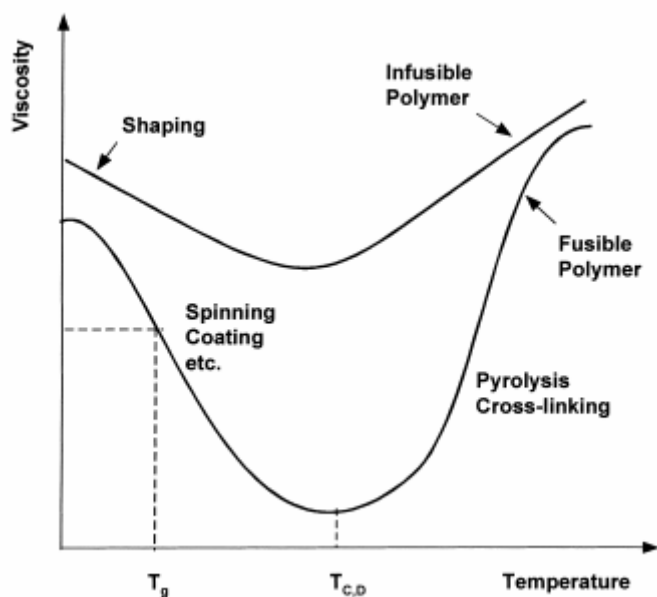


Figure 2: The schematic behavior of the viscosity as a function of temperature for fusible and infusible polysilazanes.

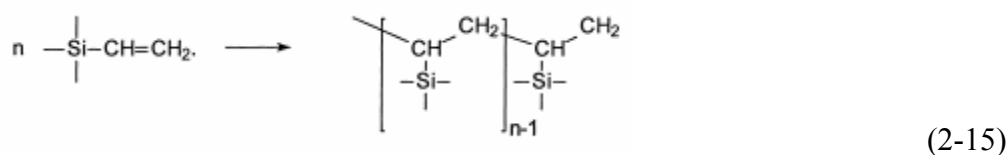
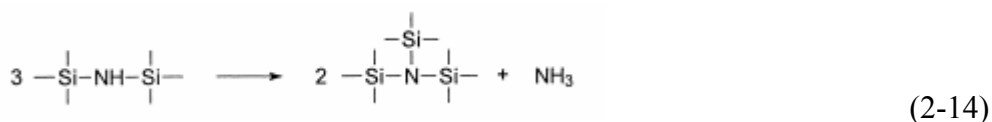
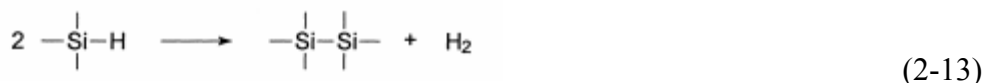
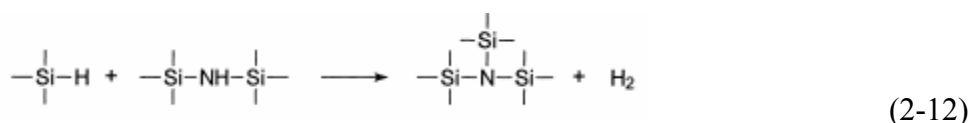
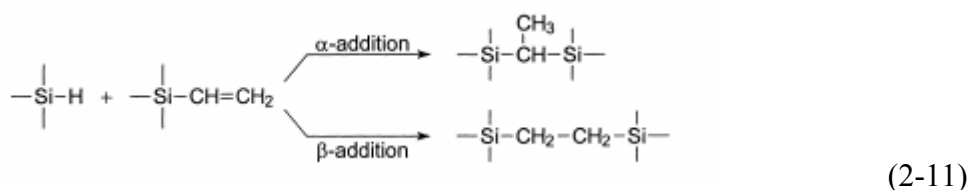
As can be seen in Figure 2, there is a wide range of viscosity that can be obtained from a fusible silazane when heated. Spinning fibers and coating films are possible in a temperature range where a suitable viscosity is attained but no enhanced cross-linking and decomposition occurs. For the infusible polymer, shaping the precursor powders is carried out around the glass temperature where the polymer particles show softening and allow plastic forming.

2.1.3.1 Cross-linking of the precursors

One of the most important steps in the preparation of ceramics by pyrolysis of polymer precursors is cross-linking. Cross-linking results in the oligomeric silazanes into large molecules

with highly interlocked backbones, which is required to avoid the evaporation of oligomers during pyrolysis⁹⁴.

The effective cross-linking can be obtained by either thermally or chemically using radical initiators like peroxides or catalysts. Thermal cross-linking is preferred on consideration of the control of elemental and phase composition of the final ceramics because no additional elements are introduced to the polymer. Thermal cross-linking requires the presence of reactive functional groups such as vinyl or silyl groups in the precursors. The major cross-linking reactions involved in the pyrolyzing polysilazanes are a) hydrosilylation of vinyl groups as shown in the Eq. (2-11), b) dehydrocoupling of Si-H and N-H as shown in Eq. (2-12) and (2-13), c) transaminations by trisilating nitrogen atoms as shown in Eq. (2-14), and d) vinyl polymerization reaction as shown in Eq.(2-15)^{23, 95, 96, 97}.



The effects of the different functional groups on thermal cross-linking behavior of polymer precursors were systematically investigated by Choong Kwet Yive *et al.*. They found the enhanced cross-linking reaction with an increasing number of active vinyl and Si-H groups. Based on their experimental results, the cross-linking activity can be arranged in the following order:

Hydrosilylation > dehydrocoupling > transaminations > vinyl group polymerization.

The study on PUMVS-Ceraset by Seyferth and his co-workers⁹⁸ showed that the presence of Si-H and vinyl groups in Ceraset makes it possible to cross-link it at a relatively low temperature. The Ceraset solidifies mainly by the hydrosilylation reaction. Intense cross-linking results in a highly interconnected backbone structure that is infusible and easy to shape by powder processing.

2.1.3.2 Conversion process to ceramics

The polymer precursors usually have the density of about 1g/cm^3 , while the pyrolyzed product of ceramics has the density of about 2.5g/cm^3 . Even for a yield of 100% for the conversion from polymer to ceramics, the linear shrinkage would be 26%. Since the diffusivity and deformability of Si/C/N ceramics are low, the higher shrinkage during pyrolysis may result in defects such as cracks and bubbles. Therefore, it is imperative for the precursor to have a high yield in order to produce a high quality ceramic product. The ceramic yield of polymer precursors strongly depends on their chemistry, including backbone structure and the functionality as well as the degree of cross-linking. Boury *et al.*⁹⁹ showed that the ceramic yield of poly(carbosilane) was enhanced due to the increased degree of cross-linking. Lucke *et al.*¹⁰⁰

systematically investigated the effects of substituent and backbone structure of polysilazanes on their pyrolysis behavior. They prepared branched and unbranched polysilazanes with different substitution patterns such as Si-H, Si-CH₃, Si-CH=CH₂, Si(NH₂), and performed TGA analysis under argon atmosphere. The results showed that the unbranched silazane gave a very low ceramic yield <11wt.% at 1000°C, while the branched silazanes showed a higher ceramic yield of 51-77wt.%. In addition to the precursor chemistry and pyrolysis temperatures, the ceramic yield is also affected by the pyrolysis conditions including heating rate¹⁰¹ and the pyrolysis atmosphere. The higher heating rate will reduce the volatility of the oligomers at low temperatures, which leads to a higher ceramic yield. However, the higher heating rate may lead to cracking and other defects during pyrolysis.

The weight loss during pyrolysis was caused predominately by the evolution of oligomers at lower temperatures and by-product gases at higher temperatures. A three-stage weight loss was generally observed for the polysilazanes¹⁰². First, weight loss occurs at temperatures lower than 400°C due to the evaporation of light molecular weight oligomers and transamination reaction. There is also a contribution from hydrosilylation reaction in case of precursors with reactive groups of Si-H and CH=CH₂. The second weight loss comes from the loss of hydrocarbons such as CH₄, C₂H₆ and others in the temperature range of 400-750°C. Also, there is some dehydrogenative coupling with Si-H and N-H groups. Above 750°C, the weight loss is mainly due to hydrogen evolution. The exact temperatures of gas evaporation change with the different polymer structure and the degree of cross-linking. There is also some variability due to the heating rate and pyrolysis environment.

The elemental composition of the final amorphous ceramics after pyrolysis at 800-1200°C depends on the factors such as chemical composition of the starting materials¹⁰³,

pyrolysis environment^{109, 104}, degree of cross-linking, and the reactive groups in the polymer precursors.

During the pyrolysis process, the carbon in the polymer precursor will be redistributed. Some is gaseous evolution as hydrocarbons, some retains in the structure as free carbon which is present as basic structural units of turbostratic carbon around the silicon network, and the other is present in the silicon network environment of the amorphous structure as $\text{SiC}_x\text{N}_{4-x}$ ¹⁰⁵. The carbon in the structure can act as a diffusion barrier and prevents crystallization of stable phases such as SiC and Si_3N_4 . The presence of carbon is thought to be the reason for increased stability of the materials. The carbon content in the polymer-derived ceramics can be adjusted to a certain extent through pyrolysis or isothermal annealing in active gases like ammonia. This treatment reduces the carbon content by the formation of methane as described in Eq.2-16.

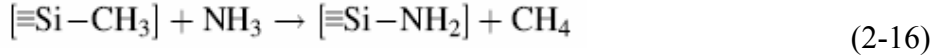


Figure 3¹⁰⁶ shows the composition of SiCN ceramics derived from polymer precursors. The stable phases SiC and Si_3N_4 are shown in the figure. The tie line joining Si_3N_4 and SiC separates the diagram into two important domains. The domain below the tie line shows there is an excess of silicon. The one above the line has an excess of carbon. Generally, the composition range lies within the triangle bound by SiC, Si_3N_4 , and carbon. Thus, their composition can be expressed as $\text{SiC}_n\text{Si}_3\text{N}_4x\text{C}$. The ratio, n , is a measure of the relative amounts of Si–N and Si–C bonds in the amorphous structure, while x measures the free-carbon atoms bonded to themselves.

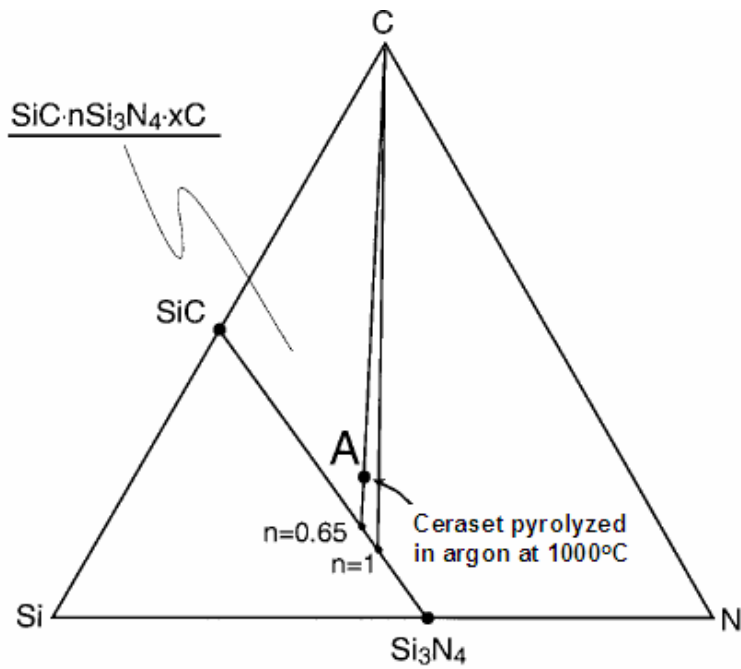
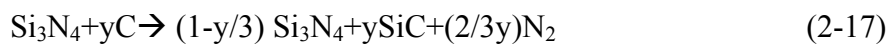


Figure 3: Composition diagram for Si–C–N system. Tie line represents “stoichiometric” ternary compositions so that all carbon and nitrogen atoms are bonded to silicon.

At high temperatures, the amorphous structure will evolve to the thermal stable phases such as SiC and Si₃N₄. Considering the thermodynamic stability of the system of SiC, Si₃N₄, and C, three reactions (Eq.2-16~2-18) are to be considered in the first approach. These reactions depend strongly on the nitrogen pressure and on the temperature as it is shown in Figure 4¹⁰⁷.



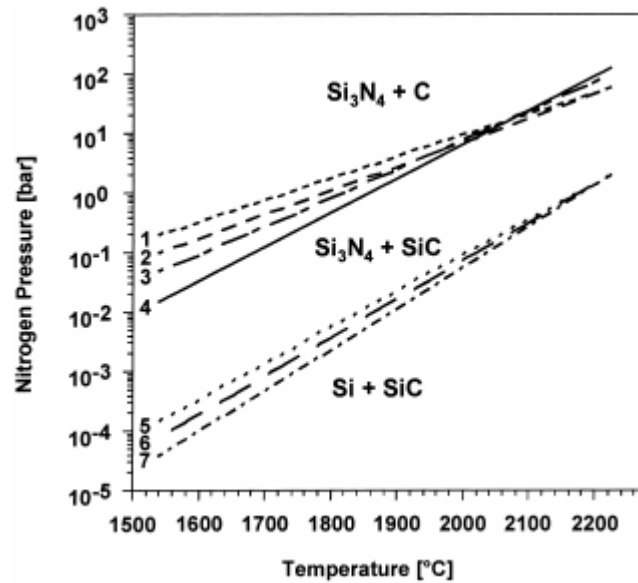


Figure 4: Thermodynamic stability range of Si_3N_4 and SiC relative to temperature and nitrogen pressure.

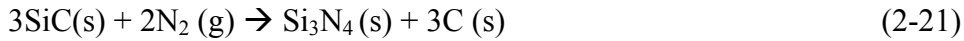
Under given nitrogen pressure, the lower bound of the stability range in Figure 4 is defined by the Eq. 2-19:



Since Si_3N_4 and C are in contact, reaction (2-19) occurs at temperatures above 1440°C under a nitrogen pressure of 0.1 MPa^{108} . This reaction leads to the formation of nitrogen and is consequently accompanied by a weight loss. The upper bound of the stability range of Si_3N_4 and SiC in Figure 4 is given by reaction 2-20.



Under gas pressure conditions, i.e. using high nitrogen pressures, the nitridation of SiC according to reaction Eq. 2-21 (reverse of reaction 2-20) may occur. Reaction 2-21 implies incorporation of nitrogen from the atmosphere and, therefore, leads to a weight gain.



As amorphous Si/C/N powders generally contain an excess of carbon, this intermediate step is carried out in order to remove carbon according to Eq.2-20. By using this procedure, the evolution of nitrogen due to reaction (2-17) during liquid phase sintering can be avoided.

The thermal stability of polymer derived ceramics is the stability against chemical decomposition and crystallization. The region of metastability shown in Figure 3 represents the compositions with certain SiCN composition. The stability of these compositions can be explained as the presence of carbon in the silicon-nitrogen network. As reported by many investigators^{109, 110, 111, 112}, the amorphous structure of SiCN consists of the mixed tetrahedra of SiC₄, SiC₃N, SiC₂N₂, SiCN₃, and SiN₄. These tetrahedra decide the crystallization temperatures and the phases. As expected, SiCN₃ and SiN₄ tetrahedra will crystallize in Si₃N₄ crystallites, and SiC₃N and SiC₄ will crystallize as SiC. SiC₂N₂, referred to as a magic composition, requires the most numerous substitution jumps to provoke the nucleation of the stable SiC or Si₃N₄ phase. The presence of different tetrahedra depends on various parameters such as the chemical composition of the starting precursors, the degree of cross-linking, and the pyrolysis conditions.

The composition of the starting precursors and the degree of cross-linking determines the composition of the final pyrolyzed amorphous ceramics. The rearrangements during pyrolysis depend on the reactions that the specimen undergoes, resulting in various combinations of silicon tetrahedra in the pyrolyzed ceramics. As shown in Figure 3, the stable compositions are above the tie line between SiC and Si₃N₄, which prevents the liquid or gaseous decomposition of excess silicon. Also, the excess of carbon is in the composition; otherwise, the materials would start crystallization at about 1200°C, such as amorphous SiC^{113,114} and amorphous Si₃N₄¹¹⁵ because of

the presence of only SiC_4 and SiN_4 tetrahedra. The presence of mixed tetrahedra determines the thermal stability of polymer derived SiCN ceramics.

2.1.4 The properties of PDCs

Some mechanical properties of bulk silicon carbonitride amorphous ceramics derived from polymer precursors have been reported. The mechanical strength of amorphous ceramics derived from NCP200 is about 375 MPa, and the Vickers hardness is about 9.5 GPa. The hardness value is lower than that of sintered crystalline SiC (27-30 GPa) and Si_3N_4 (18-20 GPa), but is comparable to that of reaction bonded silicon nitride¹¹⁶. This may be due to the presence of appreciable open porosity in the ceramic bodies (7%). The improvement of the preparation and pyrolysis process led to the formation of fully dense Si/C/N ceramics with significantly enhanced hardness (26GPa) and the fracture strength (1.1GPa)¹¹⁷. The reduction of porosity in the ceramics can account for the increase (Figure 5).

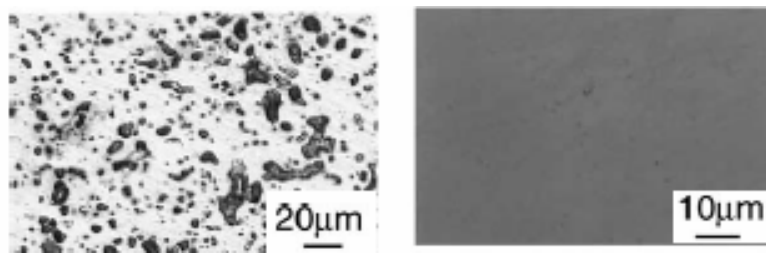


Figure 5: Optical micrographs of specimens prepared by the powder and the pressure casting routes.

Due to the fact that the polymer derived Si/C/N ceramics do not contain any oxide additives in the amorphous network, increased high temperature properties can be expected. The results of creep studies on the polysilazane derived amorphous Si/C/N ($\text{Si}_{1.7}\text{C}_{1.0}\text{N}_{1.5}$) and polyborosilazane derived Si/B/CN ($\text{Si}_2\text{B}_{1.0}\text{C}_{3.4}\text{N}_{2.3}$) showed that both materials exhibited an exceptionally low creep rates^{118, 119} (Figure 6). Both materials exhibited a three-stage creep behavior: (1) the creep rate declined, which was associated with the further densification; (2) the strain rate approached a steady state, and (3) it resumed a declining strain rate that ultimately decreased below the measuring limit of the system (Figure 6). The density of the tested Si/C/N ceramics increased from 2.06 at the beginning of the experiment to 2.30 g/cm^3 at the end of the stage (1) and then remained constant during stages (2) and (3). The enhanced creep resistance in stage (3) was related to crystallization in the samples (about 5% crystalline Si_3N_4 was detected in the 1280°C tested Si/C/N ceramics).

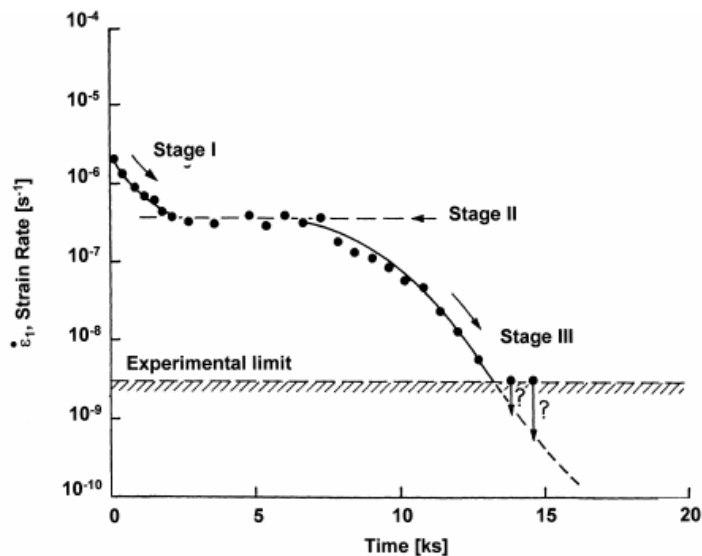


Figure 6: Change of the strain rate in Si/(B)/C/N vs. time showing three different stages.

Polymer derived Si/C/N ceramics will release the N₂ gas at the temperatures above 1400°C, which causes the undesirable degradation of silicon carbonitride ceramics. However, this situation can be circumvented by heating the material in air. In the dry oxygen or air environment, polymer derived ceramics showed good resistance to oxidation^{120, 121}. The oxidation rate for SiCN ceramics is close to that for pure SiC or Si₃N₄. Our research showed that aluminum doped SiCN ceramics exhibit much better than SiCN ceramics, CVD SiC, and CVD Si₃N₄. The details will be discussed in the oxidation section.

In general, ternary Si/C/N materials were characterized by semiconductive electrical behavior^{88, 122}. The electrical properties of this class of materials strongly depend on the starting composition of the precursor material, the type of microstructure obtained, and the utilized processing technology in terms of pressing and pyrolyzing conditions^{123, 124}. Depending on the above-mentioned parameters, the dc-conductivity of polysilazane (PHMS) derived amorphous Si/C/N materials can be adjusted between 10⁰ and 10⁻¹⁵ Ω⁻¹ cm⁻¹ at room temperature¹²⁵. Decreasing the carbon content of the Si/C/N ceramics by performing the pyrolysis in a reductive ammonia atmosphere results in decreased dc-conductivity, whereas an increased conductivity is observed by annealing the material in a nitrogen atmosphere. Starting phase separation and beginning crystallization at annealing temperatures of 1300°C results in high conductivity. The DC conductivity of the polymer derived ceramics shows a T^{-1/4} dependence at low temperatures, which indicates that electron transport is realized occupying midgap-states by variable-range-hopping¹²⁶. At higher temperatures, a change of the charge transport mechanism is observed utilizing tail-states by polarone-tunneling¹²⁷. Comparable results were obtained by the preparation of polymer derived amorphous Si/B/C/N materials (Figure 7). Polymer derived

amorphous Si/(B)/C/N semiconductors have high potential for future applications in microelectronic devices due to their tunable wide range conductivity.

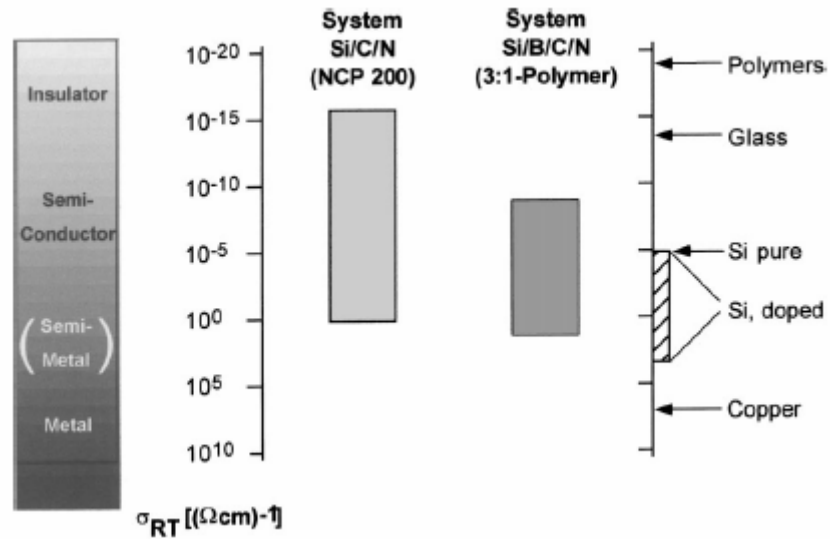


Figure 7: Specific electrical resistance of Si/C/N ceramics derived from PHMS (NCP2000) and Si/B/C/N ceramics. From comparison some typical values for insulators, semiconductors and conductors are also shown.

2.2 Oxidation behavior of silicon-based materials

2.2.1 Oxidation behavior of pure silicon

Before discussing the oxidation of silicon-based ceramics, it is appropriate to review the oxidation of pure silicon for it sets a basic for all silicon-based ceramics. The classic paper in this area was written by Deal and Grove¹²⁸. In this paper, it was assumed that oxidation proceeded by

inward movement of oxidant rather than outward movement of silicon in accordance with the experimental evidence for silicon^{129, 130, 131}. They viewed the oxidation process as consisting of three distinct steps, as shown in Figure 8:

1. Transfer of the gaseous oxidant to the outer surface where it reacts or is absorbed.
2. Transport of oxidant across the oxide film towards the silicon.
3. React at the silicon surface to form a new layer of SiO₂.

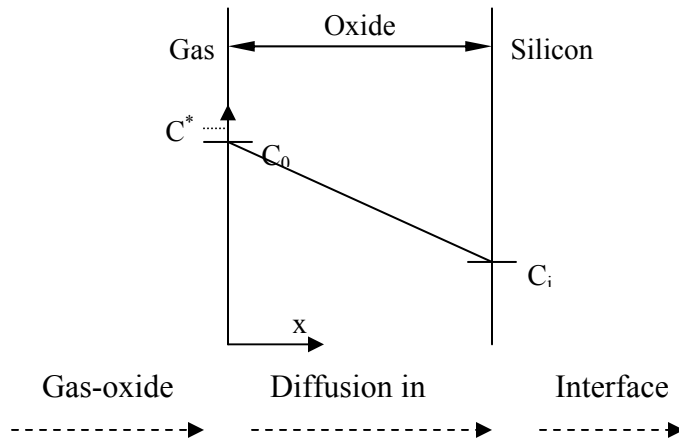


Figure 8: Process involved in Silicon oxidation.

From the above steps, the following linear-parabolic equation was derived:

$$x^2 + Ax = k_p(t + \tau) \quad (2-22)$$

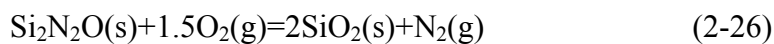
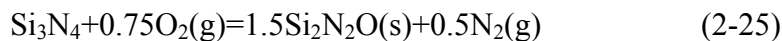
where x is the scale thickness, k_p the parabolic rate constant, t the time, and τ the time shift corresponding to the presence of an initial oxide layer. The quantity of k_p/A is the linear rate constant. The parabolic rate constant is given by:

$$k_p = 2D_{\text{eff}}C^*(\text{O}_2)/N_0 \quad (2-23)$$

where D_{eff} is the diffusion coefficient through the film, $C^*(\text{O}_2)$ the equilibrium concentration of oxidant in the scale, N_0 the number of oxygen molecules incorporated into the SiO_2 scale per volume. For relatively small oxidation times, $t \ll A^2/4k_p$, $x \cong k_p/A(t+\tau)$, oxidation follows a linear rate law. The physical interpretation of the linear region is still controversial. It has been attributed to interface reaction control or to diffusion control which is nonparabolic due to strain effects in the oxide¹³². For longer times ($t \gg A^2/4K_p$ and $t \gg \tau$), oxidation follows a parabolic law, and the diffusion through the thicker oxide is rate control. The activation energy can be calculated by a plot of $\ln k_p$ vs $1/T$. The magnitude of the activation energy can reveal useful information about the diffusion process. The Eq.2-22 describes a wide range of oxidation data. Calculations of parabolic rate constant that are based on the molecular oxygen diffusion coefficient of Norton¹³³ show good agreement with the measured values, and the activation energy for parabolic oxidation is close to that for molecular oxygen diffusion through SiO_2 . Thus, it is generally accepted that molecular oxygen diffusion through the SiO_2 layer is the rate-controlling step^{134, 135}.

2.2.2 Oxidation behavior of SiC and Si₃N₄

The oxidation behaviors of SiC and Si₃N₄ are more complex. In both ceramics, there is a countercurrent gas. The following reactions are generally accepted¹³⁶:



Therefore oxidation process for SiC and Si₃N₄ involves five steps:

1. Transport of molecular oxygen gas to the oxide surface
2. Diffusion of oxygen through the oxide film
3. Reaction at the oxide/ceramic interface
4. Transport of product gases (e. g. CO or nitrogen)
5. Transport of product gases away from the surface

The process is even more complex in Si_3N_4 case because of the formation of duplex film. Many questions still remain about these steps. The key question is what the rate-controlling step is. Furthermore, it is still unknown that either oxygen molecular diffusion in or network exchange of O^{2-} ion is the mechanism for the permeation of oxygen through the network. Even less is known about the transport mechanism of product gas outward through the SiO_2 scale. First, consider the oxidation of SiC. The key observations have been summarized by several investigators^{137, 138, 139}. Generally, only one SiO_2 oxide scale forms though there is limited evidence that an oxycarbide may form between the SiC and the oxide^{140, 141, 142, 143, 144}. The key question concerns the rate-controlling step. There are three possibilities: (1) oxygen diffusion inward, (2) CO diffusion outward, and (3) an interfacial reaction.

Motzfeld¹⁴⁵ carefully compared the rate constants for silicon and SiC. After correcting for the stoichiometry difference (the additional oxygen necessary to oxidize carbon), he finds that silicon and SiC have essentially the same rates and the same activation energies. Therefore, he concludes that the same process that controls silicon oxidation also controls SiC oxidation (i.e., oxygen diffusion inward). Consider the activation energies for oxidation of high-purity SiC, the results showed that there was generally a low temperature regime (<1623K) and a high temperature regime (>1623K). At the low temperature regime, the activation energies for SiC are about 120-140kJ/mol, similar to that for oxidation of silicon and molecular oxygen diffusion

through amorphous SiO₂. This supports molecular oxygen diffusion inward as a rate-controlling step for SiC oxidation below 1623K. At temperatures higher than 1623K, the activation energy for oxidation of SiC becomes much larger. Zheng *et al.*^{146, 147} attributed this to the mixture of network exchange diffusion and molecular oxygen diffusion. However, Ramberg and Worrell¹⁴⁸ find that the high-temperature transition from interstitial-dominant to network-dominant oxygen transportation is a property of amorphous silica scales and does not exist for cristobalite after they carefully evaluated the previous results and their own data. They also conclude that for high-purity silica scales, there is no difference between the rates of interstitial oxygen transport in amorphous SiO₂ and in β-cristobalite.

The difference between molecular oxygen diffusion and the network oxygen diffusion should be reflected in the dependence of the parabolic rate constant k_p on the oxygen pressure P_{O_2} . For the molecular oxygen diffusion, the rate constant should be proportional to P_{O_2} , assuming that the solubility of oxygen in SiO₂ obeys Henry's law. For network exchange diffusion, one expects k_p to show a weak dependence on P_{O_2} ^{147, 149}. Zheng *et al.* have found that k_p was dependent on $p_{O_2}^n$, where n varies from 0.6 at 1473K to 0.3 at 1773K. This result is consistent with the proposed transition between the two types of diffusion. At low temperatures, one expects a value of n closer to 1 for molecular oxygen diffusion. Zhang *et al.* contributed the difference to deviation from Henry's law for the solubility of oxygen in SiO₂.

Some investigators have attributed the higher activation energies at higher temperatures to a transition to CO-diffusion-outward rate control^{150, 151}. There are two facts tending to discount this point. One is the oxidation experiment of Si¹³C done by Zhang *et al.*. The result shows no carbon gradient, as one would expect if CO diffuses outward slowly. On the other hand, the thermodynamic calculation rejected the possibility that the CO diffusion outward was the

controlling process since if the CO-diffusion-outward is a rate-controlling process, P_{CO} has a value of about 10^{32} Pa at 1600K at oxide/substrate interface. Extremely high pressure would be expected to blow the scale off, but this is not observed.

If the interfacial reaction was the controlling process, the oxidation kinetics should be linear behavior. However, most of oxidation data of pure SiC indicated the parabolic kinetics for the majority of the reaction period. Consequently, the oxygen diffusion inward is the control process for oxidation of SiC.

Next, consider Si_3N_4 oxidation. The oxidation of Si_3N_4 is more complex because of the formation of duplex layers. The activation energy is substantially higher than that of Silicon. In addition, the oxidation rates are slower than pure Si and SiC in certain temperature range. These facts suggest that the oxidation mechanism for Si_3N_4 is different from that for SiC.

Luthra has systematically investigated the possible rate-controlling steps for Si_3N_4 . Most investigators have observed parabolic kinetics, suggesting that either oxygen diffusion inward or nitrogen diffusion outward is a rate-controlling step^{140, 152, 153, 154}. The parabolic rate constant varies linearly with oxygen pressure at 1523-1673K, suggesting a molecular oxygen diffusion mechanism. The double oxidation experiments with $^{18}O_2$ and $^{16}O_2$ also suggested that permeation by molecular oxygen is the primary diffusion mechanism and that considerable exchange with network occurs at higher temperatures¹⁵⁵. The higher activation energy for Si_3N_4 as compared with that of silicon has been attributed to oxygen transport through Si_2N_2O ¹⁵⁶. Same as the SiC case, rate control by diffusion of gaseous outward is unlikely because that leads to a very large nitrogen pressure at oxide/matrix interface. Oxidation studies at very high temperatures showed only limited bubbling. An interfacial reaction is not likely to be the rate-controlling step because no obvious linear rates have been observed.

The difficulty with oxygen diffusion inward as a rate-controlling step arises from the substantially slower rate of Si_3N_4 as compared with silicon. The fact leads to unreasonably high pressures at the $\text{SiO}_2/\text{Si}_2\text{N}_2\text{O}$ interface. This had been discussed by both Du *et al.* and Luthra. There are three possible explanations: (1) thermodynamic equilibrium is not attained at the interface, (2) SiO_2 scale formed on Si_3N_4 may be different from that formed on silicon, (3) network exchange diffusion may occur in Si_3N_4 case at the temperature at which molecular oxygen diffusion occurs in the silicon case. If the first assumption was true, diffusion would not be truly rate controlling. There is also no clear evidence of different types of SiO_2 scale being formed on Si_3N_4 or on silicon. Some investigators suggested that the nitrogen or nitrogen compounds diffusing outward may create a sort of blocking effect to oxygen diffusion inward, but this is difficult to prove experimentally. If nitrogen had such an effect, one would expect a dependence of the rate on P_{N_2} , which has not been observed. The double oxidation experiment supports the oxygen molecular diffusion for both silicon and Si_3N_4 , discounting the third explanation.

Du *et al.*^{140, 156} explained the differences between SiC and Si_3N_4 on the basis of duplex layer formation on Si_3N_4 . Du *et al.*^{140, 156} proposed that oxygen diffusion inward was a rate-controlling step and that $\text{Si}_2\text{N}_2\text{O}$ layer had a lower permeability to oxygen than SiO_2 and thus acted as a diffusion barrier. However, the inconsistencies for rate control by oxygen diffusion inward still remains.

In summary, a lot of questions are still unsolved although a fundamental understanding of SiC and Si_3N_4 oxidation is emerging. These deal with the rate-controlling step and transport mechanism through the SiO_2 scales.

2.2.3 Oxidation behavior of additive-containing materials

The discussion above has been focused on the oxidation behavior of high purity materials. In practice, sintered SiC and Si₃N₄ materials contain densification aids, such as magnesium oxide (MgO), alumina (Al₂O₃), and yttria (Y₂O₃). These oxides tend to migrate out to the SiO₂ scale and form the corresponding silicate^{157, 158, 159, 160, 161, 162, 163, 164, 165, 166, 167, 168, 169, 170}. Clarke has reported two driving forces of these transition metals diffusing to the surface. Initially, a pure SiO₂ layer is formed and the additives are present as a grain-boundary silicate glass. Then, the concentration gradient drives the cations to diffuse into the SiO₂ glass.

In the case of SiC hot-pressed with Al₂O₃ sintering aid, an observed pressure dependence on oxygen suggests that oxygen diffusion inward is still the rate-controlling step. However, aluminum diffuses into the scale to form an aluminosilicate that appears to accelerate oxidation rate^{141, 158}. In case of SiC sintered with boron and carbon sintering aids, boron diffuses into the scale. It creates a lower viscosity scale, which leads to somewhat higher oxidation rates over pure SiC. It has also been suggested that the formation of boron hydroxide is responsible for the bubbling from oxidation observed in this material. The high thermodynamic stability of boron hydroxide indicates it can be formed at substantial pressures with a small pressure of water vapor and small amount of boron.

As for the hot-pressed Si₃N₄ with MgO and Y₂O₃ additives, no pressure dependence on oxygen has been found^{160, 165}. This differs from the observations for CVD Si₃N₄ and indicates another oxidation mechanism. Cubicciotti and Lau^{164, 165} have performed re-oxidation experiments on MgO- and Y₂O₃-containing Si₃N₄. First, they oxidized the materials for a time interval, polished the scale off, and re-oxidized them. It was found that the process simply

continues, as shown in Figure 9. From this phenomena and other analysis, they concluded that the oxidation is controlled by migration of the magnesium or yttrium cations outward through the grain-boundary phase. However, the result of Andrews and Riley indicates that both cation outward diffusion and oxygen inward diffusion are important for some types of Si_3N_4 .

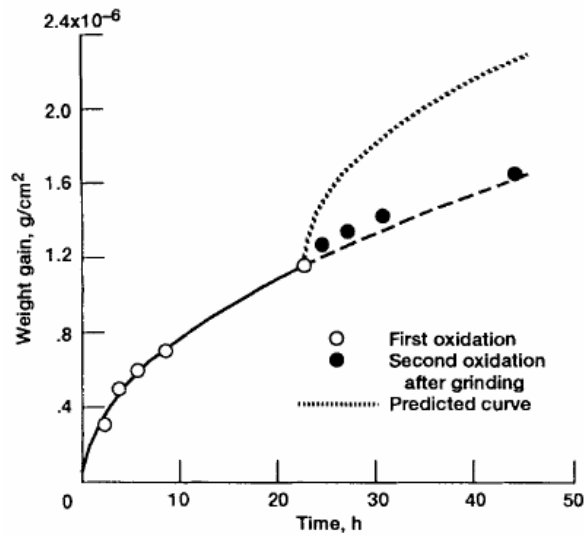


Figure 9: Re-oxidation curve for Si_3N_4 with MgO additives.

The additives also show other effects on oxidation. The oxidation rate will increase with the amount of additives. Some additives lead to deviations from the parabolic rate law. Also, it is noted that certain compositions of a Y_2O_3 -containing Si_3N_4 have been found to catastrophically oxidize at 1273 K. It is due to the oxidation of a grain-boundary phase and the associated volume expansion¹⁷¹. The surface oxide does not form in a sufficient quantity to protect the grain boundaries at 1273 K.

Related to this is the oxidation of porous SiC and Si_3N_4 materials. There are several studies on reaction-sintered Si_3N_4 , which is about 15% porous^{172, 173}. In general, these studies

show that internal oxidation of the pores is critical. Porz and Thummler have shown that the extent of internal oxidation is governed by the radius of the pore channels allowing the oxygen to penetrate the specimen. In their work, the channel is narrow so that the velocity of oxygen transportation through the channel is very low compared to the reaction rate of oxygen with Si_3N_4 . Due to these two concurrent processes an oxygen gradient is built up along the channel axis leading to SiO_2 formation mainly at the channel mouth [Figure 10(a)]. The typical oxidation of reaction-sintered Si_3N_4 is presented by an asymptotic law. However, for the oxidation of porous polymer-derived SiCN ceramic powders, the situation is different for two reasons: (1) the pores are oxidized uniformly through the thickness of the specimen and (2) the weight gain is proportional to the volume of the specimen, not its surface area. Raj and co-workers propose another model [Figure 10(b)] in which growth rate is slower than oxygen penetration rate, leading to uniform oxidation through this specimen.

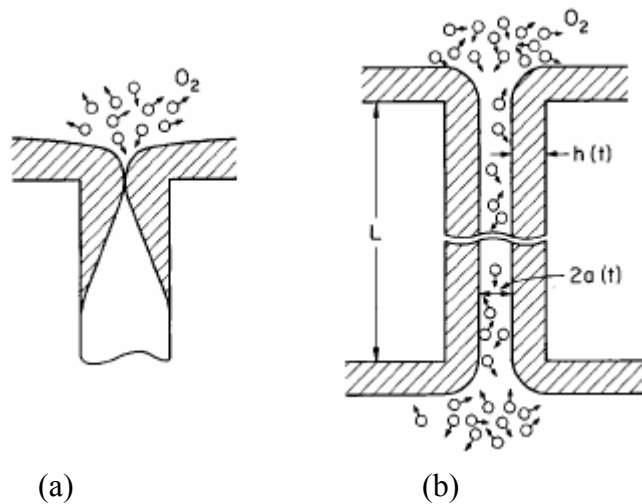


Figure 10: Two extreme cases for morphology of oxide overgrowth on pore surface. (a) growth rate is faster than supply rate of oxygen from atmosphere into pore, leading to pore clogging near surface. (b) growth rate is slower than oxygen supply rate, leading to uniform oxidation through specimen.

2.2.4 Oxidation behavior of sialon

Sialon ceramics are another important class of high temperature structural ceramics. In comparison with SiC and Si₃N₄ ceramics, the oxidation of sialon has been less studied. Singhal and Lange¹⁷⁴ reported that the oxidation of hot-press sialon compacts followed a parabolic rate law with increased oxidation resistance as the Al content increased. Mullite (Al₆Si₂O₁₃) was the only identifiable crystalline oxidation product. M.H. Lewis and P.Barnard¹⁷⁵ studied the oxidation mechanism of sialon ceramics. They found the oxidation kinetics was controlled by outward diffusion of grain boundary segregated impurities. Chartier *et al.*¹⁷⁶ suggested the same mechanism occurred to β'-sialon (Z=0.4). However, the parabolic law and activation energy of oxidation for sialon powder showed that the rate-controlling step was the permeation of molecular oxygen through the oxide layer¹⁷⁷.

2.2.5 Oxidation of polymer derived ceramics

The earliest study of the oxidation of SiCN was done by Bahloul *et al.*. He concluded that the oxidation of free carbon was retarded by surrounding amorphous SiCN. In 1993, Mocaer *et al.*, studied the oxidation behavior of SiCN(O) filaments. Some studies on the oxidation of boron-containing SiCN have been reported as well in recent years^{109, 106}.

In most of studies, the oxidation rate is very low, close to or a little over the oxidation rate of pure SiC and Si₃N₄ ceramics. Reidel attributed the improved thermal stability of bulk silicon carbonitride covered by a protective silica surface layer to the low nitrogen diffusion coefficient through SiO₂ that hinders the solid-state reaction. Thus, the equilibrium of the reaction is shifted

to the side of the products, enabling the formation of novel metastable bulk composite materials in the ternary system Si/C/N, with Si_3N_4 , SiC and C as discrete phases. Moreover, due to the low oxygen diffusion coefficient of 10^{-11} - 10^{-16} cm^2/s at 900 and 1400 $^\circ\text{C}$, respectively, the passivating dense SiO_2 layer effectively protects the bulk silicon carbonitride from further oxidation. Raj *et al.* found asymptotic behavior during oxidizing SiCN powders and attributed it to the saturated weight gain analogous to the oxidation behavior of reaction-bonded Si_3N_4 ceramics.

Some k_p values of silicon-based ceramics are summarized and shown in Figure 11.

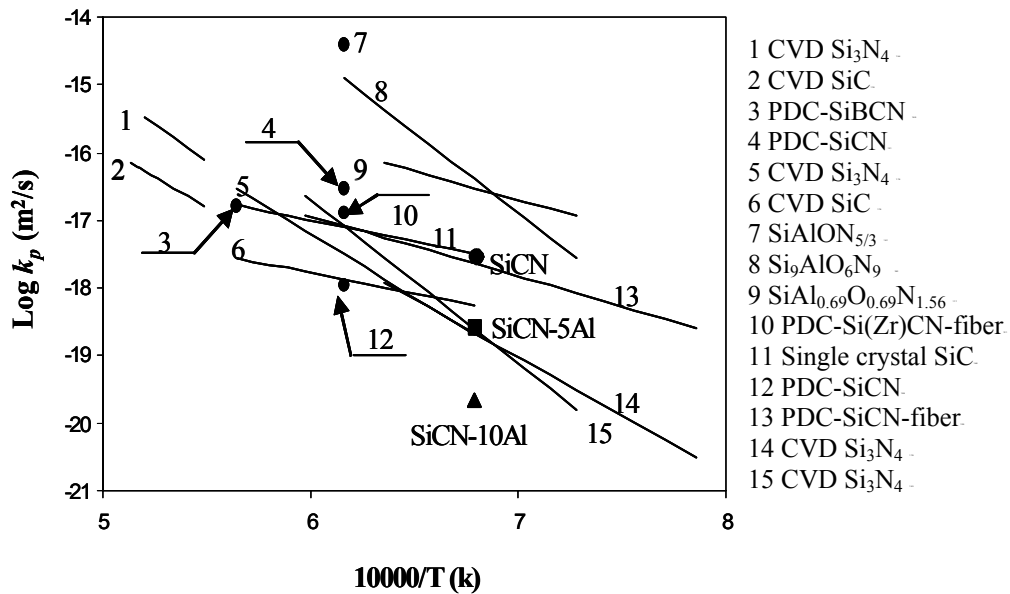


Figure 11: Some k_p values of silicon-based ceramics.

2.3 Wet oxidation behavior of silicon-based materials

When silicon-based materials are exposed to high temperature water vapor, two reactions occur simultaneously: (1) the material reacts with water vapor to form silicon dioxide (referred as to oxidation) and (2) the silicon dioxide reacts with water vapor to form highly volatile products, such as $\text{Si}(\text{HO})_4$ (referred as to corrosion). They will be discussed in detail in the following sections.

2.3.1 Oxidation of silicon-based materials in wet environments

Considering the effect of water on the oxidation of pure silicon, Deal and Grove have shown that silicon oxidizes over an order of magnitude faster in wet oxygen than in dry oxygen. They attribute this to the higher solubility of water in SiO_2 than that of molecular oxygen in SiO_2 according to Eq 2-23. Deal and Grove further show that silicon oxidizes at the same rate regardless of whether the mixture is $\text{H}_2\text{O}/\text{Ar}$ or $\text{H}_2\text{O}/\text{O}_2$. This indicates that H_2O is the primary oxidizing species. Irene and Ghez¹⁸³ have shown that H_2O also disrupts the SiO_2 network that permits faster H_2O transport.

There is general agreement that water accelerates the oxidation of SiC ^{144, 159, 184, 185, 186, 187, 188}. The major reaction is very likely:



The study done by Jorgensen *et al.* on the oxidation of SiC powders showed the rates to be proportional to $\log P_{\text{H}_2\text{O}}$. Cappelen *et al.* have observed that the rate in $\text{H}_2\text{O}/\text{N}_2$, and $\text{H}_2\text{O}/\text{O}_2$ is the same indicating that as in pure silicon, the primary oxidizing species is H_2O . The study of

SiC in wet oxygen for longer times showed an initial linear region followed by a parabolic region. Unlike oxidation in dry oxygen, the linear region lasts long enough (about 1 h) to allow the measurement of reliable linear rate constants. Apparently the rapid permeation of H₂O extends the period of interfacial reaction control. Tressler *et al.* have examined the effect of water vapor on the oxidation of single-crystal SiC and sintered a-SiC. In both cases, steam accelerated oxidation by about 10 to 20 times, which is attributed to more rapid permeation of the H₂O molecules.

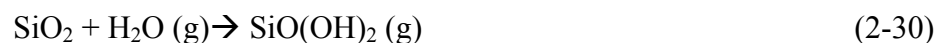
Choi *et al.* examined the oxidation of Si₃N₄ in wet oxygen. The results showed somewhat different behavior than for wet oxidation of silicon or SiC. For wet oxidation in H₂O/Ar, the pressure of H₂O has no effect on the rates. However, in the case of H₂O/O₂, the rates show a complex dependence on pressure of water vapor. They attribute the wet oxidation to the following reactions:



They suggest that the product gases such as NH₃ and NO block the outward diffusion paths, which leads to increase solubility of H₂O versus molecular oxygen in SiO₂.

2.3.2 Corrosion of silicon-based materials in wet environment

Silica scale formed by water oxidation may simultaneously volatilize by forming a silicon hydroxide or silicon oxyhydroxide species under atmosphere pressures. Some possible reactions are as follows¹⁸⁹:





The rate of oxidation can be described by a parabolic rate constant, k_p . The rate of volatilization is given by a linear reaction constant, k_l . When the oxidation and the volatilization occur simultaneously, the overall kinetics is described by more complex parabolic kinetics. Parabolic oxide scale thickness kinetics has been mathematically described by Tedmon for Cr_2O_3 -forming Fe-Cr alloys¹⁹⁰. The expression is as follows:

$$t = \frac{k_p'}{2k_l'} \left[-\frac{2k_l'x}{k_p'} - \ln\left(1 - \frac{2k_l'x}{k_p'}\right) \right] \quad (2-33)$$

where t is the oxidation time, x the oxidation thickness, k_p' the parabolic rate constant for oxidation in the units of thickness² per unit time, and k_l' the linear rate constant for scale volatilization in units of thickness per unit time.

The flux in the real system is different from the measured one. The measured flux can be compared with the calculated one¹⁹¹. The appropriate relation for the flux of the volatile species from a flat plate through a gaseous boundary layer under laminar flow conditions is as follows¹⁹²:

$$J = 0.664 \left(\frac{\rho' v L}{\eta} \right)^{1/2} \left(\frac{\eta}{\rho' D} \right)^{1/3} \frac{D \rho}{L} \quad (2-34)$$

where J is the flux, ρ' the concentration of the major gas species, v the linear gas velocity, L the sample length, η the gas viscosity, D the interdiffusion coefficient for the diffusing species in the major gas species, and ρ the concentration of the diffusion gas species at the solid-gas interface. Gas concentration is calculated using the ideal gas law. Using the data of Hashimoto¹⁹³, Krikorian¹⁹⁴, and Allendorf¹⁹⁵, one can calculate vapor pressures of Si-O-H species. The results

of calculation show that the Si(OH)_4 is the primary volatile species. Thus the magnitude and the temperature dependence of the measured flux are best described by Si(OH)_4 formation. For the approximation, the diffusion coefficient (D) is proportional to $1/P_{\text{total}}$, and ρ proportional to P_{total} . Because the Si(OH)_4 (g) is the only volatile species and is formed via the reaction (2-31), ρ is proportional to $P_{\text{Si(OH)}_4}$:

$$k_l \propto \frac{v^{1/2} P_{\text{H}_2\text{O}}^2}{P_{\text{total}}^{1/2}} \quad (2-35)$$

The effects of additives on the volatilization of silica in water vapor were discussed by Opila *et al.*¹⁹⁶. It was found that the rare-earth cations diffuse to the surface and form the rare-earth disilicates. The silica activity in these silicates is not low enough that the dense adherent rare-earth disilicate surface layer in-situ formed on the additive-containing silicon-based ceramics is not sufficient protection for these materials in combustion environments.

CHAPTER THREE: CHARACTERIZATION OF POLYMER DERIVED CERAMICS

In this chapter, the process for fabricating fully dense silicon carbonitride (SiCN) and silicoaluminum carbonitride (SiAlCN) ceramics is described. ^{29}Si NMR and ^{27}Al NMR are applied to investigate the structural evolution during thermal pyrolysis and post-pyrolysis heat treatment. XRD is used to investigate the crystallization behavior of SiCN and SiAlCN ceramics. It is found that the aluminum greatly affects the structural evolution during post-pyrolysis heat treatment. Higher aluminum content in the Si-C-N leads to more SiCN_3 unit, which provides more stable amorphous phases and, as a result, contributes to higher thermal stability comparing with SiCN without Al doping. In addition, the effect of aluminum on the crystallization phase of SiAlCN is also discussed.

3.1 Experimental procedure

3.1.1 Processing of fully dense monolithic ceramics

Commercially available polyureamethylvinylsilazane (PUMVS, CerasetTM (Kion Corp., PA) is used as the precursor for preparation of SiCN ceramics. Ceraset is a versatile, liquid thermosetting resin. This polymer contains repeat units in which silicon and nitrogen atoms are bonded in an alternating sequence. The structure is described in Figure 12¹⁹⁷.

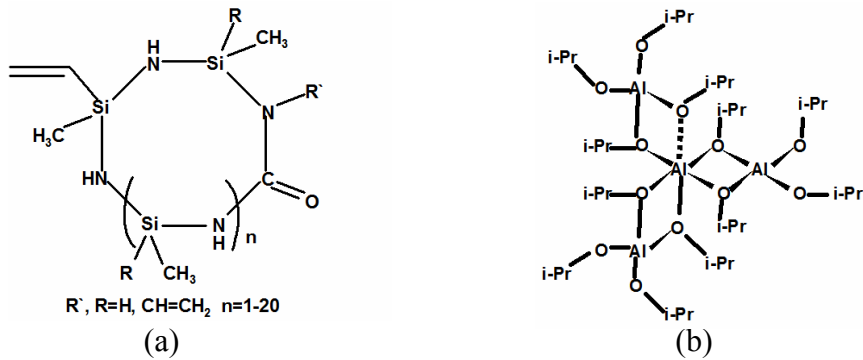


Figure 12: Structure of (a) CerasetTM and (b) Aluminum isopropoxide.

Liquid Ceraset is mixed with 2-5wt% thermal initiator, Dicumyl Peroxide (Acros Organics) under continuously stirring until the thermal initiator is totally dissolved. Then the precursor is cross-linked at 120-150⁰C for 2 hours to produce transparent polymer rods. The discs of 2-3mm thick are cut from the rods, and pyrolyzed at 1000⁰C for 5 hours under 50MPa isostatic-pressure in nitrogen atmosphere. The typical sintering procedure is shown in Figure 13.

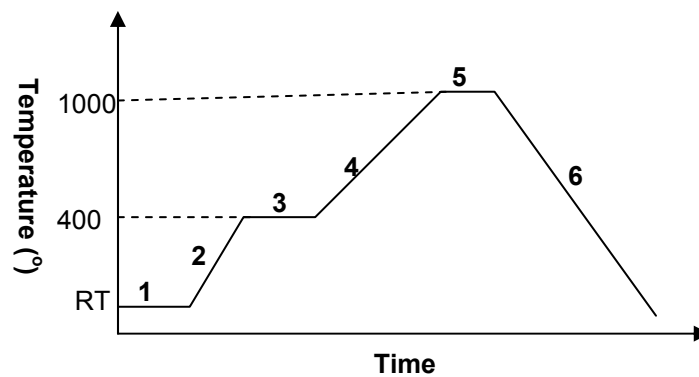


Figure 13: The Schematic Sintering Procedure for SiCN and SiAlCN ceramics

1. Increase the pressure to 50 MPa
2. Raise the temperature to 400°C with the ramp rate of 1°C/min
3. Hold the temperature at 400°C for 4 hours
4. Raise the temperature to 1000°C with the ramp rate of 0.3-0.5°C/min
5. Hold the temperature at 1000°C for 4-8 hours
6. Cool down to RT at the rate of 2-5°C/min

For SiAlCN ceramics, liquid Ceraset and solid aluminum isopropoxide (98+% Assay, Alfa Aesar, The structure is shown in Figure 12 (b)) are used as starting materials. They are mixed together under continuously stirring for several hours until aluminum isopropoxide is completely dissolved. Gaseous by-products are removed by placing the mixture in a vacuum before the thermal-setting step. This precursor is then mixed with 2-5wt% thermal initiator, dicumyl peroxide. The cross-linking and pyrolysis process are the same as that for the SiCN ceramics.

SiCN and SiAlCN powders are also prepared. For powder samples, the starting materials are the same as aforementioned. After being cured at 150°C, these polymers are further cross-linked at 350°C-400°C under flowing argon or nitrogen gas protection. Then the polymers are ball-milled for different times to get different size powders. These powders are then pyrolyzed using the same procedure as shown in Figure 13. The compositions of the SiCN and SiAlCN ceramics are measured using a combination of elemental analysis and secondary hydrochloric acid ICP. The results are listed in Table 1.

Table 1: The Composition of Si(Al)CN Samples.

	(Ceraset : Al-Isopropoxide)	Compositions
SiCN	100:0	$\text{SiC}_{0.99}\text{N}_{0.85}\text{O}_{0.11}$
SiAlCN-5	95:5	$\text{SiAl}_{0.02}\text{C}_{0.84}\text{N}_{0.90}\text{O}_{0.12}$
SiAlCN-10	90:10	$\text{SiAl}_{0.04}\text{C}_{0.83}\text{N}_{0.93}\text{O}_{0.14}$
SiAlCN-20	80:20	$\text{SiAl}_{0.08}\text{C}_{0.80}\text{N}_{0.95}\text{O}_{0.15}$
SiAlCN-30	70:30	$\text{SiAl}_{0.12}\text{C}_{0.78}\text{N}_{0.97}\text{O}_{0.15}$

3.1.2 Structural characterization

The structural evolutions during the polymer-to-ceramic transformation and post-pyrolysis heat-treatment are very complex and have not been completely understood. This is partly due to the poorly defined structure of the highly cross-linked polysilazanes and the resultant amorphous ceramics. By applying solid state Nuclear Magnetic Resonance (NMR), Fourier Transform Infrared Spectroscopy (FTIR), X-ray Diffraction (XRD) and other characterization technologies, it is possible to investigate the pyrolysis reactions and the structural evolution during post-pyrolysis heat-treatment.

FTIR is a powerful tool for identifying different types of chemical bonds in a molecule by producing an infrared absorption spectrum that is like a molecular "fingerprint". It is used to analyze the starting liquid precursors. FTIR spectra of liquid samples can be easily obtained by placing one drop of the sample between two plates of sodium chloride (salt) which is transparent to infrared light; and then placing the sample in FT-IR instrument (Perkin Elmer Spectrum One) for analysis.

In order to understand the material evolution during heat-treatment, the samples heated at different temperatures up to 1500°C were analyzed with solid state NMR.

In NMR, unlike other types of spectroscopy, the quality of the sample has a profound effect on the quality of the resulting spectrum. The sample should be carefully so that useful information is not lost or obscured in the spectrum. Before preparing the NMR samples, the tubes should be rinsed with acetone or some other suitable solvent, and then dried with a blast of dry air or nitrogen. Do not dry tubes in a hot oven because it does not remove solvent vapor effectively, and solvent peaks will appear in the spectrum. Tubes must be capped, and caps should be treated the same way as tubes. The solid powders should be so fine that they can be compacted densely and uniformly in the tube. The height of sample in the tube should be suitable so that the sealed pellet can fit into the tube. NMR tubes with a chipped or broken top must be forbidden because they are dangerous, and very likely to splinter lengthwise.

High resolution ^{27}Al and ^{29}Si solid state magic angle spinning (MAS) NMR experiments are carried out on a Chemagnetics 300 MHz Infinity spectrometer at Larmor frequencies of 78.2 and 59.6 MHz for ^{27}Al and ^{29}Si , respectively. A standard CP/MAS probe with a 7.5-mm pencil rotor system is used. The sample spin rate of 5kHz and 10kHz are used for ^{29}Si and ^{27}Al , respectively. All the ^{27}Al and ^{29}Si spectra are acquired using a standard single pulse sequence with a tip angle of about 45 degrees and a recycle delay time of 0.5s (^{27}Al) and 10s (^{29}Si) with accumulation numbers varied between several hundred to 30,000 scans. The ^{27}Al chemical shifts are referenced to $\text{Al}(\text{H}_2\text{O})_6^{+3}$ (1M Aluminum nitrate) and the ^{29}Si chemical shifts are referenced to tetrakis(trimethylsilyl)silane (TTMS).

The materials annealed at different conditions are also characterized by X-ray Diffraction (XRD, a Rigaku diffractometer) with Cu K_α radiation. Powder samples are used for the

diffraction. The diffraction samples are prepared by impacting the powder into a square hole of an amorphous aluminum plate sample holder and then are scanned in the range of angle (2θ) from 10 to 90° .

Microstructures of selected samples are observed by high-resolution transmission electron microscopy (HRTEM) using a JEOL JEM 2010F microscope. First, the bulk sample is cut to small piece using diamond saw and is mounted on the glass holder by wax. One side of the sample is polished with diamond lapping film to $1\mu\text{m}$ finish using tri-pod. Then the sample is remounted by gluing the polished surface to the glass holder with super-glue. The other side is then polished to 20-50 μm thick with diamond lapping films to $1\mu\text{m}$ finish using tri-pod. Then the sample on the glass holder is immersed in acetone to dissolve super-glue. The polished sample is mounted on a nickel or copper ring and then is further polished by ion-beam milling to reduce the thickness of the center of the sample until a small hole appears.

3.2 Results and discussion

3.2.1 Structural evolution

The reaction to synthesize polyaluminasilazanes was characterized by FTIR (Figure 14). The spectrum of Ceraset is similar to that reported previously¹⁹⁸. The bands ascribed to vinylsilyl groups ($\text{H}_2\text{C}=\text{CHSi}$) are the C-H vibration at 3047 cm^{-1} and the C=C stretching at 1591 cm^{-1} . The bands attributed to Si-NH-Si groups are N-H stretching at 3374 cm^{-1} and Si-N vibration at 1160 cm^{-1} . The bands related to Si- CH_3 groups are the characteristic band at 1253 cm^{-1} and methyl vibrations at 2954 and 2896 cm^{-1} . A strong band at 2111 cm^{-1} is

assigned to Si-H. The broad bands between 640 to 1000 cm^{-1} result from the mixture of two bonds: Si-N and Si-C. The FTIR spectrum of the reaction product of Ceraset and aluminum isopropoxide is significantly different from that of pure Ceraset. The intensities of absorption bands ascribed to N-H, Si-CH₃, vinylsilyl group, and Si-H are all significantly reduced. The broad bands between 640 and 1000 cm^{-1} exhibited in original Ceraset spectrum shift to the range between 700 and 1200 cm^{-1} , and split into three peaks centered at 1030, 900 and 760 cm^{-1} , respectively. The reduction of Si-CH₃, vinylsilyl group and Si-H is due to the partially cross-linking of Ceraset. The reduction of N-H results from the reaction between Ceraset and aluminum isopropoxide, as stated below.

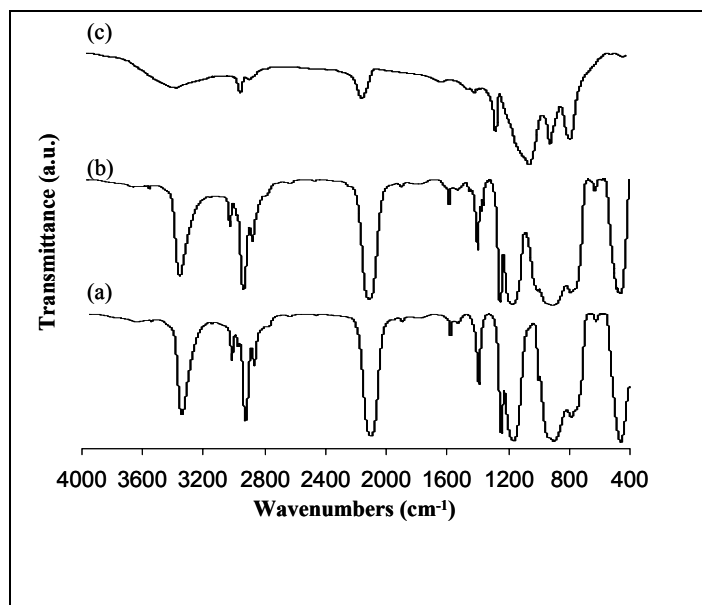


Figure 14: FTIR spectra of Ceraset as obtained (a), CER-10AIs mixed at room temperature (b) and CER-10AIs heat-treated at 150 °C (c).

The gaseous phase evaporated at 150°C was analyzed by MS¹⁹⁹. The results indicated that gaseous phase is predominantly isopropyl alcohol (HOCH(CH₃)₂). Combined with the information of the reduction of N-H in FTIR spectra at 150°C, it is suggested that the following reaction occurs between Ceraset and aluminum isopropoxide at 150 °C:



The formation of Al-N units through dehydrocoupling is a favored reaction^{200, 6, 84}.

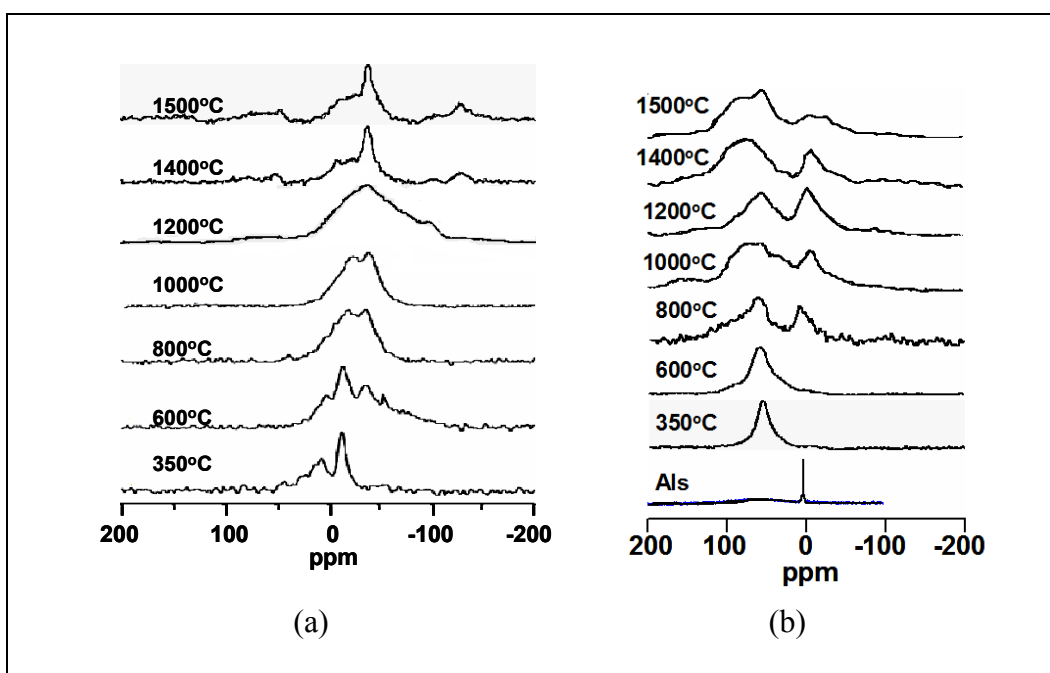


Figure 15: Solid-state NMR spectra of SiAlCN-10 heat-treated at different temperatures: (a) ²⁹Si NMR, (b) ²⁷Al NMR.

Figure 15 (a) shows ²⁹Si solid-state NMR spectra of the SiAlCN-10 precursor heat-treated at different temperatures up to 1500°C. Two peaks centered at 8 and -11 ppm are shown in the spectrum of the SiAlCN-10 heated at 350 °C. The peak at 8 ppm can be assigned to SiC₃N

units²⁰¹, whereas SiC₂N₂ or SiHCN₂ groups, which are present in Ceraset structures (Figure 12), are responsible for the peak at -11 ppm^{201, 202}. Formation of the SiC₃N unit, which is not present in original Ceraset structure (Figure 1), can be explained by the following cross-linking reaction of Ceraset between 250 to 350 °C as proposed previously:



Heating the sample to 600 °C results in reduced intensity of SiC₃N and SiC₂N₂ signals, while two new peaks appear at -34 and -50 ppm. These new peaks are attributed to SiCN₃ (-34 ppm) and SiN₄ (-50 ppm) groups, respectively. The formation of SiCN₃ and SiN₄ unit dues to the thermal decomposition reaction of Ceraset at 550 to 600 °C, which results in the release of CH₄ and H₂ gases. Upon heat-treatment at the temperature of 600°C, the ²⁹Si resonances corresponding to different groups do not overlap with each other, suggesting the transition from the polymeric preceramic structure to the amorphous ceramic is not yet completed at this stage. The signal ascribed to the SiC₂N₂ unit is dominant up to 600°C, indicating the backbone structure in original Ceraset is retained up to this temperature.

Further heating the polyaluminasilazanes to 800°C causes the intensity of peaks associated with SiC₃N (0 ppm) and SiN₄ (-48 to -50 ppm) to decrease significantly. Meanwhile, the intensity of the SiCN₃ peak (-37 ppm) increases to the level as strong as the SiC₂N₂ peak (-21 ppm). Upon heating samples to 1000 °C, the signal of SiCN₃ becomes higher than that of SiC₂N₂. At the temperature of 1200°C, SiCN₃ group is dominant and the spectrum shape is totally different from those at lower temperatures. These changes in NMR spectra suggest that the SiC₃N and SiN₄ units formed earlier during cross-linking and earlier stages of thermal decomposition convert to more stable SiCN₃ units. This result reflects the completion of thermal decomposition and the onset of full transformation of the preceramic network into the

amorphous ceramics which is observed at 800 °C. Further increase in the intensity of the SiCN₃ signal at the expense of SiC₂N₂ suggests gradual structure rearrangement at higher temperatures. The gradual formation of SiCN₃ may be due to the decomposition of SiC₂N₂ with free carbon by-product. This is also observed in other research^{203, 204, 205}. The reaction in this process may include the following:



Annealing the samples at temperatures above 1200°C leads to the continual increases in the intensity of SiCN₃ signal, the peak also becomes sharper. It suggests that the structural evolution to SiCN₃ still continues and that the structure of SiCN₃ is becoming more ordered.

Figure 15b shows ²⁷Al solid-state NMR spectra of the SiAlCN-10 precursor heat-treated at different temperatures. The spectra obtained at lower temperatures (350 and 600 °C) show a single peak centered at 51 ppm, which should be assigned to the 5-coordinated Al. The NMR spectrum of aluminum isopropoxide shows that the dominant feature in precursor is 6-coordinated Al-O, which is indicated by the 0ppm peak. The NMR spectra of SiAlCN-10 at 350°C and 600°C confirm that the complete reaction between aluminum isopropoxide and Ceraset, because no aluminum isopropoxide is left. According to the results of FT-IR and MS, Al-N bonds should be dominant, although a small amount of Al-O cannot be avoided²⁰⁶. This is also the reason that the addition of aluminum isopropoxide does not significantly change the oxygen content in the final ceramics when comparing with SiCN ceramics without Al-doping. At 800 °C, the new peak (8ppm) corresponding to six-coordinated Al appears; meanwhile, the intensity of the peak at 51ppm decreases. Just as it is aforementioned, the structural rearrangement occurred at the

temperatures higher than 800°C. At the temperature of 1200°C, the ^{27}Al NMR shows an increase of 5-coordinated Al at the expense of 4-coordinated Al. This demonstrates the structural rearrangement at this temperature, which is confirmed by ^{29}Si NMR at 1200°C. At the temperature of 1400°C, the peak for 4-coordinate Al appears again while that for 6-coordinated Al peak remains. At the temperature of 1500°C, both peaks are divided into two peaks, indicating Al atoms exist in two different environments. It is believed that the structure is rearranging so that it is ready for the crystallization. Some aluminum is still in the amorphous matrix, and the other is in the highly ordered phase. This distribution will affect the crystallization behavior of Si-Al-C-N, which will be discussed later.

It is also noticed that at temperatures higher than 800°C, 6-coordinated Al appears and SiCN_3 also becomes dominant in the ^{29}Si NMR spectra (Figure 15). Up to the temperature of 1400°C, 6-coordinated Al is always there and SiCN_3 becomes stronger with increasing temperature. According to NMR spectra, SiCN_3 appears accompanying with AlN_6 , the structure of SiAlCN ceramics can be deduced and shown in (Figure 16).

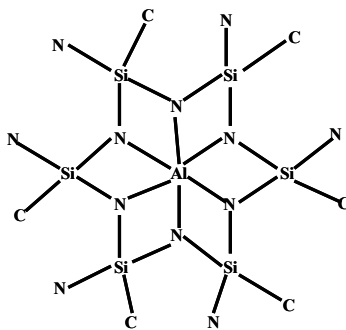


Figure 16: The Schematic Structure of SiAlCN ceramics.

The effect of Al-content on the structures of the amorphous ceramics was characterized by using solid-state NMR. At different temperatures, this effect is similar, so only ^{29}Si NMR

spectra of the ceramics treated at 1000°C is shown here as an example (Figure 17). The significant effect of Al-content on the structure of amorphous ceramics is evident from the spectra. While the SiC_2N_2 unit (-20 ppm) is the major building block for the ceramic synthesized from pure Ceraset, the material also contains significant amount of SiC_3N (0 ppm) and SiCN_3 (-38 ppm) units. When Al is added, the amount of SiC_3N units significantly decreases, but the amount of SiCN_3 unit increases at the expense of SiC_3N and SiC_2N_2 . With increasing Al-content, more SiC_3N and SiC_2N_2 transform to SiCN_3 . For ceramics synthesized from SiAlCN-20, SiCN_3 units become dominant. This can be understood according to the structure described in Figure 16: the more aluminum, the more the SiCN_3 units required. It is noticed that the crystallization temperature is increased from 1400°C for SiCN to 1600°C for SiAlCN-20. It is believed that this is due to the increase of SiCN_3 , which can be stable to higher temperatures to prevent the material from crystallizing.

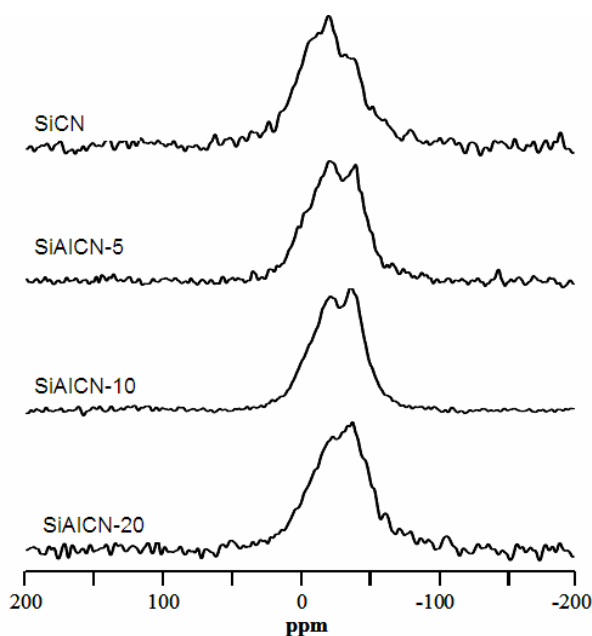


Figure 17: ^{29}Si solid-state NMR spectra of the ceramics obtained at 1000 °C from pure Ceraset (SiCN), CER-5Als (SiAlCN-5), CER-10Als (SiAlCN-10), and CER-20Als (SiAlCN-20).

3.2.2 The crystallization behavior of Si-Al-C-N ceramics

From the results of XRD investigation (Figure 18), all SiCN and SiAlCN ceramics are amorphous after heat-treated at the temperature of 1400°C. After annealed at 1500 °C, SiCN, SiAlCN-5, and SiAlCN-10 begin to crystallize, but SiAlCN-20 still remains amorphous. After being heat-treated at 1600°C in the N₂ atmosphere, all samples (SiCN, SiAlCN-5, SiAlCN-10Al, and SiAlCN-20) become crystallized. It is also interesting to note that the crystallization phases are both α -Si₃N₄ and β -Si₃N₄ for the SiCN, but the crystalline phase is only β -Si₃N₄ for SiAlCN-20. It is indicated the aluminum affects the crystallization behavior of SiCN ceramics.

Figure 19 shows the TEM results of SiAlCN-10 post-pyrolyzed at 1400°C. Most of the area is amorphous (Region 1 in Figure 19), but some local (Region 2 in Figure 19) area is crystallized. The crystallines include turbostratic carbon and another phase, most likely the (100) face of Si₃N₄. However, from the information of XRD and NMR, the signal for Si₃N₄ crystal phase is very weak. It is possible that the crystalline phases are too small to be detected.

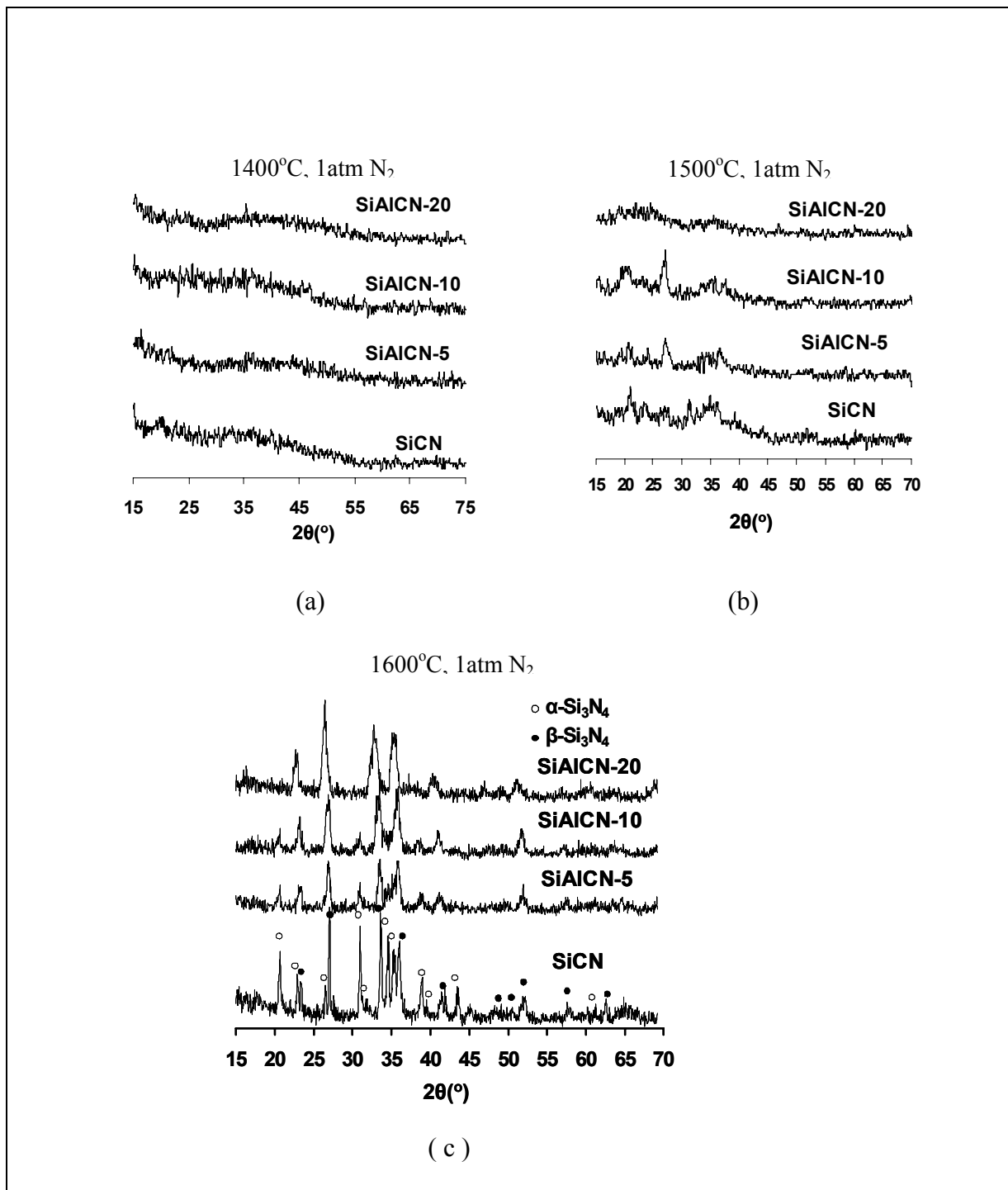
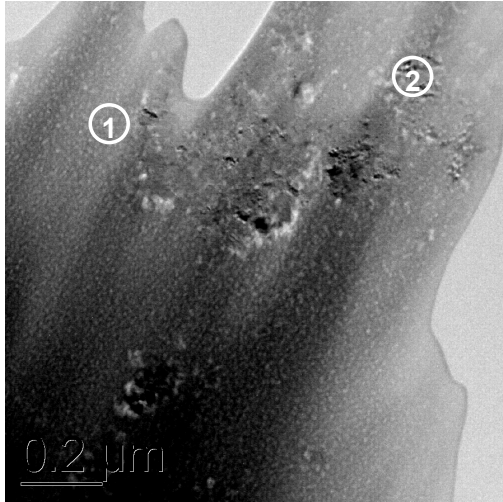


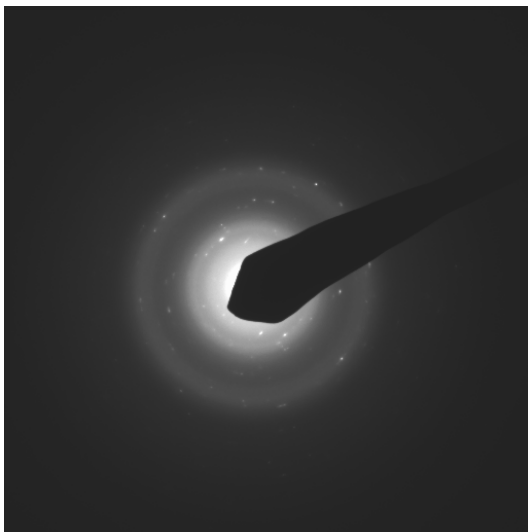
Figure 18: XRD of SiCN, SiAlCN-5, SiAlCN-10, and SiAlCN-20 at (a) 1400°C, (b) 1500°C, and (c) 1600°C.



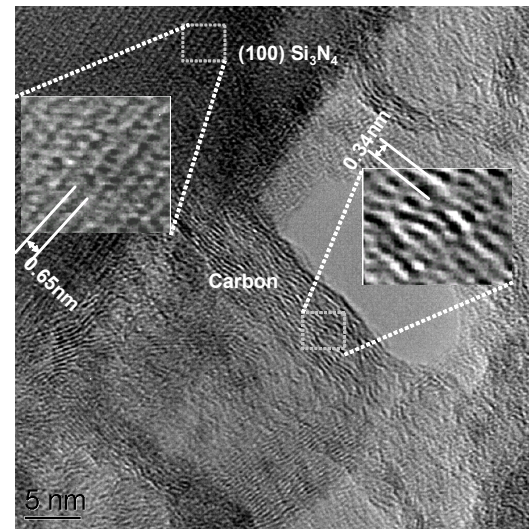
(a)



(b)



(c)



(d)

Figure 19: TEM results of SiAlCN-10 heat-treated at 1400⁰C. (a) The morphology of the SiAlCN-10 sample; (b) diffraction pattern for region 1; (c) diffraction pattern for region 2; (d) HRTEM for region 2, showing some crystallines.

The ideal crystal structure of α -, and β - Si_3N_4 was proposed by Hardie and Jack²⁰⁷, and Popper and Ruddlesden²⁰⁸. In both forms, the basic building unit is the Si-N tetrahedron in which a silicon atom lies at the center with nitrogen atom at each corner. The SiN_4 tetrahedrons are joined each other by sharing corners in such a way that the each nitrogen atom is common to three SiN_4 . The structures can be visualized as the stack of puckered Si-N layers (Figure 20). The ideal structure of silicon nitride can be described as a stacking of ABCDABCD... sequence for α - Si_3N_4 , or ABAB... sequence for β - Si_3N_4 .

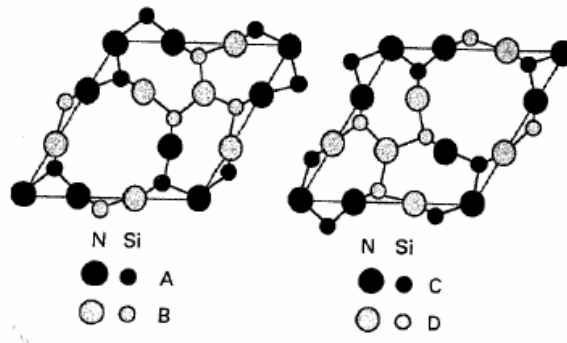


Figure 20: The idealized Si-N layers in α -, and β - Si_3N_4 structure^{207, 208}.

While β -phase is the thermally stable phase, the formation of the two phases is controlled by formation mechanism, rather than by thermodynamic consideration²⁰⁹. Formation of α - Si_3N_4 is favored by presentation of oxygen during silicon nitridation²¹⁰. β - Si_3N_4 would rather be the form when liquid exists²¹¹. According to previous works and our study, the SiCN ceramics contain oxygen^{4, 212}. Oxygen can stable the α -phase during crystallization^{213, 214}. For the Si-Al-C-N ceramics, we do not agree that the presence of liquid phase is responsible for the fully crystallized β -phase for two reasons: First, according to ²⁷Al NMR (Figure 15b), most Al bonds

with N, suggesting there is no liquid phase present in this system. Second, the particle size of β - Si_3N_4 in SiAlCN-20 ceramics is smaller than that in SiCN ceramics, evident by the broader peaks shown in Figure 18. It is more likely the β - Si_3N_4 is obtained by directly pyrolysis of SiCN₃ units ($\text{SiCN}_3 \rightarrow \text{Si}_3\text{N}_4 + \text{C}$) rather than liquid phase based nucleation-growth. Consequently, we propose that the formation of β - Si_3N_4 phase is only due to aluminum dissolute in the Si_3N_4 structure during crystallization. From the structure proposed in Figure 16, it is believed that aluminum evolved in Si_3N_4 structure during decomposition of SiCN₃ units. The aforementioned ²⁷Al NMR at 1500°C also suggests that some aluminum dissolves in the crystalline phase. Furthermore, from the lattice constants (listed in Table 2) calculated from XRD pattern (Figure 18 c), it is noted that with the aluminum content increases, the lattice constants for β - Si_3N_4 also increase, while the lattice constants of α - Si_3N_4 keep almost the same. It is believed that the expansion of lattice constant is due to the dissolution of aluminum in the Si_3N_4 structure. The same phenomenon was also observed by others during sintering Si_3N_4 ceramics²¹⁵.

Table 2: The lattice constants of Si_3N_4 calculated from XRD pattern.

α		SiCN	SiAlCN-5	SiAlCN-10	SiAlCN-20
β - Si_3N_4	a=b (nm)	0.7620	0.7648	0.7662	0.77903
	c (nm)	0.2918	0.2921	0.2925	0.2994
α - Si_3N_4	a=b (nm)	0.7794	0.7816	0.7816	-
	c (nm)	0.5573	0.5563	0.5563	-

3.3 Summary

In this section, the detailed procedure to fabricate SiCN and SiAlCN ceramics are stated. The structural evolution during the pyrolysis is discussed by analyzing FT-IR and NMR spectra. The structural evolution during post-pyrolysis annealing is studied by using NMR, XRD, and TEM. The effect of different aluminum content on the material structures is indicated: more aluminum results in more SiCN₃ structural unit. The high content of SiCN₃ structural unit is the reason for structural stability to resist crystallizing. The effect of aluminum on the crystallization phases is also discussed.

CHAPTER FOUR: OXIDATION BEHAVIOR OF POLYMER DERIVED SiCN AND SiAlCN CERAMICS

The aim of this chapter is to study the oxidation behaviors of SiAlCN ceramics in both a low temperature region (Oxide scales are amorphous) and a high temperature region (Oxide scales are crystalline). In comparison, the oxidation behaviors of SiCN ceramics are also studied in both temperature regions. In both cases, the oxidation kinetics is determined by measuring the thickness of oxide scales as a function of the temperature. The structures of the oxide scales are studied by XRD and solid state NMR. The experiment of $^{18}\text{O}_2$ tracer diffusing through the oxide scales is carried out to understand the oxidation mechanism. A physical model of the oxide structure is advanced to account for the oxidation behavior of polymer derived SiAlCN ceramics.

4.1 Experimental procedures

4.1.1 Oxidation experiments for SiCN and SiAlCN bulk ceramics

Fully dense SiCN and SiAlCN specimens are used in the oxidation experiments. The procedure for preparing these specimens was described in section 3.1.1.

Before oxidation, the samples are treated at different temperatures to stabilize the structure. For oxidation at temperatures equal to or less than 1200°C , the samples are heat-treated

at 1220°C for 5 hours. For oxidation at the temperature of 1400°C, the samples are heat-treated at 1420°C for 5 hours.

After heat-treatment, and prior to oxidation, one side of the samples is polished to 0.5µm finish. The samples are first mounted on a holder using wax. The samples are then ground on the 30µm lapping film followed by polishing them from 15µm down to 0.5µm by using diamond lapping films (Allied High Tech Products Inc., CA, USA). These polished samples are then cleaned in acetone by using an ultrasonic cleaner (Fisher Scientific, USA) for about 10 minutes to remove any contamination on the samples during polishing and handling.

After polishing, the oxidation process is carried out in the air at different temperatures including: 900°C, 1000°C, 1100°C, 1200°C, and 1400°C for 20, 50, 100, and 200 hours in the high-temperature tube furnaces.

For oxidation at temperatures equal to or less than 1200°C, the SiCN and SiAlCN samples are loaded in a high purity quartz tube with polished surface up. The oxidation experiments are carried out in an auto-programmable Thermolyne alumina tube furnace (Barnsted/Thermolyne, Texas). The quartz tube is used to avoid any contamination from the alumina working tube. The furnace is then programmed to reach the desired temperature with a rate of 25°C/min and is held there for a certain time.

For oxidation at 1400°C, the SiCN and SiAlCN samples are loaded in alumina crucibles, and the experiments are performed in a Thermolyne alumina tube furnace (F54500, Barnsted/Thermolyne, Texas). Here, the quartz tube is not used because it will crystallize at 1400°C in the air. The furnace is programmed to reach 1400°C with a rate of 20°C/min and held at the temperature for different times.

After oxidation, the polished surface of the SiCN and SiAlCN samples are coated with chromium of about 400-500nm in thickness using the Precision Etching Coating System (PECS) (Gatan Inc., USA) to protect the oxide surface. After coating Cr, a thin glass slide is bound to the surface with Epoxybond 110TM (Allied High Tech Inc., CA, USA) to protect the soft chromium metal from damage during cross-section polishing. The cross-section of the sample is polished with the diamond lapping film down to 0.5 μ m. The polishing process is the same as described above. After polishing, the cross-section of the sample is etched by Buffered Oxide Etchants (BOE). It gives very clear interface between the substrate and the oxide. The thickness of the oxide layer is then measured using SEM.

4.1.2 Characterization of oxide structure

In order to understand the oxidation mechanism, the structure of the oxide scale is characterized using solid state NMR and XRD. Powder samples are used for these characterizations. The SiCN and SiAlCN ceramic powders are prepared according to section 3.1.1. These powders are oxidized using the same conditions as that for oxidizing the bulk specimens, which were described in the section 4.1.1. The sample preparation and experimental process for XRD and solid state NMR are the same as described in section 3.1.2.

4.1.3 ¹⁸O₂ diffusion in the oxide produced by oxidation of SiCN and SiAlCN ceramics

In order to further understand the oxidation behavior of the SiCN and SiAlCN ceramics, ¹⁶O₂-¹⁸O₂ double diffusion experiments are carried out on SiCN and SiAlCN-10 specimens. The polished samples are put in the quartz tubes and oxidized at 1200 °C for 200 hours. The detailed

oxidation procedure is described in the section 4.1.1. The oxide scales obtained are cleaned using the following steps: (1) rinse in distilled water, (2) rinse in acetone with ultrasonic agitation, (3) repeat step 1, (4) rinse in methanol with ultrasonic agitation, (5) repeat step 1, and (6) dry the surface by compressed air.

The isotope gas used is a mixture of an ^{18}O and N_2 (Isotech Inc. OH, USA). The composition of the mixture is $^{18}\text{O}_2:\text{N}_2= 1:4$, close to the oxygen concentration in the air. A schematic diagram of the annealing apparatus is shown in Figure 21. The apparatus is constructed of a long quartz tube (Technical Glass Products Inc) in an alumina tubing furnace. Both ends of the quartz tube are sealed by plugs. Samples rest on a fused quartz tube inside the long quartz tube. The diffusion experiments are conducted under a pressure of 1 atm.

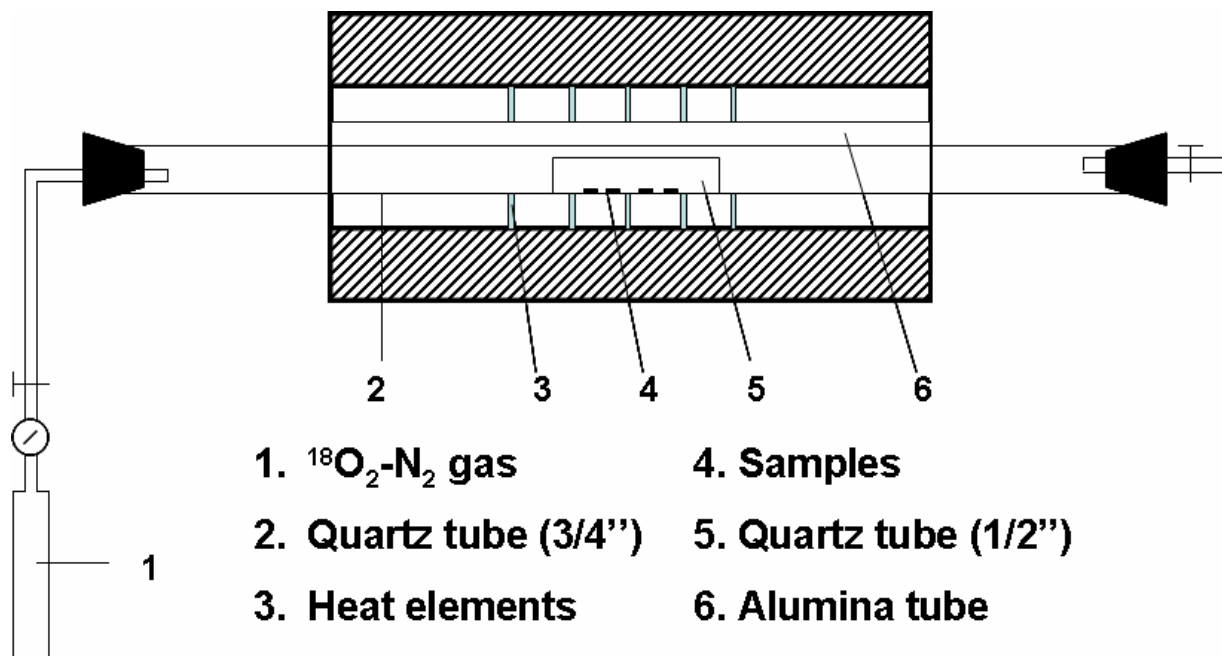


Figure 21: Schematic diagram of annealing apparatus for ^{18}O tracer diffusion.

The experiments are carried out in the temperature range between 1050°C and 1150°C for 3 to 15 hours. Before introducing the isotope gas in the system, the long quartz tube is vacuumed by a mechanical pump for at least 10 minutes. The furnace is then heated to the desired temperature at a rate of 20°C/min. When the temperature reaches the set-point, the system is heated for another 20 minutes before introducing the isotope gas to stabilize the system. Then, the isotope gas is introduced into the quartz tube. After annealing for a desired time, the isotope gas is stopped and the system is cooling down as soon as possible to minimize the effect of the cooling period on the diffusion. Usually, the temperature can drop more than 100 °C within the first two minutes.

After annealing, the samples are analyzed using a Secondary Ion Mass Spectrometer (SIMS) (Adept 1010, Physical Electronics) to obtain ^{18}O depth profiles using a 3.0-kV Cs^+ beam of 30 nA beam current rastered over a $250\ \mu\text{m}^2$. Data are collected from the central $25\ \mu\text{m}^2$ region. The depth of the sputtered crater is measured using a profilometer with an accuracy of 10%. Sputter time is converted to depth by assuming a constant sputter rate. Sputtering rates were experimentally determined for each sample and ranged from 0.05 to 0.117 nm/s. The total instrumental broadening associated with the SIMS is assumed to be a Gaussian function and the full width at half maximum (FWHM) is approximately 10 nm.

4.2 Oxidation at the temperatures lower than 1200°C

4.2.1. Results

The oxide scales were examined using SEM and XRD. XRD was performed on powder samples. The results revealed that all oxide scales are amorphous, dense, and free of bubbles or cracks regardless of oxidation conditions and substrate materials. Figure 22 is a typical SEM micrograph showing the cross-section of an oxidized specimen. Figure 23 gives typical XRD patterns of oxidized powders, revealing amorphous nature of the oxide scales.

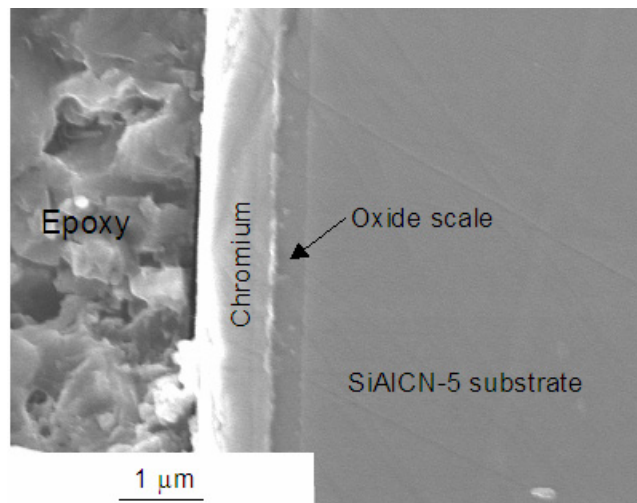


Figure 22: SEM micrograph showing the morphology of the cross-section of the SiAlCN-5 oxidized at 1100 °C for 20 hours.

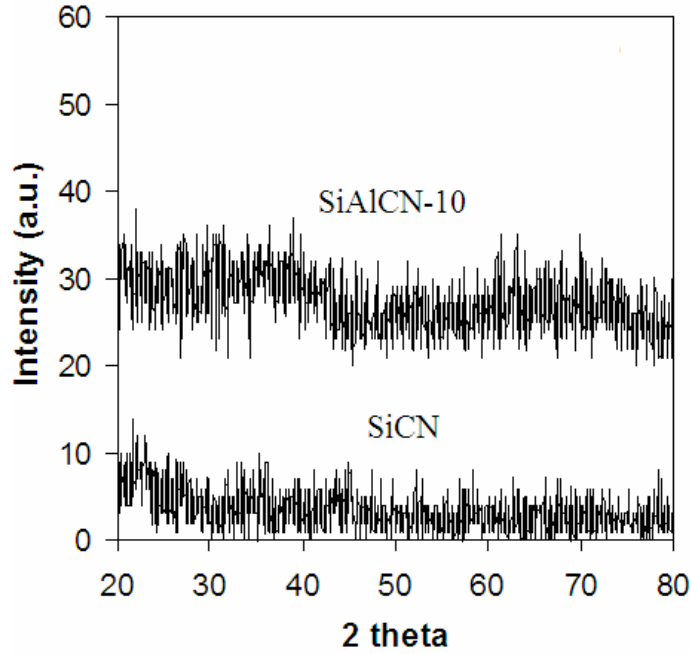


Figure 23: XRD patterns of SiAlCN-10 (top) and SiCN (bottom) oxidized at 1200 °C for 200 hours.

Figure 24 plots the square of the thickness of the oxide scales as a function of annealing time for the SiCN and SiAlCN ceramics at different temperatures. The slope of the curve in such a plot is corresponding to a parabolic rate constant according to the following equation:

$$h^2 = k_p t \quad (4-1)$$

where h is the thickness of oxide scale, t oxidation time, and k_p the parabolic rate constant. Several features can be seen from Figure 24. At 900 °C, all three materials follow typical parabolic oxidation kinetics - linear dependence of h^2 on annealing time t . At this temperature, the oxidation rate constants measured for three materials are comparable to each other (Table 3). At higher temperatures (1000°C–1200°C), the oxidation of the SiCN ceramics still follows parabolic behavior. However, the two SiAlCN ceramics show a decrease in the oxidation rates

with annealing time. For the SiAlCN ceramics, the oxidation curve can be divided into three regions: the initial stage, the transition stage where oxidation rate decreases, and the steady stage where the oxidation rate becomes constant at low level. The oxidation rates of the initial stage (the first 50-hours for 1000 and 1100 °C, and the first 20 hours data for 1200 °C) are close to that of the SiCN (Table 3). Also, the oxidation rates for SiAlCN ceramics after the initial stage are calculated and listed in Table 4. For samples oxidized at 1200 °C, the steady stage oxidation rates for the SiAlCN-5 and SiAlCN-10 are calculated using last 100-hours data to be 0.3×10^{-18} and 0.025×10^{-18} m²/sec, respectively. These oxidation rates of the SiAlCN-5 and SiAlCN-10 are about 20 and 200 times lower than that of the SiCN (4.8×10^{-18} m²/sec), respectively. The long-term oxidation rate of the SiAlCN-10 is even an order of magnitude lower than the lowest data measured from CVD SiC (0.55×10^{-18} m²/sec) and Si₃N₄ (0.22×10^{-18} m²/sec) obtained at similar conditions. For samples oxidized at 1000°C and 1100 °C, it seems that the steady stage was not fully reached since the oxidation rate calculated by using the last 100-hours data is still higher than that obtained from samples oxidized at 1200 °C.

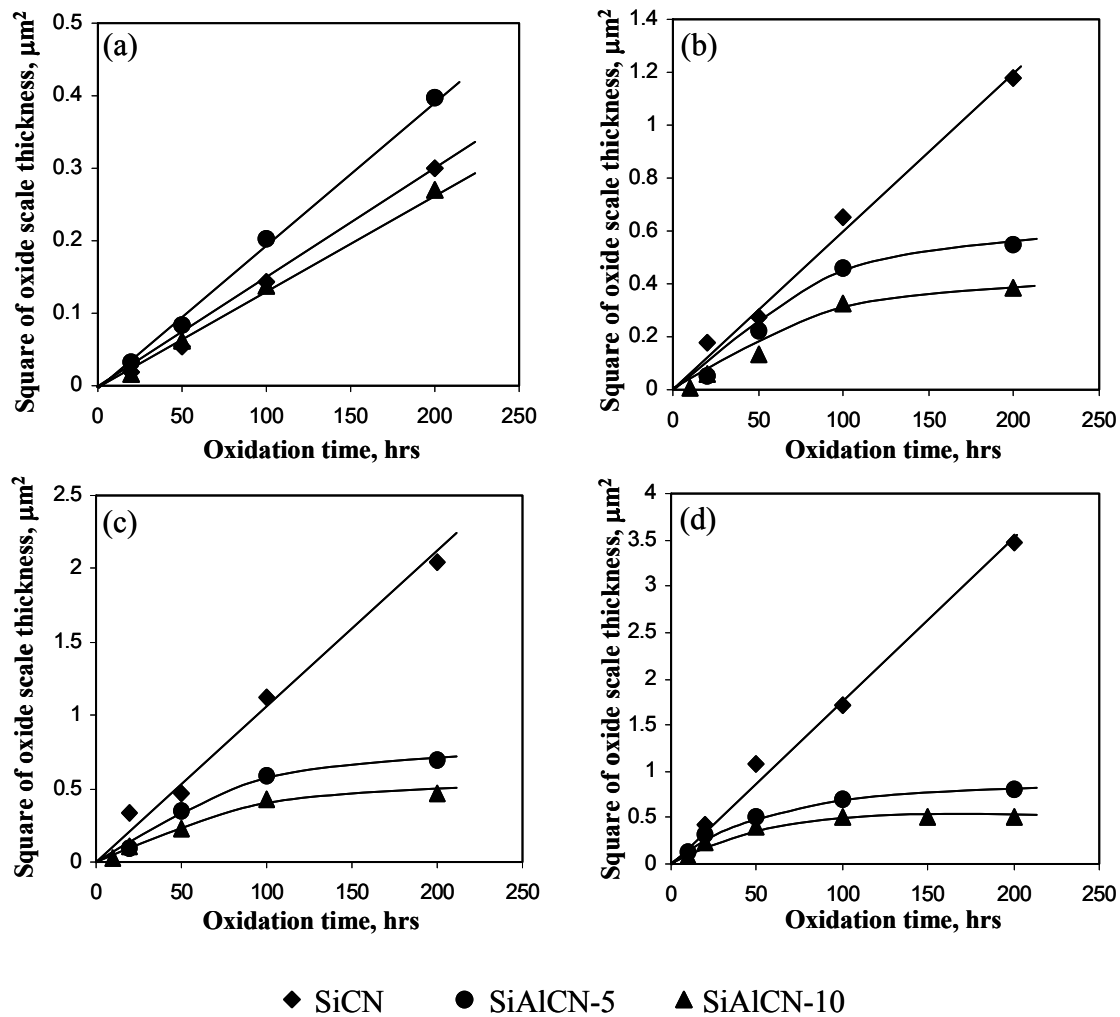


Figure 24: Plots of the square of the oxide scale thickness as a function of annealing times for the SiCN, SiAlCN-5 and SiAlCN-10 at temperatures (a) 900, (b) 1000, (c) 1100 and (d) 1200 °C.

Table 3: Parabolic rate constants and activation energies for the SiCN ceramics and SiAlCN ceramics at the initial oxidation stage.

Materials	Parabolic rate constants ($\times 10^{18} \text{ m}^2/\text{sec}$)				Activation energy (KJ/mole)
	900 °C	1000 °C	1100 °C	1200 °C	
SiCN	0.39	1.3	2.8	4.8	120
SiAlCN-5	0.56	1.2	2.3	5.3	115
SiAlCN-10	0.39	0.98	1.6	3.9	115

Table 4: Parabolic rate constants and activation energies for the SiCN ceramics and SiAlCN ceramics after the initial oxidation stage

Materials	Parabolic rate constants ($\times 10^{18} \text{ m}^2/\text{sec}$)				
	SiCN	SiAlCN-5	SiAlCN-10	SiC	Si ₃ N ₄
1200 °C	4.8	0.30	0.025	0.55	0.22

The apparent activation energy of the oxidation can be calculated from the rate constants measured at the different temperatures using Arrhenius equation:

$$k_p = A_o \exp\left(-\frac{Q_A}{RT}\right) \quad (4-2)$$

where Q_A is the oxidation activation energy. Figure 25 plots the $\ln(k_p)$ as a function of reciprocal temperature (the earlier-stage data listed in Table 3 are used for the SiAlCN ceramics). It can be

seen that fairly good linear relationships are obtained for all three materials. The activation energies calculated for all three materials are very close to each other (Table 3), and are also similar to that of high purity SiC (such as CVD and single crystal SiC) and single crystal silicon, but much less than that of CVD silicon nitride^{136, 216}. This suggests that at low temperature or high temperature short-term, the oxidation of the SiAlCN ceramics follows the same mechanism as the SiCN, which is similar to that of SiC oxidation.

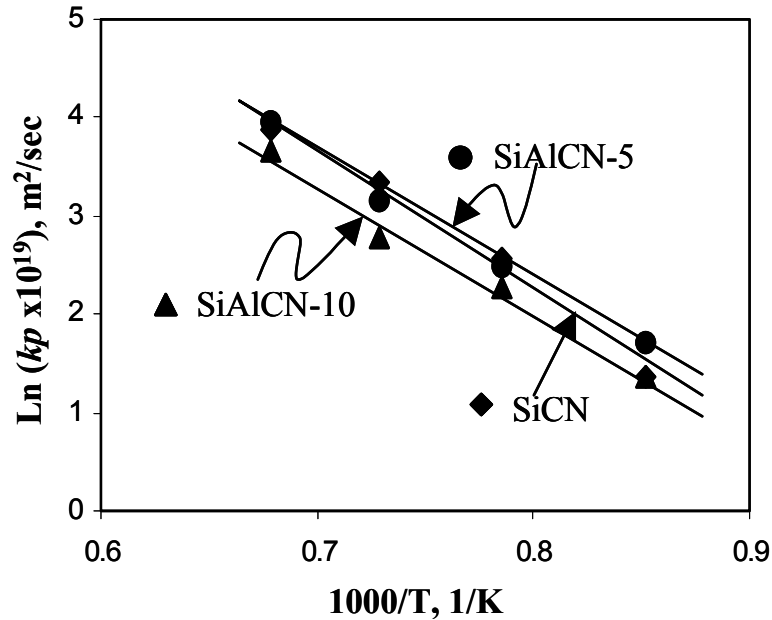


Figure 25: Plot of log parabolic rate constants as a function of reciprocal of temperature for SiCN, SiAlCN-5 and SiAlCN-10. The rate constants of SiAlCN-5 and SiAlCN-10 for temperatures higher than 1000 °C were calculated using initial stage data.

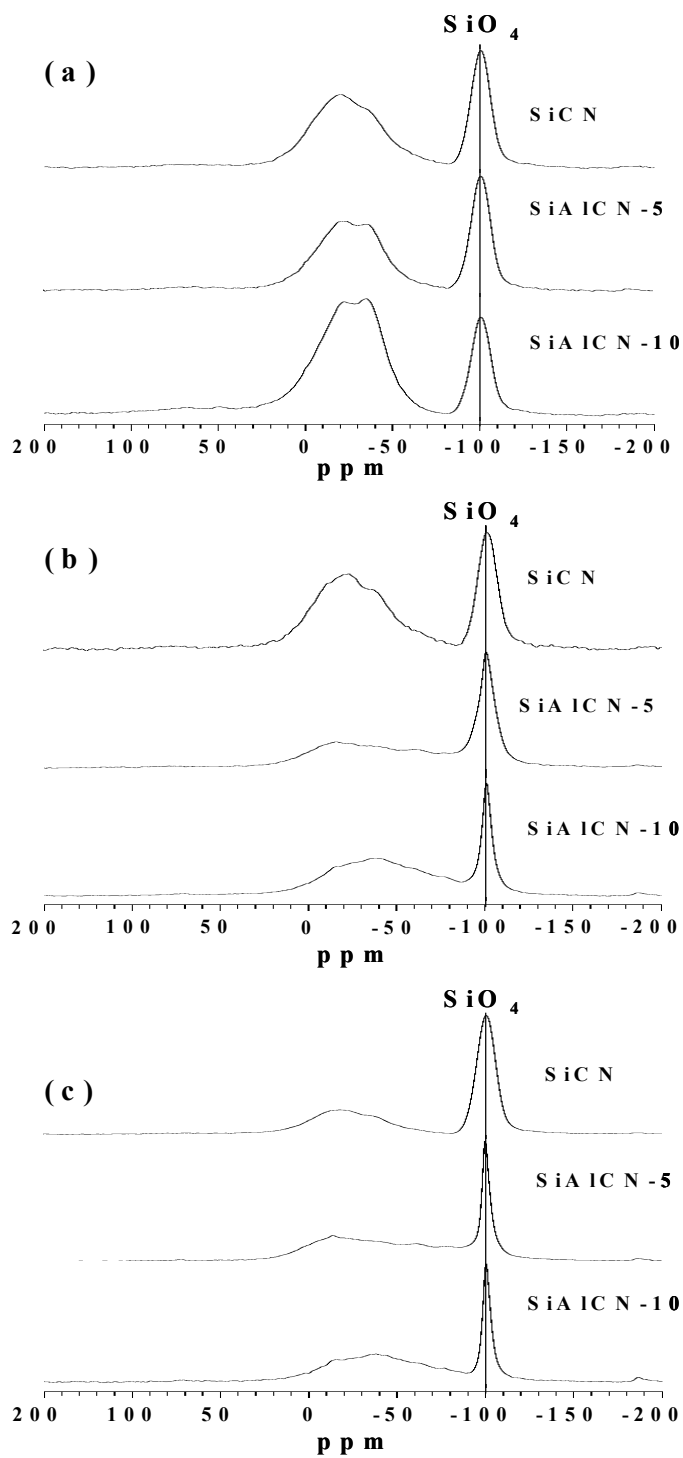


Figure 26: ^{29}Si NMR spectra of the SiCN and SiAlCNs oxidized at (a) 900 °C x 50 hours, (b) 1200 °C x 20 hours and (c) 1200 °C x 200 hours.

Figure 26 shows ^{29}Si spectra of SiCN and SiAlCN ceramics oxidized at different conditions. The signals between 0-75 ppm result from the un-oxidized substrates. The spectra suggest that at 900°C, a significant amount of SiCN and SiAlCN substrates remain un-oxidized after 50 hours of annealing; while at 1200°C, most of substrates were oxidized. This is consistent with the oxide scale thickness measurement. The strong signal centered at -100 ppm is assigned to SiO_4 tetrahedral²¹⁷, formed by oxidation. The position of this signal remains unchanged for all samples, which suggests the aluminum atoms are not incorporated into the SiO_2 network^{218, 219}. Furthermore, the similarity between the shape of the signals from SiCN ceramics oxidized at all conditions and that of the SiAlCN ceramics oxidized at 900°C suggests that their SiO_2 network structures are similar to each other. However, at 1200°C the signals from SiAlCN ceramic specimens become sharper with increasing time, suggesting that the SiO_2 structures become more order. The results also suggest that the structures of the SiO_2 scale formed on SiAlCN ceramics are rearranged over time at higher oxidation temperatures.

4.2.2. Discussion

As described earlier, polymer-derived SiAlCN ceramics exhibited unique oxidation behaviors, including: (i) the oxidation rate decreases with annealing time, (ii) the steady stage oxidation rate measured for SiAlCN-10 at 1200 °C is about 10 times lower than the lowest reported values for CVD SiC and Si_3N_4 under similar conditions, and (iii) the oxidation rate decreases with increasing aluminum content. Here, we would like to emphasize that the decrease in oxidation rates with time observed in SiAlCN ceramics is not the same as that observed in porous materials through weight change measurement^{106, 173}. In porous materials, the decrease in

weight gain is due to pore sealing and can only be measured by weight change. In the contrast, the oxidation rates shown in Figure 24 were obtained by directly measuring the thickness of oxide scale.

The oxidation rate of silicon-based materials is controlled by oxygen diffusion through oxide layer (under the current condition, temperatures ≤ 1200 °C, oxygen diffusion occurs by interstitial transportation of oxygen molecules)^{136, 216}, which leads to parabolic kinetics. For silicon and silicon carbide, the oxide scale comprises of a single layer of SiO₂; while for silicon nitride, a bi-layer scale structure consisting of SiO₂ outer-layer and Si₂N₂O middle-layer between the SiO₂ layer and the substrate was observed²²⁰. Since the oxynitride layer has a lower permeability to oxygen comparing with SiO₂ and acts as a diffusion barrier^{220, 156}, silicon nitride has lower oxidation rate and higher activation energy. However, the theory of the silicon oxynitride layer is not applicable to the SiAlCN ceramics for three reasons. First, the oxynitride layer was not observed in the oxide scales; second, the oxidation rate of the SiAlCN is even much lower than that for Si₃N₄; and third the undoped SiCN exhibits oxidation behavior similar to that of SiC.

A possible explanation for the decrease in the oxidation rate of SiAlCN ceramics is that aluminum atoms modified the network structure of the oxide scale. To understand this mechanism, it is important to review the current understanding of silica network structure and oxygen diffusion within it. The structure of amorphous silica can be characterized by connected rings comprising of SiO₄ tetrahedral²²¹, which gives a medium-range ordering to the material. Raman spectrum studies^{222, 223, 224} indicated that the majority of these rings are 6-membered or higher, only a few percentages of them are three or four-membered. A previous study²²⁵ revealed

that the calculated activation energy of oxygen molecules pass through 6-membered rings was comparable to that measured for the oxidation of silicon/silicon carbide. These results suggest that the 6-membered rings are the barriers for the diffusion of oxygen molecules in amorphous silica. Among all simple oxides, SiO₂ possesses lowest oxygen permeability²²⁶. The presence of impurities usually damages the network structure of the SiO₂ and results in the increase in oxygen diffusion and higher oxidation rates^{136, 216} by providing easier diffusion path.

The XRD study indicates that all oxide scales in this study are amorphous. The ²⁹Si NMR results (Figure 26) suggest that the oxide scale formed on the surface of the SiAlCN samples becomes more orderly with annealing time (the signal corresponding to SiO₄ sharpened with time). Here we argue that the ordering of the oxide scale cannot cause the decrease in oxygen diffusion. The ordering can decrease the diffusion by decreasing the average free volume only when the diffusion is controlled by the free volume mechanism. In case of oxygen molecules diffusing through interstitials of silica glass, the barrier is the 6-membered SiO₄ rings. The size of these rings should not be changed (at least not significantly) with ordering, thus oxygen transportation should not be affected. We can even extend this argument to crystalline silica, in which interstitial oxygen molecule diffusion should not be much different from that in amorphous form since in both cases it is the 6-membered rings that controlled the diffusion. Recently, Ramberg and Worrell experimentally demonstrated that there is no difference between the rates of interstitial oxygen transport in amorphous SiO₂ and in β-cristobalite. This point is very important for the oxidation behavior of SiCN ceramics and SiAlCN ceramics, which will be described in the next section.

Hereby, it is proposed that the oxide scale formed on the SiAlCN ceramics has a unique network structure, namely aluminum atoms (at least part of them) sit in the center of the 6-membered rings (Figure 27). These aluminum atoms block the path of oxygen diffusion so that oxygen molecules have to take longer transportation path, leading to lower oxidation rate for SiAlCN ceramics. While the aluminum content is relatively low (ratio of Al to Si is 0.02 and 0.04 for SiAlCN-5 and SiAlCN-10, respectively), the number of the blocked rings may not reach the percolation values. It is further proposed that the unique network structure of Al-blocking 6-membered Si-O rings is formed gradually with time through structural rearrangement, as evidenced in the NMR spectra (Figure 26). The rearrangement requires high temperature and time for the kinetic reason. At 900 °C or initial stage of higher-temperatures, the rearrangement did not occur or just began due to the low temperature or shorter time, thus the oxidation of the SiAlCN ceramics is similar to that for the SiCN. At higher temperatures, the structural rearrangement leads to the decrease in oxidation rate. This model can also easily explain the fact that the oxidation rates decrease with increasing aluminum content since more rings are blocked. More evidence to support this model will be discussed in section 4-4.

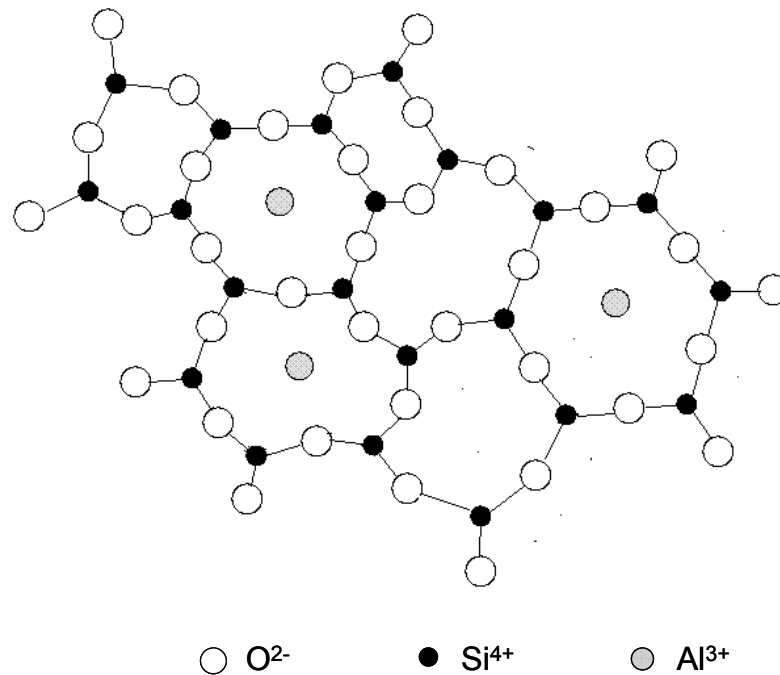


Figure 27: Two-dimensional schematic showing the proposed structure of silica oxide scale, in which aluminum atoms sit in the center of the 6-membered rings of Si-O to block the diffusion of oxygen.

Here, the proposed model will be compared with other Al-containing Si-based ceramics. The decrease in oxidation rate with time has also been observed previously in sialon ceramics at the temperature range of 1400-1600 °C^{182, 227}. The authors attributed this to the formation of fused silica layer containing octahedral Al. However, the reason that octahedral Al can slow the oxidation was not discussed. It is possible that these aluminum atoms also sit in the center of 6-membered SiO₄ rings. Oxidation behavior of polymer-derived ceramics SiBCNAl ceramics has been reported recently^{228, 229}. These studies revealed that compared to aluminum-free SiBCN ceramics, aluminum-containing SiBCNAl ceramics exhibited a slightly higher oxidation rate; but

aluminum did help to improve the oxide scale quality in terms of adhesion, cracking, bubble formation and crystallization. Compared to our materials, these previously studied materials contain boron and higher Al-to-Si ratios. This could be the reason why improved oxidation resistance was not observed in these SiBCNAl materials.

4.3 Oxidation at the temperature of 1400°C

SEM observations of the oxide scales reveals that all oxide scales are dense and free of bubbles or cracks, regardless of oxidation conditions and substrate materials. Figure 28 shows a typical SEM micrograph showing the cross-section of an oxidized specimen.

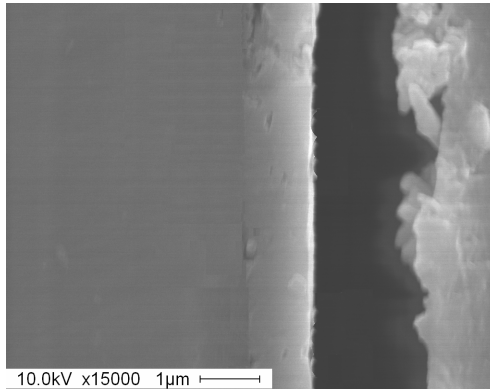


Figure 28: SEM morphology of cross-section of oxide scale for SiAlCN-10 ceramics oxidized at 1400°C for 20 hours.

Figure 29 plots the square of the thickness of the oxide scale (h^2) as a function of oxidation time t . It can be seen that the SiCN obeys the typical parabolic kinetics (linear relationship between h^2 and t). While the linear dependences of h^2 on t are also observed for

three SiAlCNs, the extrapolations of the lines have positive intercepts with the y-axis. This indicates that the oxidation rates of the SiAlCNs are much higher at the short-term than in the long-term. Similar oxidation behavior has also been observed for SiAlCNs at lower temperatures where the oxide scale was amorphous, and was attributed to the rearrangement of aluminum in the oxide scale that led to the decrease in oxidation rates.

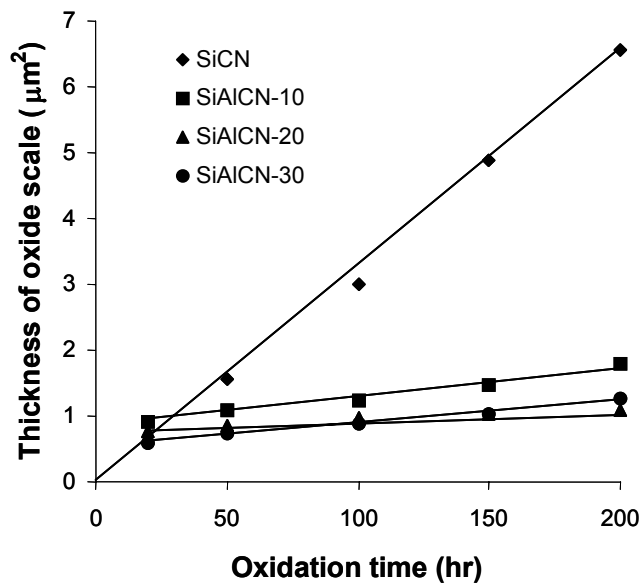


Figure 29: The Square of oxide scale thickness as a function of oxidation time.

The parabolic rate constants, k_p , can be measured from the slope of the lines presented in Figure 29 according to the Eq 4-1. The measured parabolic rate constants are summarized in Figure 30 together with those for various silicon-based materials. The data for SiC and Si₃N₄ are those measured from the high-purity materials and represent the lowest values for the corresponding materials^{141, 148, 152, 153, 154, 178, 179, 230, 231, 232}. The data for the SiCN/SiAlCN at lower temperatures (≤ 1200 °C) are taken from Chapter 4-2. It can be seen clearly that while SiCN

behaves very similar to pure SiC, SiAlCNs exhibit lower oxidation rates than all other silicon-based ceramics. It should also be noted that the oxidation rates of the SiAlCNs strongly depend on the aluminum content. SiAlCN-20, in which the ratio of Si to Al is 1:0.08, shows the lowest oxidation rate, which is more than an order of magnitude lower than those for all other silicon-based ceramics.

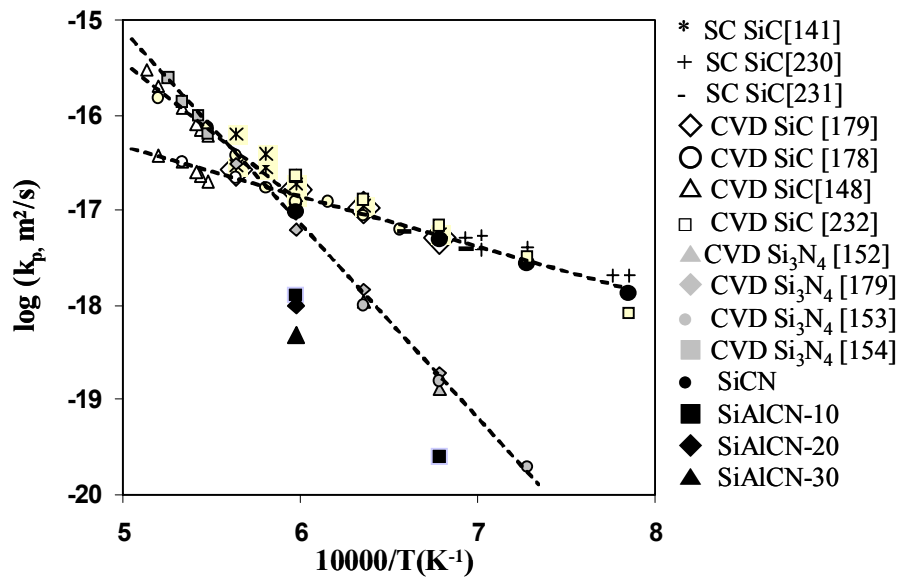


Figure 30: Comparison of oxidation rate constants for different silicon-based ceramics (SC: single crystal).

In order to understand the oxidation behavior of SiCN/SiAlCNs, their oxide scales were characterized using XRD (Figure 31). Different with those obtained at lower temperatures (Figure 23), the oxide scales obtained at the present temperature consist of crystalline phases, similar to what was observed for SiC and Si₃N₄^{148, 154}. Within the accuracy of our XRD, it is estimated that the oxide scales are fully crystallized without residual amorphous phases. It is

clear that the aluminum content has a strong effect on the formation of crystalline phases. For the SiCN and SiAlCN-10 the oxide scales consist of cristobalite only; for the SiAlCN-30 the oxide scale consists of mullite in addition to a major cristobalite phase; and the oxide scale of the SiAlCN-20 also consists of a slight amount of mullite. The lattice constants of the cristobalite are calculated from the XRD patterns and listed in Table 5. The lattice constants of the cristobalite increase with increasing aluminum content at the beginning, suggesting that aluminum has dissolved into the cristobalite. Further increases in the aluminum content (SiAlCN-30) leads to the decrease in the lattice parameters. This is possibly because of the formation of the mullite, which extracts aluminum from the cristobalite to decrease the solution of aluminum in the latter.

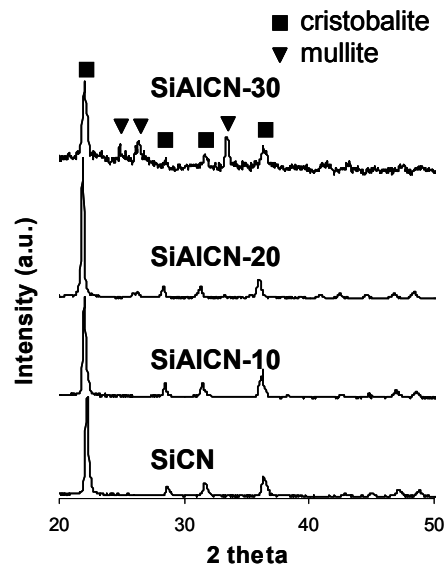


Figure 31: XRD patterns of the SiCN, SiAlCN-10, SiAlCN-20 and SiAlCN-30 oxidized at 1400°C for 200 hours.

Table 5: The lattice constants of cristobalite formed on different materials.

	SiCN	SiAlCN-10	SiAlCN-20	SiAlCN-30
a = b (nm)	0.4936	0.4946	0.4979	0.4939
c (nm)	0.6780	0.7007	0.7104	0.6960

The oxidation rate of silicon-based materials is controlled by the oxygen diffusion through the oxide layer. At low temperatures (<1350 °C), the oxide is amorphous, which consists of the 6-membered SiO₄ rings. It is demonstrated that the oxidation rate is controlled by oxygen molecules passing through the rings. At high temperatures (> 1350 °C) the oxide scale is crystallized. It is commonly believed that at high temperatures the oxidation mechanism will change from the oxygen molecular interstitial diffusion to oxygen atom/ion lattice diffusion. However, recent study clearly demonstrated that SiC exhibits the same oxidation behavior regardless if the oxide scale is amorphous or crystalline phase; the above-mentioned transition of oxidation mechanism only occurred when the oxide scale is partially crystallized or the crystalline phase contains impurities. This result implied that oxygen diffusion mechanism is the same in amorphous silica as in crystalline silica: oxygen molecule diffusion through 6-membered SiO₄ rings that exist also in the cristobalite structure.

Based on these evidences, we propose that the oxidation of SiC/SiAlCN ceramics at 1400°C is controlled by oxygen molecule interstitial diffusion through 6-membered SiO₄ rings of cristobalite, similar to what occurred at lower temperatures. The aluminum atoms dissolved in cristobalite block the rings and reduce the diffusion rate of oxygen, thus increasing the oxidation resistance. The more aluminum atoms dissolve in cristobalite, the lower the oxidation rate becomes. Since mullite is a thermodynamically stable phase, when the concentration of

aluminum in cristobalite is higher than a certain value, mullite will be formed, which will extract aluminum from cristobalite to decreasing the solution of aluminum. Thus the SiAlCN-30 has a higher oxidation rate than the SiAlCN-20. We further propose that the formation of the unique structure, where aluminum atoms block the 6-membered SiO_4 rings of cristobalite to reduce oxygen diffusion rate, occurred gradually to lead to the asymmetric oxidation kinetics in short-term (Figure 2). This is the same mechanism as that of lower temperatures. The only difference in that the process to rearrange aluminum takes 50 to 100 hours to reach equilibrium at lower temperatures, but it takes much shorter time (< 20 hours) at 1400°C .

4.4 $^{18}\text{O}_2$ tracer diffusion

Both ^{16}O and ^{18}O profiles are recorded by SIMS. In order to get the concentration-depth relationship, the concept of fractional concentration is used. The fraction concentration of ^{18}O is calculated using $I_{\text{O-18}}/(I_{\text{O-18}}+I_{\text{O-16}})$, where I is the number of counts.

The modeling of oxygen diffusion in the oxide scales is based on the following assumptions²³³:

1. Initially, the fractional tracer concentration in both the network, C , and the interstitials, C_i , is equal to the same low background. $C(x \geq 0, t=0) = C_i(x \geq 0, t=0) = C_b$.
2. Upon exposure to the tracer atmosphere, both the network and the interstitials immediately establish equilibrium with the gas. $C(x=0, t > 0) = C_i(x=0, t > 0) = C_g$.
3. Diffusion occurs in parallel through the network and interstices. Interstitial diffusion is considered to occur quickly relative to that in the network. $D_n > D_i$.

According to assumption 3, at any finite depth into the sample the fractional enrichment of the interstitial oxygen is always greater than that in the network. Thus, isotopic exchange between network and interstitial oxygen always results in network enrichment. The rate of network-interstitial exchange is assumed to be directly proportional to the difference in fractional concentration, and, therefore, at large depths where the concentration is determined solely by network-interstitial exchange this may be expressed as:

$$\frac{\partial C}{\partial t}_{x=\infty} = -\beta(C_{(x=\infty)} - C_{i(x=\infty)}) \quad (4-3)$$

β is the network-interstitial exchange coefficient and has a unit of reciprocal of second. If the rate of exchange reaction is much slower compared to that of interstitial diffusion, the concentration of interstitial ^{18}O can be considered as a constant and equal to C_g^{234} . This is because the interstitial oxygen is in equilibrium with the atmosphere. It has been observed in previous studies that D_i is much greater than D_n . Therefore, the gradient in the interstitial oxygen is negligibly small over a distance much larger than $(D_n t)^{1/2}$.

Due to the fact that the absolute concentration of interstitials is small, a few ppm, the signal which is detected during experimentation, reflects only the gradient in C . The diffusion equation modified with the consideration of the network-interstitial reaction by the addition of a source term is:

$$\frac{\partial C}{\partial t} = D_n \left(\frac{\partial^2 C}{\partial x^2} \right) + \beta(C - C_g) \quad (4-4)$$

where $C - C_g$ is the difference in concentration between the network and interstitial oxygen.

Considering the aforementioned boundary conditions, the solution for the above differential equation (Eq 4-4) is:

$$\frac{C - C_b}{C_g - C_b} = e^{-\beta t} [\text{erfc}(\theta) - 1] + 1 \quad (4-5)$$

where erfc denotes complementary error function and $\theta = x/[2(D_n t)]^{1/2}$.

The application of this solution is restricted to the near surface, i.e., $x \ll (D_n t)^{1/2}$, and the generalization to include the surface reaction kinetics is described by Cawley and Boyce.

A χ^2 fitting method is used with Eq 4-5 to get the values of β and D . The objective function, χ , to be minimized is:

$$f = \frac{C - C_b}{C_g - C_b} - 1 \quad (4-6)$$

$$\chi^2(\beta, D) = \sum_{i=1}^n \frac{f_i^{ob} - f^{ca}(x_i, \beta, D)}{\sigma_i} \quad (4-7)$$

where f_i^{ob} is the experimentally observed value at the distance x_i . The quantity $f^{ca}(x_i, \beta, D)$ is the calculated value from Eq.4-5 at the distance x_i . The variance, σ_i , is assigned a value of unity, since the true values associated with the experimental data were not known a priori. Minimization of the objective function, $\chi^2(\beta, D)$ was accomplished by simultaneous adjustment of β and D , using the Levenberg-Marquardt technique.

Figure 32 (a) and (b) show the typical SIMS profiles of ^{18}O and ^{16}O in the oxide scales formed on the SiCN and SiAlCN specimens, respectively, after annealing in ^{18}O enriched gas at 1050 °C for 5 hours. It can be seen that there is significant accumulation of ^{18}O isotope near the oxide-substrate interface of the SiCN (Figure 32 a). The bottom of the ^{18}O profile is close to the background concentration of ^{18}O in the original oxidizing gas (0.2%) according to the calculation of $I_{O-18}/(I_{O-18} + I_{O-16})$. The observed profile is explained in terms of the transport mechanisms present, as well as by the exchange of the oxidant with the lattice oxygen. The accumulation of

^{18}O near the interface of oxide-substrate results from the permeation of oxygen molecular through the oxide and formation of a new oxide at the interface. The decreasing profile near the oxide surface into the oxide can be understood by the diffusion of the oxygen tracer through the network. In addition to the isotope diffusion into the oxide from the outer interface, the isotope can diffuse into the oxide from the newly formed oxide as well, thus an apparent sloped isotope profile appears near the original oxide-substrate interface. The above analysis suggests that oxygen interstitial diffusion is the controlling process for the oxidation of the SiCN. However, at the same annealing conditions, there is no ^{18}O accumulation near the oxide-substrate interface for the SiAlCN; while ^{18}O concentration is not uniform across the oxide either (Figure 32 b). Figure 32c shows the profiles of ^{18}O and ^{16}O in the oxide scales formed on the SiAlCN after annealing in ^{18}O enriched gas at 1050°C for 15 hours. Slight accumulation of ^{18}O near the oxide-substrate interface can be observed, suggesting that the oxidation of the SiAlCN is also controlled by interstitial diffusion. The above results clearly demonstrate that the interstitial diffusion is faster than network diffusion at the testing conditions and is the rate control process for the oxidation of both SiCN and SiAlCN and that the interstitial diffusion rate is much lower for the aluminum-doped silica (formed on the SiAlCN) than the pure silica (formed on the SiCN). The experiments shown in Chapter 4.2 reveal that the oxidation rate of the SiCN was about 200 times higher than that of the SiAlCN, indicating the oxygen interstitial diffusion rate can be lowered by two order of magnitude with only about 4% (based on Si content) of aluminum doping.

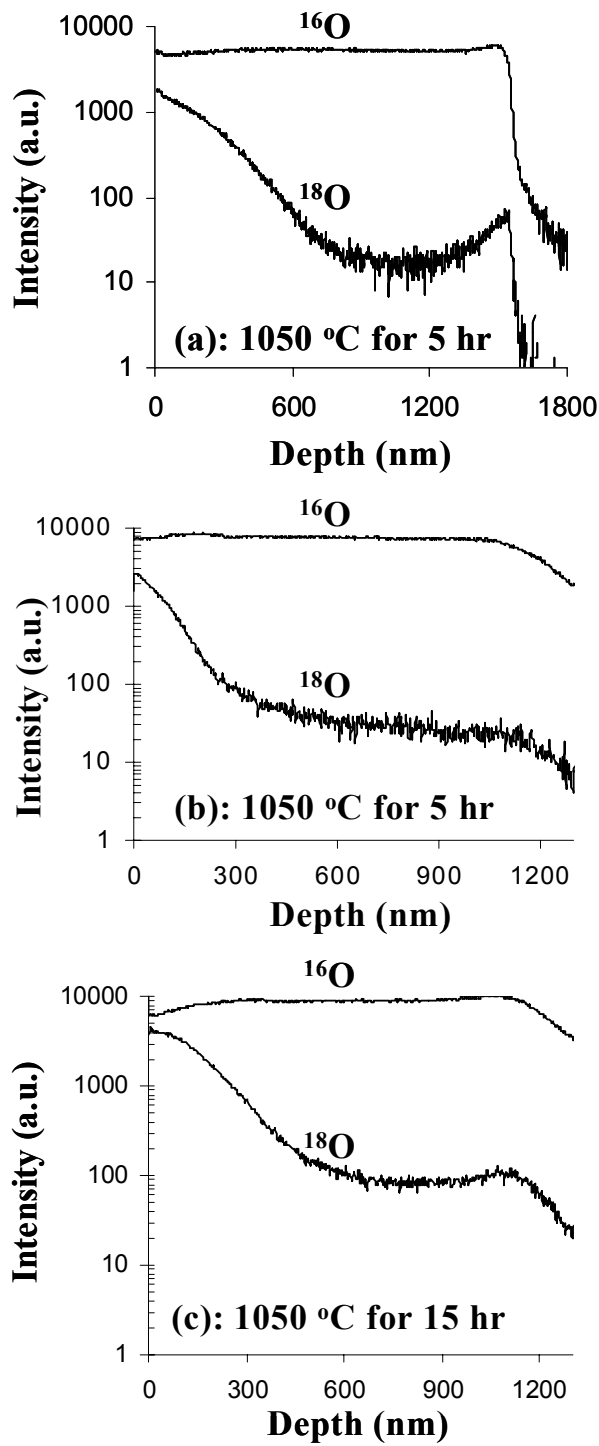


Figure 32: SIMS profiles of ^{16}O and ^{18}O in the oxide scales formed on (a) the SiCN, (b) and (c) the SiAlCN after annealing in ^{18}O enriched gas.

The profiles presented in Figure 32 can also be used to determine the network diffusivity by fitting them with proper diffusion models. Raw data from SIMS was first converted to the concentration-penetration profile of ^{18}O , which can be done by dividing the ^{18}O signal by the sum of the ^{18}O and ^{16}O signals. Figure 33 shows a typical ^{18}O concentration-penetration profile obtained for the aluminum-containing silica. Due to the existence of the interstitial diffusion, the internal exchange between interstitial and network oxygen needs to be considered for determining pure network-diffusion. Kalen *et al.*²³³ and Cawley and Boyce suggested that ^{18}O concentration profile such as presented in Figure 33 can be modeled to obtain pure network-diffusivity by using the relation:

$$\frac{C - C_0}{C_s - C_0} = \exp[-\beta t] \left[\operatorname{erfc}\left(\frac{x}{2\sqrt{D_n t}}\right) - 1 \right] + 1 \quad (4-8)$$

where D_n is the oxygen network-diffusion coefficient to be determined; C tracer concentration at any given position, C_s tracer concentration at surface, C_0 the natural abundance of ^{18}O (0.2%), β the network-interstitial exchange coefficient, t the annealing time, and x the penetration distance. It can be seen from Figure 33 that the experimental data can be modeled by Eq. (4-8) very well.

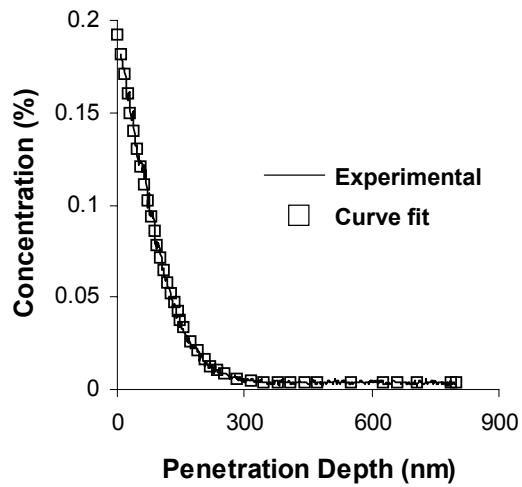


Figure 33: Comparison between the experimental ^{18}O concentration-penetration profiles obtained from the SiAlCN after annealing in ^{18}O enriched gas at $1100\text{ }^\circ\text{C}$ for 3 hours and that calculated using equation (4-8).

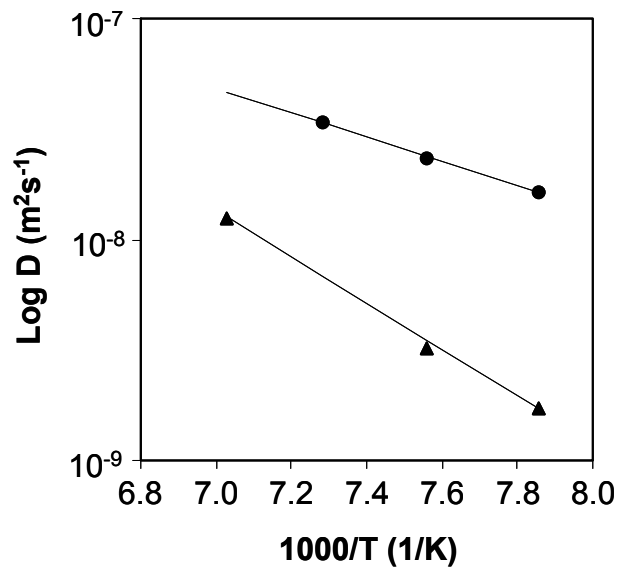


Figure 34: Arrhenius plot for the oxygen network-diffusion in pure silica and Al-doped silica.

The coefficients of network-diffusion determined from concentration-penetration profiles of ^{18}O by using Eq. (4-8) are presented in Figure 34 for the pure silica and aluminum-doped silica. It can be seen that the diffusion coefficients exhibit Arrhenius dependence on temperature according to the relation:

$$D_n = D_o \exp(-Q/RT) \quad (4-8)$$

where D_o is the pre-exponential factor and Q the activation energy of diffusion. The calculated D_o and Q for the pure silica and Al-doped silica are reported in

Table 6. The diffusion coefficients for the Al-doped silica are about an order of magnitude lower than those for the pure silica, suggesting Al-doping can also reduce the network diffusion of oxygen. More importantly, the activation energy for the Al-doped silica is about twice of that for the pure silica. The activation energy for the network diffusion is closely relates to the free energy of the formation of oxygen vacancies²³⁵. The higher activation energy indicates that the oxygen vacancies are more difficult to form in Al-doped silica, suggesting that Al doping could enhance the stability of the network oxygen. This may explain the lower corrosion rate observed in the SiAlCN.

Table 6: D_o and Q values for ^{18}O diffusion in SiCN and SiAlCN-10 ceramics

Materials	SiCN	SiAlCN
D_o (m ² /s)	3.5×10^{-14}	2.9×10^{-11}
Q (kJ/mol)	106	201

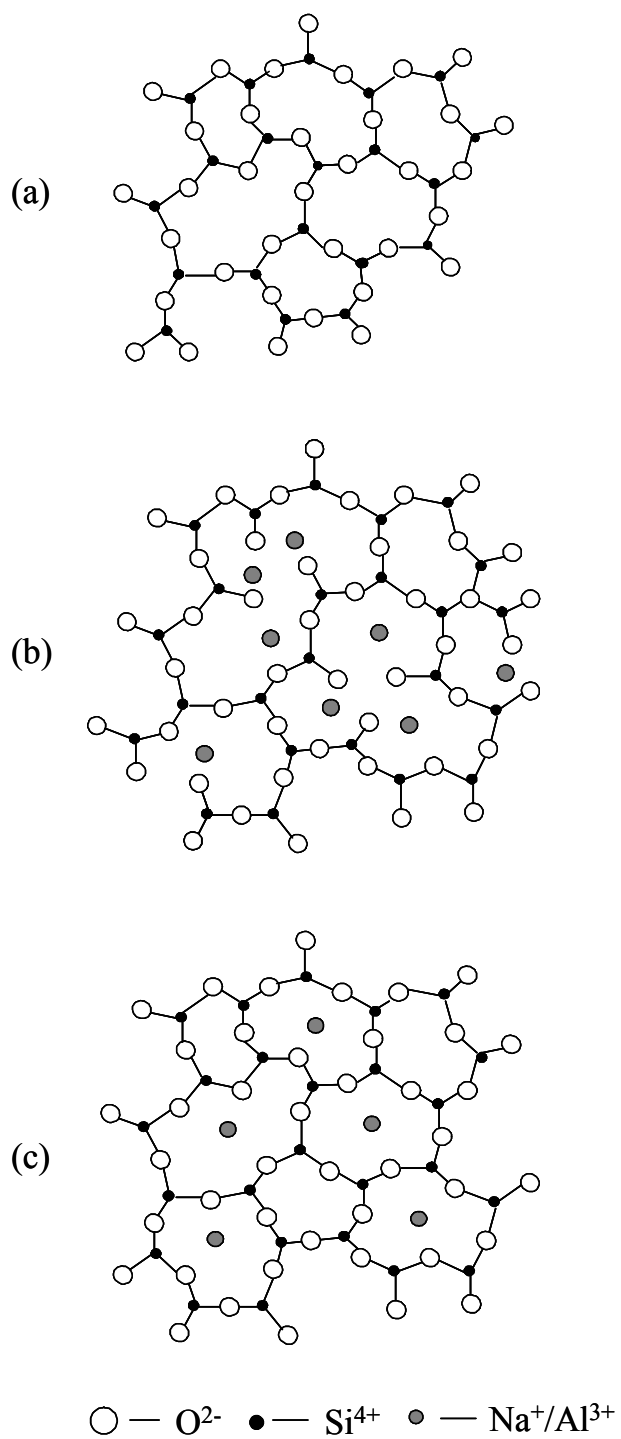


Figure 35: A schematic diagram of the two-dimensional structures of (a) pure silica, (b) silica with impurities (conventional model) and (c) Al-doped silica (currently proposed).

The structure of amorphous silica can be characterized by connected rings comprising of SiO_4 tetrahedral (Figure 35 a). The majority of these rings are 6-membered or higher^{222, 223, 224}. Therefore, the interstitial diffusion of oxygen through amorphous silica is controlled by oxygen molecules passing through the 6-membered rings. According to conventional understanding, the presence of impurities can destroy the original “perfect” network structure of pure silica and results in the formation of non-bridging oxygen (Figure 35 b)²³⁶, thus enhancing oxygen diffusion. The current study, however, demonstrates that aluminum doping leads to a decrease in oxygen interstitial diffusivity, and thus suggests that the aluminum doping must either block part of the 6-membered rings or significantly alternate the structure of otherwise pure silica. Previous NMR study¹³ suggested that the structure of Al-doped silica is similar to that of the pure silica and the aluminum were not incorporated into the SiO_2 network to replace silicon atoms. Accordingly, we propose a new structural model for Al-doped silica in which aluminum sit at the center of the 6-membered rings (Figure 35 c). This model can be used to explain the lower interstitial diffusivity observed in Al-doped silica. The model can also be used to explain the higher activation energy of network diffusion for Al-doped silica. Figure 35 c shows that in this new model, Al contributes additional bond energy toward surrounding oxygen, which is already bonded to two silicon atoms. In other word, compared to pure silica, the generation of oxygen vacancy in the Al-doped silica need to break extra Al-O attraction in addition to two Si-O bonds. The proposed model is a prospective one, and further characterization of the aluminum position in such Al-doped silica is needed to fully understand the observed phenomena.

4.5 Summary

In this chapter, the oxidation behaviors of SiAlCN ceramics are discussed. The results show that small amount aluminum doped in SiCN ceramics greatly decreases the oxidation rate. A physical model to account for the phenomena is advanced. The ^{18}O tracer diffusion experiment gives the support to the proposed model. It is also pointed out that the aluminum has a percolation value. If the amount of aluminum in SiAlCN is over the value, the aluminum will increase of the oxidation rate.

CHAPTER FIVE: WET OXIDATION AND HOT-CORROSION OF SiCN AND SiAlCN CERAMICS

This chapter will discuss the oxidation and hot corrosion behavior of polymer-derived SiCN ceramics and SiAlCN ceramics in water-vapor environments. The kinetic constants of the oxidation and corrosion of the materials are derived by fitting the weight change-annealing time curves with the parabolic model. It is found that the SiAlCN ceramics have a better wet oxidation/corrosion resistance than that of the SiCN, CVD SiC and Si₃N₄ ceramics. The mechanism for the high resistance to wet-oxidation/corrosion possessed by the SiAlCNs is discussed in term of the network/microstructures of the oxide scales. The results of hot corrosion in sodium chloride environment are also presented. It is shown that adding aluminum can also improve resist to the sodium associated hot-corrosion.

5.1 Experimental procedure

Fully dense ceramics are prepared in order to study the oxidation of Si(Al)CN ceramics in the water vapor. The procedure for preparing these ceramics was stated in section 3.1.1. In these experiments, the discs of 1/2" diameter are used. When the ceramics are annealed at high temperatures, the structure will evolve with gas evaporation, which will cause the weight change during the wet oxidation. Therefore, before oxidized in water vapor, these discs are treated in N₂ atmosphere at 1450°C for 4 hours to stabilize the structure.

These discs are polished on both sides down to 0.2 μ m with the diamond lapping films before oxidization. The detail process for polishing is discussed in section 3.3.1. Each group includes at least 10 pieces of discs to obtain enough surface areas to ensure the accuracy of weight change measurement.

A schematic diagram of the apparatus for wet oxidation is shown in Figure 36:

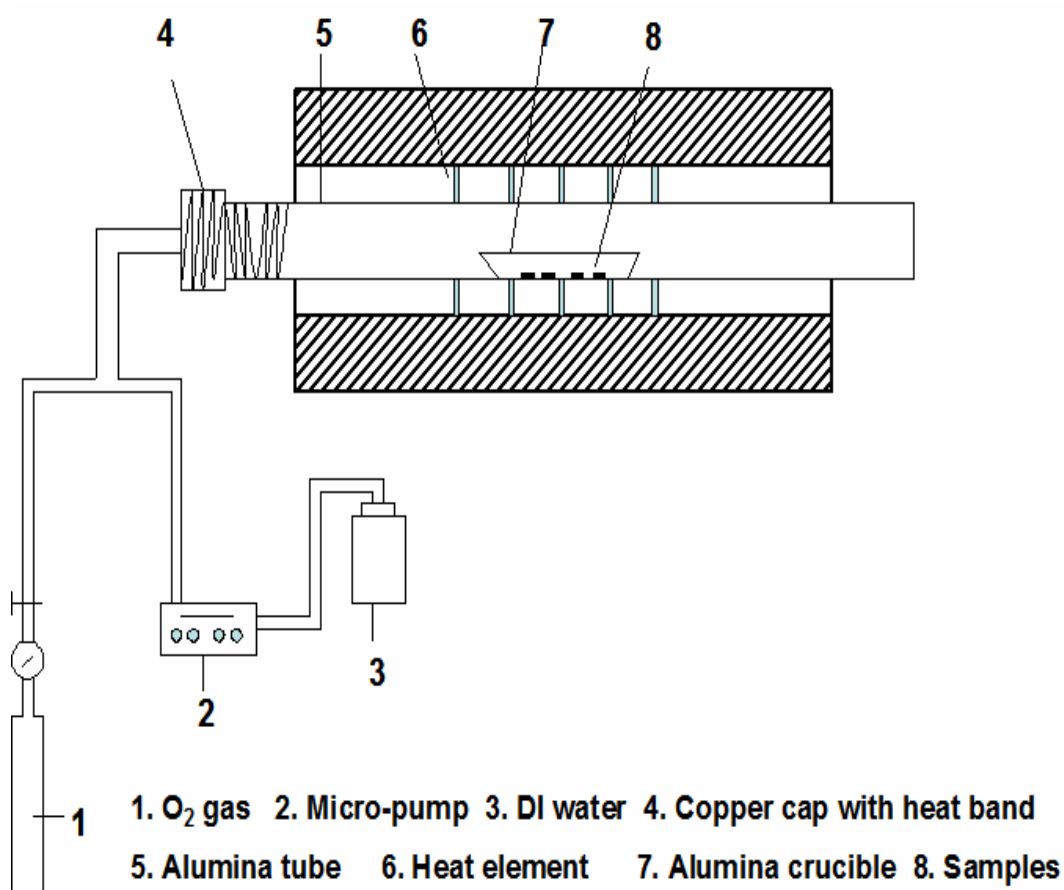


Figure 36: Schematic diagram of the apparatus for wet oxidation.

The apparatus is constructed of a long alumina tube (Coorstek, Golden, CO) in a single-zone tube furnace. One end of the alumina tube is sealed by a cap with the heating-tap. The other

end of the tube is open to the air. At the sealed end, the liquid water is vaporized at the temperature of about 200°C with the heat supported by the heating tape. To avoid of the turbulence of water vapor, a porous alumina brick is used at the sealed end. The O₂ flux is controlled by the fluid-meter. The water flux is controlled by adjusting the rate of a mini-pump (Fisher Scientific). The temperature is calibrated by the thermal couple and is controlled by the furnace. All of the wet oxidation experiments are conducted at a pressure of 1 atm.

Before the test is conducted, the samples' diameter and thickness are carefully measured to obtain the samples' total surface area. The original weight of the samples is measured by an electronic balance with the accuracy of 0.1 mg (APX-100, Denver Instrument, Denver, CO). The samples are placed in the alumina crucible and are put in the center of the furnace. The experiments are carried out at the temperatures of 1100°C and 1400°C up to 300 hours. Before adding the water vapor, the furnace raises to the desired temperature with a ramp rate of 30°C/min. Then the water and/or oxygen gas is inducted in the tube. After a certain time, the water vapor and/or oxygen stops and the furnace is shut off to order to cool down the samples as soon as possible. After that, the samples are taken out to measure their weight change with the electronic balance.

In regards to the wet oxidation at 1100°C, the condition chosen is 100% water vapor with the flowing rate of 4.4 cm/s. The alumina tube is seriously damaged after the experiment. For the wet oxidation at the temperature of 1400°C, the condition of 50% water-50%O₂ at the flowing rate of 4.4cm/s is chosen. This condition is fairly benign in comparison with a high gas velocity/high pressure environments as they are uncounted^{237, 238, 239, 196}. On the other hand the condition is the same as that used previously to measure the wet oxidation behavior of SiC and Si₃N₄^{141, 240}.

The oxidation and corrosion process of water vapor can be described by the parilinear model. For this experiment, the equation (2-33) needs to be converted to express the weight change as a function of annealing time²:

$$t = \frac{\alpha^2 k_p}{2k_l^2} \left[\frac{-2k_l \Delta w_1}{\alpha k_p} - \ln \left(1 - \frac{2k_l \Delta w_1}{\alpha k_p} \right) \right] \quad (5-1 \text{ a})$$

$$\Delta w_2 = -\beta k_l t \quad (5-1 \text{ b})$$

where Δw_1 is the weight gain due to the growth of the oxide scale, Δw_2 the weight loss due to the volatilization of the oxide scale, k_p the oxidation parabolic rate constant for oxidation in units of $\text{mg}^2/(\text{cm}^4 \text{ h})$, k_l the linear rate constant for SiO_2 volatilization in units of $\text{mg}/(\text{cm}^2 \text{ h})$, and α and β are the constants. For the ceramics with a composition of $\text{SiAl}_x\text{C}_y\text{N}_z\text{O}_u$, α and β can be expressed as follows:

$$\alpha = \frac{MW_{\text{SiO}_2} + \frac{x}{2} MW_{\text{Al}_2\text{O}_3}}{(1 + 3x/4 - u/2) MW_{\text{O}_2} - y MW_{\text{C}} - z MW_{\text{N}}} \quad (5-1 \text{ c})$$

$$\beta = \frac{MW_{\text{SiAl}_x\text{C}_y\text{N}_z}}{MW_{\text{SiO}_2} + \frac{x}{2} MW_{\text{Al}_2\text{O}_3}} \quad (5-1 \text{ d})$$

where MW stands for molecular weight. k_p and k_l , the rate constants for each material, can then be determined by nonlinear least-square analysis with the Eq.5-1. The process was discussed in detail by E.J. Opila et. al.²⁴¹. Similar to what was done in the section 4.1.3, the objective function, χ , to be minimized is:

$$\chi^2(k_p, k_l) = \sum_{i=1}^n \frac{\Delta w_i^{ob} - \Delta w^{ca}(t_i, k_p, k_l)}{\sigma_i} \quad (5-2)$$

where Δw_i^{ob} is the experimentally observed specific weight change measured at time t . The quantity $\Delta w^{ca}(t, k_p, k_l)$ is the specific weight change calculated from the parilinear kinetic model for time t . The variance, σ_i , was assigned a value of unity, since the true values associated with the experimental data were not known a priori.

The quantity $\Delta w^{ca}(t, k_p, k_l)$ is given by the relationship :

$$\Delta w_i^{ca} = \Delta w_1 + \Delta w_2 \quad (5-3)$$

The quantities Δw_1 and Δw_2 are given by Eqs (5-1a) and (5-1b), respectively. The differential-form of Eq. (5-1a) was used to compute Δw_1 by approaching the solution as an initial value problem and then applying a 4th order Runge-Kutta integration technique to solve for Δw_1 at time t_i . Minimization of the objective function $\chi^2(k_p, k_l)$ was accomplished by simultaneous adjustment of k_p and k_l using the Levenberg-Marquardt technique.

As stated in Chapter 2, at different flowing rates and system pressures, flux estimates can be made using a simplified form of Eq.2-35. Further considering the effect of annealing temperature, the corrosion rate can be expressed:

$$k_l \propto \frac{v^{1/2} P_{H_2O}^2}{P_{total}^{1/2}} \exp\left(-\frac{Q}{RT}\right) \quad (5-5)$$

where Q is activation energy and T annealing temperature. Using Eq.5-5, the data obtained at different conditions can be normalized and compared.

5.2 Wet oxidation at the temperature of 1100°C

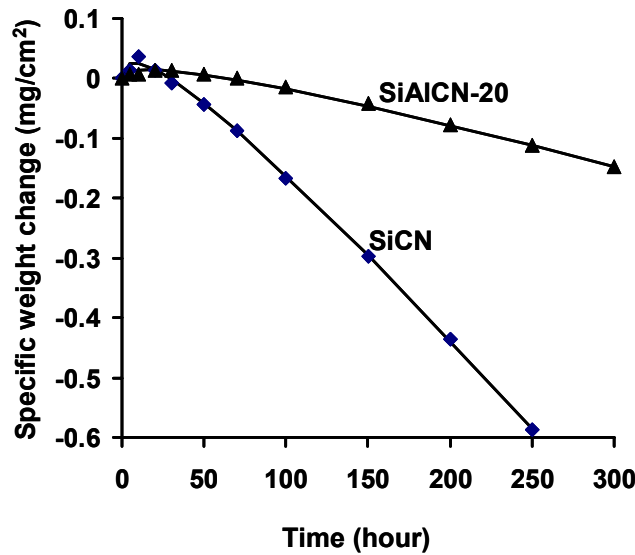


Figure 37: Weight change as a function of annealing time for the SiAlCN-20 and SiCN as indicated.

Figure 37 shows the weight change as a function of annealing time for the SiCN and SiAlCN-20. It can be seen that SiAlCN-20 exhibits much less weight loss than SiCN, suggesting that SiAlCN-20 possesses better corrosion resistance. The kinetic data for the oxidation and corrosion can be obtained by fitting the experimental data in Figure 37 by using a parabolic model as expressed in Eq.5-1. The nonlinear least-square analysis is used in the fitting process. k_p and k_l , the rate constants for each material, can then be determined. The results are listed in Table 7. It can be seen that the oxidation and corrosion rates for SiAlCN-20 are 7 and 4 times lower than those for SiCN, respectively. For the water-vapor corrosion rate, 4 times difference is considered to be significant. These results clearly demonstrate that small amount of aluminum

doping (atomic ratio of Si-to-Al is 100:8) can remarkably improve the oxidation/corrosion resistance of otherwise pure SiCN.

Corrosion kinetics obtained at different testing conditions can then be compared to each other by normalizing them using proper models. The corrosion rate strongly depends on the testing conditions such as partial pressure and flowing rate of water vapor. The dependence of the corrosion rate on these parameters can be expressed by Eq.5-5. The normalized corrosion rate constants of CVD SiC and Si₃N₄ using Eq.5-5 are also listed in Table 7. It can be seen that the corrosion rate of SiAlCN-20 is about an order of magnitude lower than those of pure SiC and Si₃N₄.

Table 7 Parabolic rate constants (k_p) and linear rate constants (k_l) for silicon based materials

Material	$k_l \times 10^3$ (mg/cm ² h)	$k_p \times 10^5$ (mg ² /cm ⁴ h)	Experimental condition	Temp. (°C)	Q (KJ/mol)	Ref.
SiCN	3.7*	38.2	100% water vapor, flowing rate: 4.4cm/s	1100	-	current
SiAlCN-20	0.96*	5.5	100% water vapor, flowing rate: 4.4cm/s	1100	-	current
CVD SiC	8.5*	-	50%H ₂ O-50%O ₂ , flowing rate: 4.4cm/s	1200-1400	35±147	241
CVD Si ₃ N ₄	14.8*	-	50%H ₂ O-50%O ₂ , flowing rate: 4.4cm/s	1200-1400	21±51	?

- k_l at 1100 °C in 100% water vapor of flowing rate of 4.4cm/s.

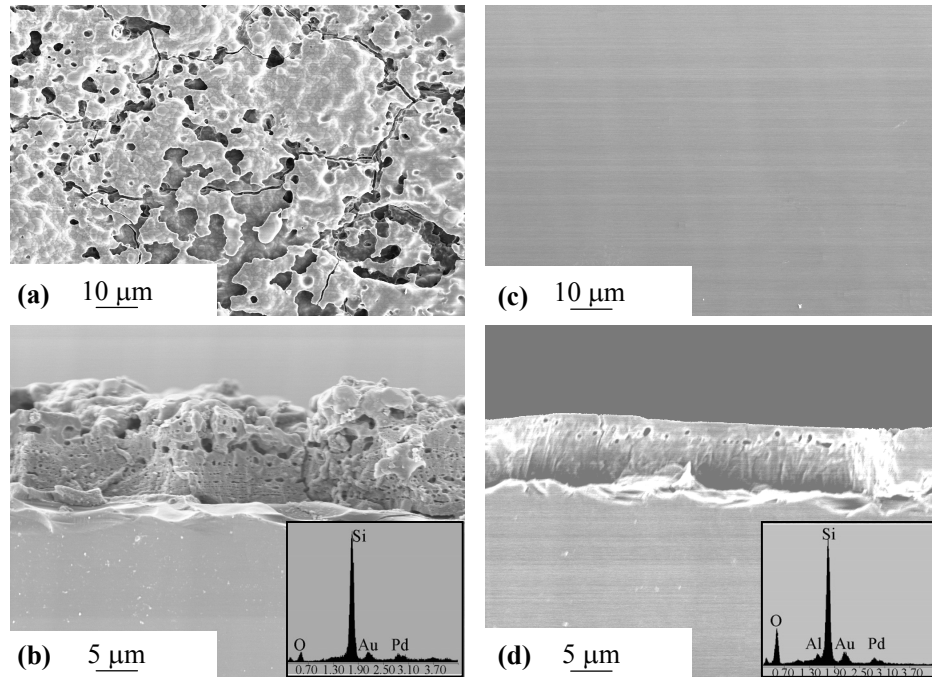


Figure 38: SEM images showing the surface (a) and cross-section (b) of the SiCN and the surface (c) and cross-section (d) of SiAlCN-20 after annealing for 100 hours.

Further evidence that demonstrates the improvement in water-vapor corrosion resistance for SiAlCN-20 comes from the observation of the morphology of oxide scales after annealing. Figure 38 shows SEM images of the oxide scales formed on SiCN and SiAlCN-20, respectively, after annealing for 100 hours. It can be noticed that the surface of SiCN is very rough and contains cracks due to the volatilization of the silica, similar to those observed in silicon carbide and nitride^{239, 196, 242}, while the surface of SiAlCN-20 is smooth and crack-free. Corrosion-associated surface defects such as cracks and roughness is one of major mechanisms to cause material degradation, which leads to a remarkable decrease in strength. Consequently, Al doping

does not only reduce material recession (lower linear rate constant) but also help to retain mechanical strength of the materials.

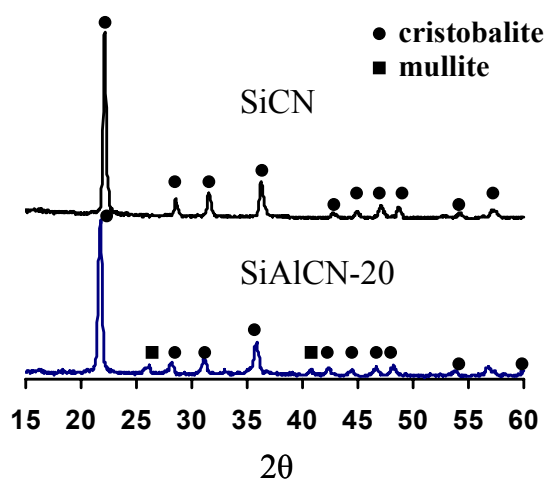


Figure 39: XRD patterns showing phase compositions in the oxide scales formed on SiCN and SiAlCN-20, respectively, after annealing for 200 hours.

XRD patterns of the oxide scales formed on SiCN and SiAlCN-20 after annealing for 200 hours are shown in Figure 39. The oxide scales for SiCN are pure cristobalite phase, while the oxide scales for SiAlCN-20 consist of cristobalite and small amounts of mullite. The lattice parameters of the cristobalite phases were calculated using XRD patterns to be for SiCN $a = 0.49836$ nm and $c = 0.67559$ nm, for SiAlCN-20 $a = 0.49980$ nm and $c = 0.70785$ nm. These values are slightly different from those for stand-free cristobalite (PDF card #00-039-1425), possibly due to the strain caused by thermal mismatch between the oxide scales and substrates. The lattice parameters of the cristobalite formed on SiAlCN-20 are larger than those of the cristobalite formed on SiCN. It is likely due to the solution of aluminum in the otherwise pure cristobalite lattice. Previously, it was demonstrated that Al-doped amorphous silica exhibits a lower rate and

higher activation energy for oxygen transportation than pure silica. We attributed such effects to a unique structure in which the aluminum sits at the center of the ring consisting of 6-membered SiO_4 tetrahedral to block the oxygen transportation and strengthen the network oxygen. It is possible that Al doping in cristoballite has a similar effect by sitting at the centers of the 6-membered SiO_4 tetrahedral rings within cristoballite to strengthen the oxygen bonding, and thus lowering the corrosion rate.

High resistance to water vapor corrosion exhibited by SiAlCN-20 is rather interesting. Previous studies²⁴³ revealed that other aluminum-containing silicon-based materials such as sialon and mullite suffer severe water vapor corrosion. This suggests that there could be an upper limit for amount of aluminum doping to effectively resist water vapor corrosion. This also suggests that the cristoballite with aluminum doping could be more stable than mullite structure in term of reaction with water vapor.

5.3 Wet oxidation at the temperature of 1400°C

Weight change as a function of oxidation time for SiAlCN and SiCN ceramics is shown in

Figure 40. The data fits parabolic model (Eq. 5-1) (solid lines) very well.

k_p and k_l , the kinetic rate constants for each data set, were determined by nonlinear least squares analysis. The detailed analysis method was described in reference 241, and the results are listed in Table 8.

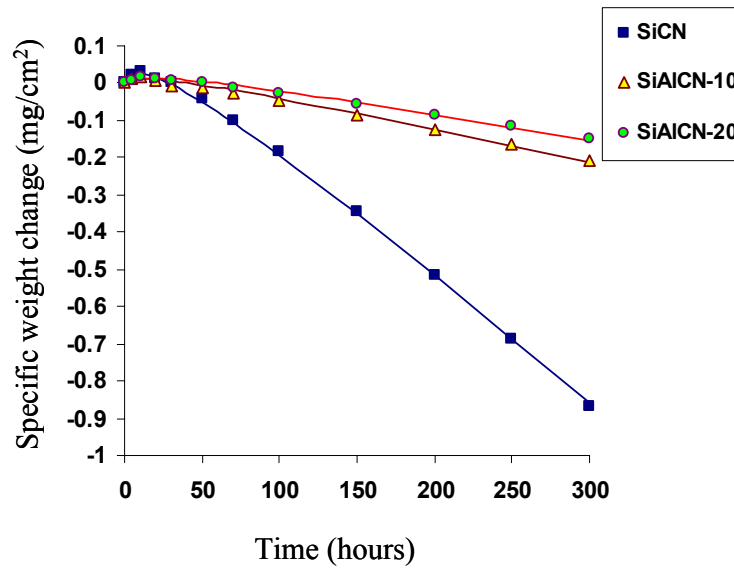


Figure 40: Weight change as a function of oxidation time at the temperature of 1400°C with 50% water-50%O₂ at the rate of 4.4cm/s.

Table 8: Comparison of k_i values of silicon-based ceramics at the condition of 50% water vapor-50%O₂ at 1400°C with the flowing rate of 4.4cm/s.

	CVD SiC	CVD Si ₃ N ₄ ²³⁹	AS 800	SiCN	SiAlCN-10	SiAlCN-20
$k_i \times 10^3$ (mg/cm ² h)	6.4	6.2	6.6	4.9	1.18	0.98
$k_p \times 10^3$ (mg ² /cm ⁴ h)	3.93	1.0	52	0.49	0.52	0.053

Compared with the other silicon-based materials under the same oxidation conditions, it can be seen that SiAlCN ceramics has the lowest k_p and k_i values.

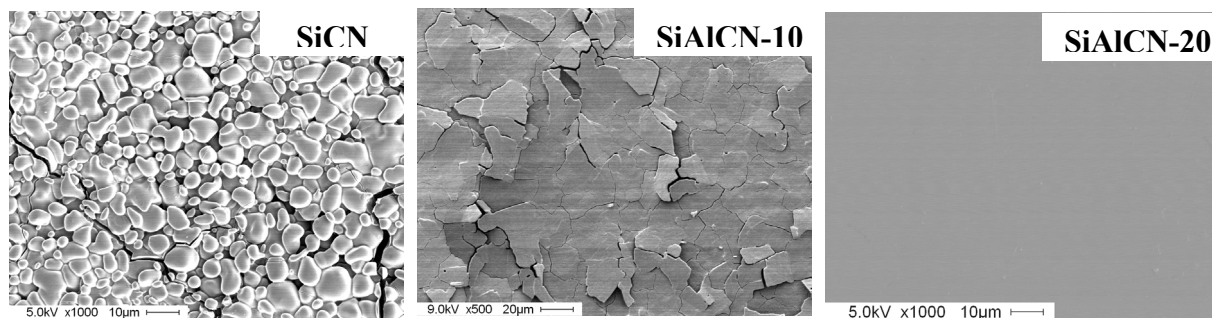


Figure 41: The corrosion surface of SiAlCN and SiCN at 1400°C with 50% H_2O -50% O_2 at the flowing rate of 4.4cm/s for 300hours.

Figure 41 shows the SEM images of the surfaces of SiAlCN and SiCN ceramics after annealing for 300 hours. It can be seen that the surfaces of SiAlCN-20 ceramics still look very smooth without any cracks on it. Compared to the surfaces of SiAlCN-20 ceramics, the surfaces of SiCN and SiAlCN-10 ceramics have been severely corroded with many cracks on them, just as many other Si-based ceramics such as SiC and Si_3N_4 ceramics suffering the cracks and evaporation on the surface due to the water corrosion. The cracks will cause that the mechanical properties of ceramics to greatly decrease in the water environments. The strength of SiCN and SiAlCN ceramics as a function of wet-oxidation time is shown in Figure 42. This figure also shows that SiCN and SiAlCN-10 ceramics almost lose 80% their strength after 300 hours corrosion in the water. However, SiAlCN-20 ceramics still keep about 70% strength in the same conditions. Moreover, the figure also indicates that the strength of SiAlCN-20 ceramics changes a little bit after 50 hours, almost at the same level.

The XRD (Figure 43) analysis shows that the phase in oxidation layer of SiCN, SiAlCN-10, and SiAlCN-20 ceramics is only cristoballite.

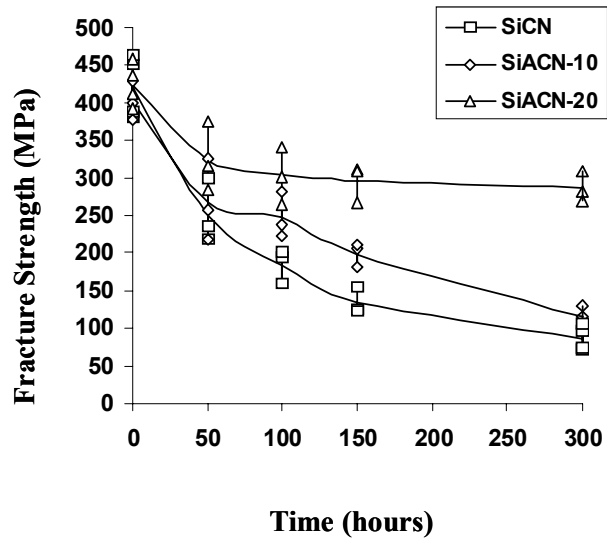


Figure 42 : Fracture strength of SiCN and SiAlCN ceramics as a function of corrosion time.

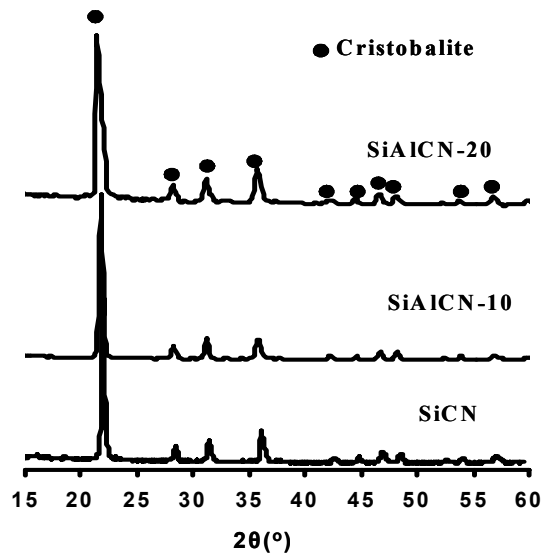


Figure 43: The XRD pattern of SiAlCN and SiCN ceramics after oxidized at 1400°C with 50%H₂O-50%O₂ at the flowing rate of 4.4cm/s for 300 hours.

Table 9: The lattice constants for cristobalite crystalline calculated from XRD results (Figure 43).

	SiCN	SiAlCN-10	SiAlCN-20
a=b(nm)	0.4972	0.4992	0.5019
c(nm)	0.6916	0.7095	0.7426

It is believed that the improvement of water corrosion to silicon ceramics is due to the decrease of silica activity in the oxide. By comparison of the corrosion results of SiCN and SiAlCN ceramics, it can be deduced that the activity of silica in the outer oxide is about 0.20~0.24 (Consider that the activity of silica on the oxide of SiCN is 1, the silica activity in the oxide on SiAlCN ceramics is calculated by the ratio of recession rate. Here, we consider all the experimental conditions are same for all kinds of ceramics). We do not believe that the formation mullite protection layer is the reason for the reduction of recession rate because the silica activity of the mullite is about 0.3-0.4, higher than the value of our study. The corrosion rate of SiAlCN-10 and SiAlCN-20 ceramics is very low although the oxide scales on SiAlCN-10 and SiAlCN-20 ceramics do not show any mullite phase from the XRD results. It further confirms that mullite phase is not the reason for the increase of water resistance. From the lattice constants (.

Table 9) calculated from XRD results (Figure 43), it can be seen that with the increase of aluminum content, the lattice constants also increase. Just as it was proposed in section 5.2, the dissolution of aluminum in the silica structure to strengthen the Si-O bond can account for the reduction of water corrosion. It is believed that a small amount of aluminum in silica can greatly decrease the silica activity and even can be lower than the value of crystal mullite. The experimental measurement of silica activity in $\text{Al}_2\text{O}_3\text{-SiO}_2$ system²⁴⁴ (Figure 44) also confirms

this phenomenon. Even though the experiment temperatures are higher than 1600°C, the tendency shows that at a lower temperature, the greater decrease in silica activity due to a small amount of aluminum. It can be deduced that the aluminum will have more affect on the activity of silica at the temperature of 1400°C.

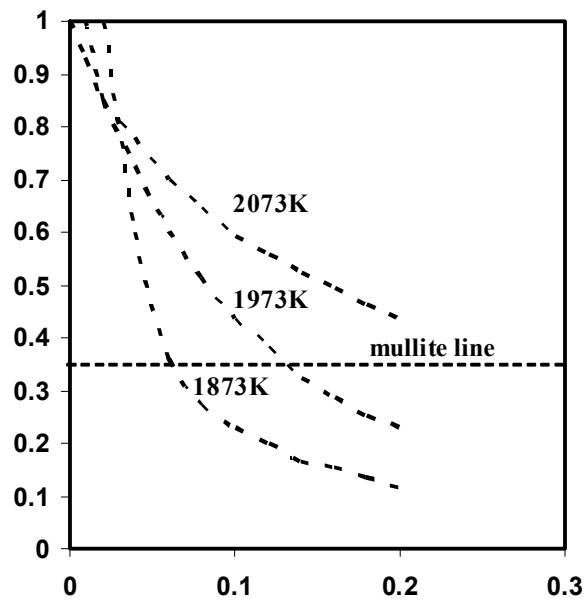


Figure 44: Activity of silica in $\text{Al}_2\text{O}_3\text{-SiO}_2$ system. The points of SiAlCN (SA) ceramics are also shown in the figure.

In summary, new kinds of silicon-based materials that possess good water corrosion resistance are found. SiAlCN ceramics have the highest water corrosion resistance till now due to the effect of a small amount of aluminum on the silica activity.

Finally, I would like to make following two comments:

- Due to its direct chemical-to-ceramic processing, the polymer-derived ceramic technique is leading to a simple, cost-efficient, and near-net shape approach to manufacture ceramic

components and devices with inconvenient shapes such as fibers, coatings, composites, micro-electro-mechanical systems (MEMS), and nanostructures. The high oxidation resistance together with high resistance to creep^{245, 119} and crystallization will extend the applications of the polymer-derived ceramics.

- While the environmental barrier coating (EBC) is currently under development to provide protection for the silicon-based materials and has been proved to be successful to a certain degree,^{8, 9, 246} the EBC is not applicable for many applications such as MEMS and heat-exchangers. With high resistance to water vapor corrosion, SiAlCN could be particularly useful in such applications.

5.4 NaCl corrosion at 1200°C

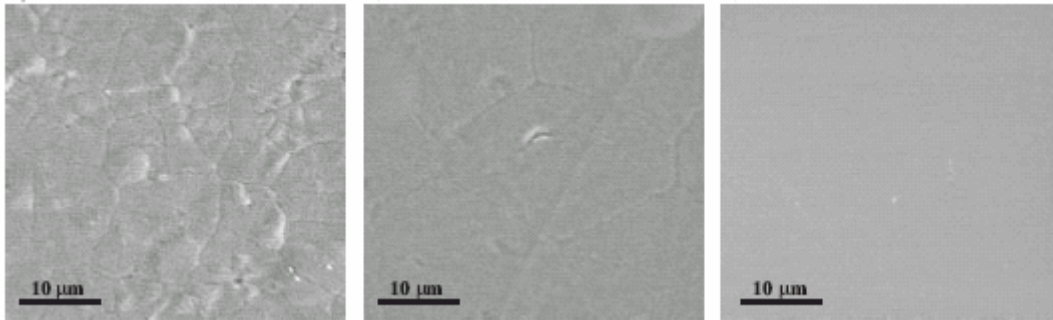


Figure 45: SEM morphologies of the surfaces of (a) SiCN, (b) SiAlCN-5, and (c) SiAlCN-10.

The specimens were first immersed in de-ionized water saturated with NaCl at 100°C and then annealed at 1200°C for 50 hours in air.

The surfaces of SiAlCN ceramics that were treated at 1200°C for 50 hours with NaCl (Figure 45) indicate that SiAlCN ceramics have good resistance to hot-corrosion of sodium. It is well known that the sodium try to break the silica compact network by forming non-bridge oxygen^{236, 247}. When aluminum evolves in the silica structure, it will try to repair the damaged structure through the formation of aluminum tetrahedral structure, reducing/eliminating non-bridging oxygen^{236, 247}. Similar behavior has previously been observed^{81, 248}.

5.5 Summary

Water corrosion behaviors of SiAlCN ceramics are demonstrated. The results show that a small amount of aluminum can greatly increase water-corrosion resistance. The reduction of silica activity in Al₂O₃-SiO₂ by a small amount of aluminum can account for the increase in water-corrosion of SiAlCN ceramics. SiAlCN ceramics also show a good resistance to sodium hot-corrosion, which can be understood by that the aluminum can prevent the sodium from damaging the silica structure.

CHAPTER SIX: CONCLUSION

From the discussion aforementioned, the following conclusions can be drawn:

1. Polymer-derived SiAlCN ceramics have better thermal stability than that of polymer-derived SiCN ceramics without Al-doping. The aluminum affects the structural evolution of SiAlCN ceramics by stabilizing the SiCN₃ structure at elevated temperatures, thus retards the crystallization of SiAlCN ceramics. The aluminum also promotes the phase transformation of α -Si₃N₄ to β -Si₃N₄ during the crystallization of polymer-derived SiAlCN ceramics.
2. Polymer-derived SiAlCN ceramics exhibit excellent oxidation resistance in air. The oxidation rate of SiAlCNs is more than an order of magnitude lower than that of the SiCN without aluminum and that of CVD SiC and Si₃N₄. The decrease in oxidation kinetic of SiAlCNs is due to the unique structures of the oxide scales formed from the SiAlCNs, in which aluminum atoms are located in the 6-membered Si-O rings blocking oxygen diffusing.
3. Polymer-derived SiAlCN ceramics demonstrate remarkable resistance to water-vapor related corrosion at high temperatures. Compared with other silicon-based non-oxide ceramics, SiAlCNs possess the lowest corrosion rate. Furthermore, SiAlCNs show smooth surfaces and retain a high strength after corrosion annealing. This unique property is due to the formation of Si-Al-O protective layer, in which a small amount of

aluminum greatly reduces the silica activity. SiAlCN ceramics also have excellent resistance to sodium hot-corrosion.

In summary, a new class of silicon-based ceramic materials, SiAlCNs, is developed. It is demonstrated that the materials have excellent high-temperature stability and oxidation/hot-corrosion resistance. Together with other unique advantages of the polymer-derived ceramic processing, the new SiAlCN ceramics are very promising for many high-temperature applications such as high-temperature MEMS micro-sensors.

LIST OF REFERENCES

- ¹ K.H. Jack, "Sialons and related nitrogen ceramics," *J. Mater. Sci.*, 11, 1135-1158 (1976).
- ² R. Riedel, G. Passing, H. SchoÈnfelder, and R.J. Brook, "Synthesis of dense silicon-based ceramics at low temperatures," *Nature* 355, 714-717(1992).
- ³ E. Kroke, Y.L. Li, C. Konetschny, E. Lecomte, C. Fasel, and R. Riedel, "Silazane Derived Ceramics and Related Materials," *Mater. Sci. and Eng. R* 26, 97-199 (2000).
- ⁴ M.A. Schiavon, G.D. Soraru, and I.V.P. Yoshida, "Synthesis of Polycyclic Silazane Network and Its Evolution to Silicon Carbonitride Glass," *J. Non-crystal. Solids*, 304, 76-83 (2002).
- ⁵ G. Jeschke and M.K.M. Jansen, "A Magnetic Resonance Study on the Structure of Amorphous Networks in the Si-B-N-(C) System," *J. Non-crystal. Solids*, 260, 216-227 (1999)
- ⁶ B. Boury and D. Seyferth, "Preparation of Si/C/Al/N Ceramics by Pyrolysis of Polyaluminasilazanes," *Appl. Organometallic Chem.*, 13, 431-440 (1999)
- ⁷ R. Riedel, A. Kienzle, W. Dressler, L. Ruwisch, J. Bill, and F. Aldinger, "A Silicoboron Carbonitride Ceramic stable to 2000°C," *Nature*, 382, 796-798 (1996).
- ⁸ K.N Lee, "Current status of environmental barrier coatings for Si-Based ceramics," *Surf. Coat. Technol.*, 133, 1-7(2000).
- ⁹ K. N. Lee, R.A. Miller and N.S. Jacobson, "New-generation of plasma-sprayed mullite coatings on silicon-carbide," *J. Am. Ceram. Soc.*, 78, 705-710 (1995).
- ¹⁰ P. Schutzenberger and H. Colson, *C. R. Acad. Sci.* 92, 1508 (1885).
- ¹¹ M. Persoz, *Ann. Chim. Phys.*, 44, 315 (1839).

-
- ¹² A. Stock and K. Somieski, "Siliconhydrides X. Nitrogen-containing Compounds," *Ber.* 54, 740-758 (1921).
- ¹³ S.D. Brever and C.P. Haber, "Alkylsilazanes and Some Related Compounds" *J. Am. Chem. Soc.* 70, 3888-3891 (1948).
- ¹⁴ R.C. Osthoff, and S.W. "Organosilazane Compounds," *Kantor, Inorg. Synth.* 5, 55-64(1957).
- ¹⁵ D.F. Weyer, "Method of Preparing Ceramic Like Articles," US Patent 3,090,691, (1963).
- ¹⁶ R.W. Rice, K.J. Wynne, and W. B. Fox, "Preparation of Ceramics," US Patent 4,097,294 (1978).
- ¹⁷ W. Verbeek and G. Winter, "Silicon Carbide Fibers," German Patent 2,236,078 (1974).
- ¹⁸ W. Verbeek, G. Winter, and M. Mansmann, "Molded Bodies of Homogeneous Mixtures of Silicon Carbide and Silicon Nitride," German Patent 2,243,527 (1974).
- ¹⁹ S. Yajima, J. Hayashi, M. Omori, and K. Okamura, "Development of A Silicon-Carbide Fiber With High-Tensile Strength," *Nature* 261, 683-685 (1976).
- ²⁰ S. Yajima, K. Okamura, J. Hayashi, and M. Omori, "Synthesis of Continuous SiC Fibers with High-Tensile Strength," *J. Amer. Ceram. Soc.* 59, 324-327 (1976).
- ²¹ P. Eigen, H. Keller-Rudek, W. Kurtz, P. Merlet, H. Schaefer, and F. Schroeder, *Gmelin Handbook of Inorganic Chemistry*, 8th Edition, Vol. B4, Silicon Suppl., Springer, Berlin, 1989.
- ²² S. Pawlenko, "Metallorganische Verbindungen Silicon," in *Methoden der organischen Chemie (Houben-Weyl)*, 4th Edition, Vol. 13, Part 5, edited by O. Bayer and E. MuÈller, Georg Thieme, Stuttgart, 1980.

-
- ²³ C.K. Narula, *Ceramic Precursor Technology and its Applications*, Marcel Dekker, New York, 1995.
- ²⁴ M. Birot, J.P. Pillot, and J. Dunogues, "Comprehensive Chemistry of Polycarbosilanes, Polysilazanes, and Polycarbosilazanes as Precursors of Ceramics," *Chem. Rev.* **95**, 1443-1477 (1995).
- ²⁵ R.M. Laine, Y.D. Blum, D. Tse, and R. Glaser, in *Inorganic and Organometallic Polymers*, edited by M. Zeldin, K.J. Wynne, and H.R. Allcock, ACS Symposium Series 360, American Chemical Society, Washington, DC, 1988.
- ²⁶ R.C.P. Cubbon, *Polymeric Precursors for Ceramic Materials*, Vol. 7, Rapra Review Report No. 76, 1994.
- ²⁷ K.J. Wynne and R.W. Rice, "Ceramics via Polymer Pyrolysis," *Annu. Rev. Mater. Sci.* **14**, 297-334 (1984)
- ²⁸ D. Seyferth, In *Inorganic and Organometallic Polymers*, edited by M. Zeldin, K.J. Wynne, H.R. and Allcock. ACS Symposium Series 360, American Chemical Society, Washington DC, 1988.
- ²⁹ S. Yajima, J. Hayashi, and M. Omori, Japanese Appl.75,50,223, 1975; *Chem. Abstr.*, **86**, 30940 1977.
- ³⁰ Nicalon form Nippon Carbon Co. Ltd. 2-6-1, Hatbochori, Chuko, Tokyo 104, Japan.
- ³¹ Tyranno from Ube Industries Ltd. , Ube-shi, Yamagushi –ken 755, Japan.
- ³² R. West, In *Ultrastructure Processing of Ceramics, Glasses and Composites*, edited by L.L. Hench, and D.R. Ulrich, Wiley Interscience, New York, 1984.

-
- ³³ W.P. Weber, "Polycarbosilanes-Polymers with Backbone Variability," *Trends polym. Sci. 1*, 356-360(1993).
- ³⁴ S. Yajima, J. Hayashi, and M. Omori, "Continuous Silicon-Carbide Fiber of High-Tensile Strength," *Chem. Lett. 9*, 931-934(1975).
- ³⁵ S. Yajima, J. Hayashi, and K. Okamura, "Pyrolysis of Polyborodiphenylsiloxane," *Nature 266*, 521-522 (1977).
- ³⁶ S. Yajima, Y. Hasegawa, K. Okamura, and T. Matsuzawa, "Development of High-Tensile Strength Silicon-carbide Fiber Using an Organosilicon Polymer Precursor," *Nature 273*, 525-527 (1978)
- ³⁷ J. Lipowitz, J.A. Rabe, and G.A. Zank, "Polycrystalline Silicon Carbide Fibers from Organosilicon Polymer," *Ceram. Engi. Sic. Prog. 12*, 1819-1831 (1991).
- ³⁸ M. Takeda, Y. Imai, H. Ichikawa, and T. Ishikawa, "Properties of the Low-oxygen-content Silicon Carbide Fiber after High Temperature Heat Treatment," *Ceram. Engi. Sic. Prog. 12*, 1007-1018(1991).
- ³⁹ K. Okamura and T. Segushi, "Application of Radiation Curing in the Preparation of Polycarbosilane-derived Silicon Carbide Fibers," *J. Inorg. Organomet. Polym. 2*, 171-179(1992).
- ⁴⁰ M. Takeda, Y. Imai, H. Ichikawa, T. Ishikawa, N. Kasai, T. Sigushi, and K. Okamura, "Thermal Stability of the Low Oxygen Silicon Carbide Fibers Derived from Polycarbosilane," *Ceram. Engi. Sic. Prog. 13*, 209-217(1992).
- ⁴¹ T. L. Smith, "Process for the Production of Silicon Carbide by the Pyrolysis of a Polycarbosilane Polymer," U.S. Patent 4,631,179, (1986).

-
- ⁴² W. A. Kriner, "The Preparation of Cyclic Siliconmethylene Compounds," *J. Org. Chem.* **29**, 1601-1606(1964).
- ⁴³ Shin Etsu Chemical Industry, "Silicon Polymers," Japanese Patent 5,867,729, (1983).
- ⁴⁴ C. L. Schilling, J.P. Wesson, and T.C. Williams, "Polycarbosilane Precursors for Silicon-Carbide," *Am Ceram. Soc. Bull.*, **62**, 912-915 (1983).
- ⁴⁵ J.P. Pillot, C. Biran, E. Bacque, P. Lapouyade, and J. Dunogues, "Process for Preparing Disilylmethanes," German Patent 3,717,265, (1986).
- ⁴⁶ D.J. Carlsson, J. Roovers, D.J. Worsfold, and L.L. Zhou, "Synthesis of Polycarbosilanes as Precursors for Silicon-Carbide Ceramics," *Polym. Prepr.* **31**, 268 (1990).
- ⁴⁷ C. L. Schilling, "Polymeric Routes to Silicon-Carbide," *Br. Polym. J.*, **18**, 355-358 (1986).
- ⁴⁸ S. Ijadi-Maghsoudi, Y. Pang, and T.J. Barton, "Efficient, One-pot Synthesis of Silylene-Acetylene and Disilylene-Acetylene Pre ceramic Polymers from Trichloroethylene," *J. Polym. Sci.; Part A, Polym. Chem.*, **28**, 955-965 (1990).
- ⁴⁹ B. Boury, L. Carpenter, and R. Corriu, *Angew. Chem.*, **102**, 818 (1990).
- ⁵⁰ B. Boury, R. Corriu, D. Leclercq, P. Mutin, J.M. Planeix, and A. Vioux, "Poly(Vinylsilane)- A Precursor to Silicon-carbide, 1. Preparation and Characterization," *Organometallics* **10**, 1457-1461 (1991).
- ⁵¹ P. Noireaux, J. Jamet, M. Parlier, and M.P. Bacos, "Process for Preparing Liquid Polysilanes," European Patent Appl. 382,651, (1990).
- ⁵² C.A. Aitken, J.F. Harrod, and E. Samuel, "Polymerization of Primary Silanes to Linear Polysilanes Catalyzed by Titanocene Derivatives," *J. Organomet. Chem.* **279**, C11-13(1985).

-
- ⁵³ O. Glemser, K. Beltz, and P. Naumann, "The Silicon-nitrogen System," *Anor. Allg. Chem.*, *291*, 51-66(1957).
- ⁵⁴ W. Verbeek, "Shaped Boron- and Carbo-containing Structures," German Patent 2,218,960, (1973).
- ⁵⁵ B.G.Penn, J.G. Daniels, F.E. Ledbetter, and J.M. Clemons, Polym. "Preparation of Silicon Carbide Fibers by the Pyrolysis of Polycarbosilazane Precursors- A Review," *Eng. Sci.* *26*, 1191-1194 (1986).
- ⁵⁶ R.M. Laine, Y.D. Blum, A. Chow, R.D. Hamlin, K.B. Schwartz, and D.J. Rowcliffe, "Catalytic Synthesis of Novel Polysilazanes including Precursors to Silicon Nitride," *Polym. Prepr.*, *28*, 393-395(1987).
- ⁵⁷ D. Seyferth and G.H. Wiseman, In *Ultrastructure Processing of Ceramics, Glasses and Composites*, edited by L.L. Hench and D.R. Ulrich, Wiley Interscience: New York, 1984.
- ⁵⁸ O. Glemser and P.Z. Naumann, "Thermal Decomposition of Silicon Diimide Si(NH)₂," *Anorg. Allg. Chem.*, *298*, 134-146(1958).
- ⁵⁹ Toyo Soda Mfg. Co. Ltd. "Fibrous Silicon Nitride," Japanese Patent 8,374,598, (1983).
- ⁶⁰ T. Hirai and S. Hayashi., "Synthesis of Beta-Si₃N₄ by Chemical Vapor Deposition," *J. Am. Ceram. Soc.* *64*, C88-89 (1981).
- ⁶¹ B.J. Aylett, In *Special Ceramics*, edited by E.P. Popper, Academic Press: New York, 1964.
- ⁶² R. E. Burks and J. L. Greene, NASA-CR-61548 (1967).
- ⁶³ M. Arai, S. Sakurada, T. Isoda, and T. Tomizawa, "Pre-ceramic Polysilazane to Silicon Nitride," *Polym. Prepr.* *28*, 407-408(1987).

-
- ⁶⁴ R.E. King, B. Kanner, S.P. Hopper, and C.L. Schilling, "Method for Making Polysilaznes," U.S. Patent 4,675,424 (1987).
- ⁶⁵ D. Seyferth, G.H. Wiseman, and C. Prud'homme, "Silicon-nitrogen Polymers and Ceramics Derived from Reaction of Dichlorosilane, H₂SiCl₂," *Mater. Sci. Res.* 17, 263-269(1984).
- ⁶⁶ K. Okamura, M. Sato, and Y. Hasegawa, "Silicon-carbide Fibers and Silicon Oxynitride Fibers Obtained by the Nitridation of Polycarbosilane," *Ceram. Int.*,13, 55-61 (1987).
- ⁶⁷ K. Okamura, M. Sato, and Y. Hasegawa, "Silicon Nitride Fibers and Silicon Oxynitride Fibers Obtained by the Nitridation of Polycarbosilane," *Mater. Scz. Monogr.* 38A, 747-754(1987).
- ⁶⁸ J.A. Rabe and D.R. Bujalski, "Process for Preparing Ceramic Materials with Reduced Carbon Levels ," US. Patent 4,761,389, (1988).
- ⁶⁹ O. Funayama, M. Arai, Y. Tashiro, H. Aoki, T. Suzuki, K. Tamura, H. Kaya, H. Nishii, and T. Isoda, *Nippon Seramikkusu Kyokai Gakujutsu Ronbunshi*, 98, 104 (1990), *Chem. Abstr.*, 112,103719(1990).
- ⁷⁰ D. Seyferth, and G.H. Wiseman, "Polysilazane Routes to Silicon Nitride,"" *Polym. Prepr.* 25, 10-12(1984).
- ⁷¹ W. Fink,"Chemistry of the Si-N bond, VII N,N-alkylated and -arylated Cyclic Disilazanes," *Helv. Chim. Acta* 47, 498-508(1964).
- ⁷² G. E. Legrow, T.F. Lim, J. Lipowitz, and R.S. Reaach, "Ceramics from Hydridopolysilazane," *Am. Ceram. Soc. Bull.* 66, 363-367(1987).
- ⁷³ J. Lipowitz, J.A. Rabe, and T.M. Carr, "Characterization of the Reaction-products of Symmetrical Dimethyltetrachlorodisilane with Hexamethyldisilane By ²⁹Si NMR Spectroscopy," *Spectrosc. Lett.* 20, 53-65(1987).

-
- ⁷⁴ J.M. Schwark, "Isocyanate- and Isothiocyanate-modified Polysilazane Ceramic Precursors," US Patent 4,929,704 (1990).
- ⁷⁵ J.M. Schwark, "Silicon Nitride Ceramics from Isocyanate- and Isothiocyanate-modified Polysilazanes," US Patent 5,001,090 (1991).
- ⁷⁶ J.M. Schwark and M.J. Sullivan, "Isocyanate-modified Polysilazanes: Conversion to Ceramics Materials," *Mater. Res. Soc. Symp. Proc.* 27, 807-812(1992).
- ⁷⁷ J.M. Schwark, "Organic Amide-modified Polysilazane Ceramic Precursors," US Patent 5,032,649 (1991).
- ⁷⁸ K.S. Mazdiyasi and R. Ruh, "High-low Modulus Si₃N₄-BN Composite for Improved Electrical and Thermal-shock Behaviors," *J. Am. Ceram. Soc.* 64, 415-419(1981)
- ⁷⁹ H.P. Baldus and M. Jansen, "Novel High-performance Ceramics-Amorphous Inorganic Networks from Molecular Precursors," *Angew. Chem.* 36, 329-343 (1997).
- ⁸⁰ O. Funayama, Y. Tashiro, A. Kamo, M. Okumura, and T. Isoda, "Conversion Mechanism of Perhydropolysilazane into Silicon Nitride-based Ceramics" *J. Mater. Sci.* 29, 4883-4888 (1994).
- ⁸¹ T. Ishikawa, Y. Kohtoku, K. Kumagawa, T. Yamamura and T. Nagasawa, "High-strength Alkali-resistant Sintered SiC fiber Stable to 2200°C," *Nature* 391, 773-775(1998).
- ⁸² J. Loffelholz and M. Jansen, "Novel Access to Polyborosilazanes and Polyalumosilazanes Suitable as Precursors for Ternary Nitride Ceramics," *Adv. Mater.* 7, 289-292 (1995).
- ⁸³ W.R. Schmidt, W.J. Hurley, R.H. Doremus, L.V. Interrante, P.S. Marchetti, in: *Advanced Composite Materials: Ceramic Transactions*, edited by M.D. Sacks, Vol. 19, American Ceramic Society, Westerville, OH, 1991.

-
- ⁸⁴ D. Seyferth, G. Brodt, and B. Boury, "Polymeric Aluminasilazane Precursors for Aluminosilicon Nitride," *J. Mater. Sci. Lett.* *15*, 348-349 (1996).
- ⁸⁵ G. Verdecia, K.L. O'Brien, W.R. Schmidt, and T.M. Apple, "Aluminum-27 and Silicon-29 Solid-state Nuclear Magnetic Resonance Study of Silicon Carbide Aluminum Nitride System: Effect of Silicon/Aluminum Ratio and Pyrolysis Temperature," *Chem. Mater.* *10*, 1003-1009 (1998).
- ⁸⁶ S.N. Borisov, M.G. Voronkov, and E.Y. Lukevits, *Organosilicon Heteropolymers, Heterocompounds*, Plenum Press, New York, 1970.
- ⁸⁷ A. Lavedrine, D. Bahloul, P. Goursat, N. Choong Kwet Yive, R. Corriu, D. Leclerq, H. Mutin, and A. Vioux, "Pyrolysis of Polyvinylsilazane Precursors to Silicon Carbonitride," *J. Eur. Ceram. Soc.* *8*, 221-227(1991).
- ⁸⁸ D. Mocaer, R. Pailler, R. Naslain, C. Richard, J.P. Pillot, J. Dunogues, C. Gerardin, and F. Taulelle, "S-C-N Ceramics with a High Microstructure Stability Elaborated from the Pyrolysis of New Polycarbosilazane Precursors. 5: Oxidation Kinetics of Model Filaments," *J. Mater. Sci.* *28*, 2615-2631(1993).
- ⁸⁹ J. Seitz and J. Bill, "Production of Compact Polysilazane-derived Si/C/N-ceramics by Plastic Forming," *J. Mater. Sci. Lett.* *15*, 391-393(1996).
- ⁹⁰ P. Greil, "Near Net Shape Manufacturing of Polymer Derived Ceramics," *J. Eur. Ceram. Soc.* *18*, 1905-1914(1998).
- ⁹¹ T. Erny, M. Seibold, O. Jarchow, and P. Greil, "Microstructure Development of Oxycarbide Composites during Active-filler-controlled Polymer Pyrolysis," *J. Am. Ceram. Soc.* *76*, 207-213(1993).

-
- ⁹² L. An, Y. Wang, L. Bharadwaj, L. Zhang, Y. Fan, D. Jiang, Y.H. Sohn, V.H. Desai, J. Kapat, and L. C. Chow “Silicoaluminum carbonitride with anomalously high resistance to oxidation and hot corrosion,” *Adv. Eng. Mater.* 6(5), 337-340 (2004).
- ⁹³ R. Riedel, A. Kienzle, and M. Friess, in: *Application of organometallic Chemistry in the Preparation and Processing of Advanced Materials*, edited by J.F. Harrod and R.M. Laine, Kluwer Academic Publishers, The Netherlands, 1995.
- ⁹⁴ D. Seyferth, in: *Euro-Ceramics 2*, Vol. 1, edited by G. Ziegler and H. Hausner, Deutsche Keramische Gesellschaft e. V., Augsburg, 1991.
- ⁹⁵ N.S. C.K. Yive, R.J.P. Corriu, D. Leclercq, P.H. Mutin, and A. Vioux, “Silicon Carbonitride from Polymeric Precursors-Thermal Cross-linking and Pyrolysis of Oligosilazane Model Compounds,” *Chem. Mater.* 4, 141-146(1992).
- ⁹⁶ D. Seyferth, in: *Silicon Based Polymer Science-A Comprehensive Resource*, edited by J.M. Ziegler and F.W.G. Feason, American Chemical Society, Washington, DC, 1990.
- ⁹⁷ M. Peuckert, T. Vaahs, and M. Bruck, “Ceramics from Organometallic Polymers,” *Adv. Mater.* 2, 398-404 (1990).
- ⁹⁸ D. Seyferth, C. Strohniann, H. J. Tracy, and J. L. Robinson, “Synthesis and Useful Reactions of Organosilicon Polymeric Precursors for Ceramics,” *Mater. Res. Soc. Symp. Proc.* 249, 1-14 (1992).
- ⁹⁹ B. Boury, R.J.P. Corriu, W.E. Douglas, “Poly(carbosilane) Precursors of Silicon-carbide- the Effect of Cross-linking on Ceramic Residue,” *Chem. Mater.* 3, 487-489(1991).

-
- ¹⁰⁰ J. LuÈcke, J. Hacker, D. Suttor, G. Ziegler, "Synthesis and Characterization of Silazane-based Polymer as Precursors for Ceramic Matrix Composites," *Appl. Organomet. Chem.* *11*, 181-194(1997).
- ¹⁰¹ D. Bahloul, M. Pereira, P. Goursat, N.S. Choong Kwet Yive, and R.J.P. Corriu, "Preparation of Silicon Carbonitrides from an Organosilicon Polymer. 1. Thermal-decomposition of the Cross-linked Polysilazane," *J. Am. Ceram. Soc.* *76*, 1156-1162 (1993).
- ¹⁰² N.S. Choong, R.J.P. Corriu, D. Leclercq, P.H. Mutin, and A. Vioux, "Thermogravimetric Analysis/Mass Spectrometry Investigation of the thermal Conversion of Organosilicon Precursors into Ceramics under Argon and Ammonia," *Chemistry of Materials*, *4*, 1263-71 (1992)
- ¹⁰³ R.J.P Corriu, "Ceramic and Nanostructures from Molecular Precursors," *Angewandte Chemie- International Edition*, *39*, 1376-98 (2000)
- ¹⁰⁴ M. Weinmann, "High Temperature Stable Ceramics from Inorganic Polymers," in *Polymer Derived Ceramics*, edited by J. Bill, F. Wakai, and F. Aldinger, Wiley-VCH Verlag GmbH, Weinheim, Germany 1999
- ¹⁰⁵ C. Haluschka, H.J. Kleebe, R. Franke, and R. Riedel, "Silicon Carbonitride Ceramics Derived from Polysilazanes Part I. Investigation of Compositional and Structural Properties," *J. Euro. Ceram. Soc.* *20*, 1355-64 (2000).
- ¹⁰⁶ R. Raj, L. An, S. Shah, R. Riedel, C. Fasel, and H.J. Kleebe, " Oxidation Kinetics of an Amorphous Silicon Carbonitride Ceramic," *J. Am. Ceram. Soc.* *84*, 1803-1810 (2001).

-
- ¹⁰⁷ S. Johnson, *The Si-Al-O-N System -- Thermodynamic Properties and Phase Diagrams*, Report of the Division of Physical Metallurgy, Royal Institute of Technology, Stockholm, Sweden, 1991.
- ¹⁰⁸ J. Weiss, H.L. Lukas, J. Lorenz, G. Petzow, and H. Krieg, "Calculation of Heterogeneous Phase-Equilibria in Oxide-nitride Systems. 1. The Quaternary System C-Si-N-O," *CALPHAD* 5, 125-140 (1981).
- ¹⁰⁹ R. Riedel, H.J. Kleebe, H. Schbrifelder, and F. Aldinger, "A covalent Micro/ Nano Composite Resistant to High temperature Oxidation," *Nature*, 374, 526-28 (1995).
- ¹¹⁰ D. Bahloul, M. Pereira, and P. Goursat, "Silicon Carbonitride Derived from an Organometallic Precursor: Influence of the Microstructure on Oxidation Behavior," *Ceram. Int.* 18, 1-9(1992).
- ¹¹¹ G. Ziegler, H.J. Kleebe, G. Motz, H. Muller, S. Trapl, and W. Weibelzahl, "Synthesis, Microstructure and Properties of SiCN Ceramics Prepared from Tailored Polymers," *Mater. Chem. Phys.* 61, 55-63 (1999)
- ¹¹² H.J Kleebe, D. Suttor, and G. Ziegler, "Microstructure Evolution and Crystallization Behavior of Polymer-Derived Si-C-N Monoliths: A TEM study," in *Polymer Derived Ceramics*, edited J. Bill, F. Wakai, and F. Aldinger, Wiley-VCH Verlag byGmbH, Weinheim, Germany, 1999
- ¹¹³ S. Yajima, "Special Heat Resisting Materials from Organometallic Polymers" *Am. Ceram. Soc. Bull.*, 62, 893-98 (1983)
- ¹¹⁴ B.A. Bender, R.W. Rice, and J.R. Spann, "Transmission electron Microscopic Characterization of Ceramics formed by Pyrolysis of Organometallic Polymer Precursors," *J. Am. Ceram. Soc.* 70, C58-60 (1987)

-
- ¹¹⁵ K.B. Schwartz, D.J. Rowcliffe, Y.D. Blum, and R. M. Laine, "Thermal conversion of Preceramic Polysilazanes to Si₃N₄: Characterization of Pyrolysis Products," *Mater. Res. Soc. Symp. Proc.* 73, 407-412 (1983)
- ¹¹⁶ G. Ziegler, J. Heinrich, G. Woëting, "Relationships Between Processing, Microstructure and Properties and Dense and Reaction-bonded Silicon-nitride," *J. Mater. Sci.* 22, 3041-3086(1987).
- ¹¹⁷ S.R. Shah and R. Raj, "Mechanical Properties of a Fully Dense Polymer Derived Ceramic Made by a Novel Pressure Casting Process" *Acta Materialia*, 50, 4093-4103 (2002).
- ¹¹⁸ L. An, R. Riedel, C. Konetschny, H.-J. Kleebe, and R. Raj, "Newtonian Viscosity of Amorphous Silicon Carbonitride at High Temperature," *J. Am. Ceram. Soc.* 81 , 1349-1352(1998).
- ¹¹⁹ R. Riedel, L.M. Ruwisch, L. An, and R. Raj, "Amorphous Silicoboron Carbonitride Ceramic with Very High Viscosity at temperatures above 1500°C" *J. Am. Ceram. Soc.* 81, 3341-3344(1998).
- ¹²⁰ D. Mocaer, G. Chollon, R. Pailler, L. Filipuzzi, and R. Naslain, "Si-C-N Ceramics With a High Microstructural Stability Elaborated from the Pyrolysis of New Polycarbosilazane Precursors. 5 Oxidation Kinetics of Model Filaments," *J. Mater. Sci.* 28, 3059–68 (1993).
- ¹²¹ A. Saha, SR. Shah, and R. Raj, "Oxidation Behavior SiCN-ZrO₂ Fiber Prepared from Alkoxide-modified Silazane," *J. Am. Ceram. Soc.* 87, 1556–1558 (2004)
- ¹²² D. Mocaer, R. Pailler, R. Naslain, C. Richard, J.P. Pillot, J. Dunogues, O. Delverdier, and M. Monthieux, "Si-C-N Ceramics with a High Microstructural Stability Elaborated from the Pyrolysis of New Polycarbosilazane Precursors. 3. Effect of Pyrolysis Conditions on the

-
- Nature and Properties of Oxygen-cured Derived Monofilaments,” *J. Mater. Sci.* 28, 2639-2653 (1993).
- ¹²³ M. Scarlete, J. He, J.F. Harrod, and I.S. Butler, in: *NATO ASI Series E: Applied Sciences*, Vol. 297, edited by J.F. Harrod and R.M. Laine, 1994.
- ¹²⁴ A. Sawaguchi, K. Toda, “Mechanical and Electrical Properties of Silicon-nitride Nanocomposite Materials,” *J. Am. Ceram. Soc.* 74, 1142-1144 (1991).
- ¹²⁵ C. Haluschka, Ph.D. Thesis, Darmstadt University of Technology, Darmstadt, 1997.
- ¹²⁶ N.F. Mott and E.A. Davies, *Electronic Processes in Non-crystalline Materials*, Clarendon Press, Oxford, 1979.
- ¹²⁷ W. Heywang, *Amorphe und polykristalline Halbleiter, Halbleiterelektronik* Bd. 18, Springer, Berlin, 1984.
- ¹²⁸ B.E. Deal and A.S. Grove, “General Relationship for the Thermal Oxidation of Silicon,” *J. App. Phys.* 36, 3770-3778 (1965).
- ¹²⁹ J. R. Ligenza and W. G. Spitzer, “The Mechanisms for Silicon Oxidation in Steam and Oxygen,” *J. Phys. Chem. Solids* 14, 131-136(1960)
- ¹³⁰ P. J. Jorgensen, “Effect of an Electric Field on Silicon Oxidation,” *J. Chem. Phys.* 37, 874-877(1962)
- ¹³¹ W.A. Pliskin and R. P. Gnall, “Evidence for Oxidation Growth at the Oxide-silicon Interface from Controlled Etch Studies,” *J. Electrochem. Soc.* 111, 872-873(1964)
- ¹³² R.H. Doremus, “Oxidation of Silicon: Test of Mechanisms” pp17-23 in *The physics and Chemistry of SiO₂ and the Si-SiO₂ interface* Edited by C. R. Helms and B.E.Deal. Plenum Press, New York, 1988

-
- ¹³³ F.J. Norton. "Gas Permeation Through the vacuum Envelope", pp 8-16 in *Transactions of the Eighth National Vacuum Symposium*, Edited by L.E. Preuss. Pergamon Press., New York, 1962
- ¹³⁴ J.A. Costello and R.E. Tressler, "Isotope labeling studies of the oxidation of Silicon at 1000⁰C and 1300⁰C", *J. Electrochem. Soc.* 131, 1944-1947(1984)
- ¹³⁵ J.D. Cawley, J.W. Halloran, and A.R. Cooper, "Oxygen-18 Tracer study of the Passive Thermal Oxidation of Silicon" *Oxid. Met.* 28, 1-16 (1987)
- ¹³⁶ N.S. Jacobson, "Corrosion of Silicon-Based Ceramics in Combustion Environments," *J. Am. Ceram. Soc.* 76, 3-28 (1993).
- ¹³⁷ K.L. Luthra, "Some New Perspectives on Oxidation of Silicon-carbide and Silicon-nitride," *J. Am. Ceram. Soc.* 4, 1095-1103 (1991)
- ¹³⁸ J. Schlichting, "Silicion Carbide as an Oxidation-resistant High-temperature (Refractory) Materials. I. Oxidation and High-temperature Corrosion Behavior," *Ber. Dtsch. Keram. Ges.* 56, 196-200 (1979)
- ¹³⁹ J. W. Fergus and W. L. Worrell, "Oxidation of Chemically Vapor Deposited Silicon Carbide": pp43-52 in *Ceramic Transactions vol 10 Corrosion and Corrosion Degradation of Ceramics*. Edited by R.E. Tressler and M. McNallen. American Ceramics Society, Westerville, OH, 1990
- ¹⁴⁰ G. H. Schiroky, R. J. Price, and J. E. Sheehan. "Oxidation Characteristics of CVD Silicon Carbide and Silicon Nitride," Rept. No. GA-A18696, GA Technologies, Inc., San Diego, CA, 1986.

-
- ¹⁴¹ J. A. Costello and R. E. Tressler, "Oxidation of Silicon Carbide Crystals and Ceramics: I. In Dry Oxygen," *J. Am. Ceram. Soc.* *69*, 674-81 (1986).
- ¹⁴² C. D. Fung and J. J. Kopanski, "Thermal Oxidation of 3C Silicon Carbide Single-Crystal Layers on Silicon," *Appl. Phys. Lett.*, *45*, 757-59 (1984).
- ¹⁴³ L. Muehlhoff, M. J. Bozack, W. J. Choyke, and J. T. Yates, Jr., "Comparative Oxidation Studies of SiC(0001) and SiC(0001) Surfaces," *J. Appl. Phys.* *60*, 2558-63 (1986).
- ¹⁴⁴ E. J. Opila, "The Oxidation Kinetics of Chemically Vapor Deposited Silicon Carbide": presented at TMS Fall Meeting, Chicago, IL, 1992.
- ¹⁴⁵ K. Motzfeld, "On the Rates of Oxidation of Silicon and Silicon Carbide in Oxygen and Correlation with Permeability of Silica Glass," *Acta Chem. Scand.* *18*, 1596-606 (1964).
- ¹⁴⁶ Z. Zheng, R.E. Tressler and K.E. Spear, "Oxidation of Single-crystal Silicon Carbide: I Experimental Studies," *J. Electrochem. Soc.*, *137*, 854-58 (1990).
- ¹⁴⁷ Z. Zheng, R.E. Tressler, and K.E. Spear, "Oxidation of Single Crystal Silicon-carbide 2. Kinetic-model," *J. Electrochem. Soc.* *137*, 2812-2816(1990)
- ¹⁴⁸ C.E. Ramberg and W.L. Worrell, "Oxygen Transport in Silica at High Temperatures: Implications of Oxidation Kinetics," *J. Am. Ceram. Soc.* *84*, 2607-2616 (2001)
- ¹⁴⁹ P. Kofstad, *High-Temperature Oxidation of Metals*; p. 125. Wiley, New York, 1966.
- ¹⁵⁰ E. Fitzer and R. Ebi, "Kinetic Studies on the Oxidation of Silicon Carbide": pp. 320-28 in *Silicon Carbide IY7.3*. Edited by R. C. Marshall, J. W. Faust, Jr., and C. E. Ryan. University of South Carolina Press, Columbia, SC, 1974.
- ¹⁵¹ D M. Mieskowski, T. E. Mitchell, and A. H. Heuer, "Bubble Formation in Oxide Scales on SiC," *J. Am. Ceram. Soc.* *67*, C-17-C-18 (1984)

-
- ¹⁵² H. Du, R. E. Tressler and C. G. Pantano, "Oxidation Studies of Crystalline CVD Silicon Nitride," *J. Electrochem. Soc.* *136*, 1527–1536 (1989).
- ¹⁵³ D. J. Choi, D. B. Fischbach and W. D. Scott, "Oxidation of Chemically Vapor Deposited Silicon Nitride and Single Crystal Silicon," *J. Am. Ceram. Soc.* *72*, 1118–23 (1989).
- ¹⁵⁴ T. Hirai, K. Niihara and T. Goto, "Oxidation of CVD Si₃N₄ at 1550° to 1650°C," *J. Am. Ceram. Soc.* *63*, 419–24 (1980).
- ¹⁵⁵ H. Du, C. A. Houser, R.E. Tressler, K. E. Spear, and C. G. Pantano. "Isotropic Studies of Oxidation of Si₃N₄ and Si using SIMS," *J. Electrochem. Soc.* *137*, 741-42 (1990)
- ¹⁵⁶ H. Du, R.E. Tressler, K. E. Spear, and C.G. Pantano, "Thermodynamics of the Si-N-O System and Kinetic Modeling of Oxidation of Si₃N₄," *J. Electrochem. Soc.* *136*, 3210-3215 (1989)
- ¹⁵⁷ C. Singhal, "Oxidation Kinetics of Hot-Pressed Silicon Carbide." *J. Mater. Sci.* *11*, 1246-53 (1976).
- ¹⁵⁸ C. Singhal and F. F. Lange, "Effect of Alumina Content on the Oxidation of Hot-Pressed Silicon Carbide," *J. Am. Cerum. Soc.* *58*, 133-35 (1975).
- ¹⁵⁹ S. C. Singhal, "Oxidation and Corrosion-Erosion Behavior of Si₃N₄, and SiC"; pp. 533-48 in *Ceramics for High-Performance Applications*. Edited by J. J. Burke. A. E. Gorum, and R. N. Katz. Metals and Ceramics Information Center, Columbus, OH, 1974
- ¹⁶⁰ S. C. Singhal, "Thermodynamics and Kinetics of Oxidation of Hot-Pressed Silicon Nitride," *J. Mater. Sci.* *11*, 500 (1976).
- ¹⁶¹ V. A. Lavrenko, I . G. Gogotsi, A. B. Goncharuk. A. F. Alekseev, O. N. Grigorev, and O. D. Shcherbina, "High-Temperature Oxidation of Reaction-Sintered Silicon Nitride with Various Additions," *Poroshk. Metnll.* *267*, 35-39 (1985).

-
- ¹⁶² J. W. Hinze, W. C. Tripp, and H. C. Graham, "The High-Temperature Oxidation of Hot-Pressed Silicon Carbide"; pp. 405-19 in *Mass Transport Phenomena in Ceramics*. Edited by A. R. Cooper and A. H. Heucr, American Ceramic Society, Columbus, OH, 1975.
- ¹⁶³ J. A. Costello, R. E. Tressler, and I. S. T. Tsong, "Boron Redistribution in Sintered α -SiC During Thermal Oxidation," *J. Am. Ceram. Soc.* *64*, 332-35 (1981).
- ¹⁶⁴ D. Cubicciotti and K. Lau, "Kinetics of Oxidation of Hot-Pressed Silicon Nitride Containing Magnesia," *J. Am. Ceram. Soc.* *61*, 512-17 (1978).
- ¹⁶⁵ D. Cubicciotti and K. H. Lau. "Kinetics of Oxidation of Yttria Hot-Pressed Silicon Nitride," *J. Electrochem. Soc.* *126*, 1723-28 (1979).
- ¹⁶⁶ W. C. Tripp and H. C. Graham, "Oxidation of S_3N_4 in the Range 1300 to 1500°C," *J. Am. Ceram. Soc.* *59*, 399-403 (1976).
- ¹⁶⁷ P. Andrews and F. L. Riley, "The Microstructure and Composition of Oxide Films Formed During High-Temperature Oxidation of a Sintered Si_3N_4 ," *J. Eur. Ceram. Soc.* *5*, 245-56 (1989).
- ¹⁶⁸ J. Schlichting and L. J. Gauckler, "Oxidation of Some β - Si_3N_4 Materials," *PowderMetall. Int.* *9*, 36-39 (1977).
- ¹⁶⁹ D. R. Clarke, "Thermodynamic Mechanism for Cation Diffusion Through an Intergranular Phase: Applications to Environmental Reactions with Nitrogen Ceramics"; pp 421-26 in *Progress in Nitrogen Ceramics*, NATO ASI Series. Series E: Applied Sciences, No. 65. Edited by F. L. Riley. Martinus Nijhoff, The Hague, Netherlands, 1983.

-
- ¹⁷⁰ J. Chen, J. Sjogger, O. Lindqvist, C. O'Meara, and L. Pejryd, "The Rate-Controlling Processes in the Oxidation of HIPed Si₃N₄ with and without Sintering Additives." *J. Eur. Ceram. Soc.* 7, 319-27 (1991).
- ¹⁷¹ J. K. Patel and D. P. Thompson, "The Low-Temperature Oxidation Problem in Ytria-Densified Silicon Nitride Ceramics," *Br. Ceram. Trans. J.* 87, 70-73 (1988).
- ¹⁷² A. G. Evans and R. W. Davidge, "The Strength and Oxidation of Reaction-Sintered Silicon Nitride," *J. Mater. Sci.* 5, 314 (1970).
- ¹⁷³ F. Porz and F. Thummler. "Oxidation Mechanism of Porous Silicon Nitride." *J. Mater. Sci.* 19, 1283-95 (1984).
- ¹⁷⁴ S.C. Singhal and F. F. Lange, "Oxidation Behavior of SiAlONs," *J. Am. Ceram. Soc.* 60, 190-191 (1977)
- ¹⁷⁵ M.H. Lewis, P. Barnard, "Oxidation Mechanisms in Si-Al-O-N Ceramics," *J. Mater. Sci.* 15, 443-448 (1980).
- ¹⁷⁶ T. Chartier, J.L. Besson and P. Goursat, "Microstructure, Oxidation, and Creep Behavior of a β'-sialon Ceramics," *Int. J. High. Tech. Ceram.* 2, 33-45(1986)
- ¹⁷⁷ K.J.D. Mackenzie, S. Shimada and T. AoKi, "Thermal Oxidation of Carbothermal beta-sialon powder: Reaction Sequence and Kinetics," *J. Mater. Chem.* 7, 527-530 (1997)
- ¹⁷⁸ T. Narushima, T. Goto, and T. Hirai, "High-Temperature Passive Oxidation of Chemically Vapor Deposited Silicon Carbide," *J. Am. Ceram. Soc.* 72, 1386-1390 (1989).
- ¹⁷⁹ L. U. J. T. Ogbuji and E. J. Opila, "A Comparison of Oxidation Kinetics of SiC and Si₃N₄," *J. Electrochem. Soc.* 142, 925-930 (1995).

-
- ¹⁸⁰ E. Butchereit, K.G. Nickel, and A. Muller, "Precursor-derived Si-B-C-N Ceramics: Oxidation Kinetics," *J. Am. Ceram. Soc.* 48, 2184-88(2001)
- ¹⁸¹ R. Ramesh, P. Byrne and M.J. Pomeroy, "Oxidation Studies of a High Al substituted Beta-Sialon," *J. Mater. Proc. Tech.* 56, 600-608(1996)
- ¹⁸² J.D.Kenneth, MacKenzie, C. M. Sheppard, and G. C. Barris, "Kinetics and Mechanism of Thermal Oxidation of Sialon Ceramic Powders," *Thermochimica Acta* 318, 91-100(1998)
- ¹⁸³ E. A. Irene and R. Ghez, "Silicon Oxidation Studies: The Role of H₂O," *J. Electrochem. Soc.* 124, 1757-1761 (1977).
- ¹⁸⁴ P. J. Jorgensen. M. E. Wadsworth, and I . B. Cutler, "Effects of Water Vapor on Oxidation of Silicon Carbide," *J. Am. Ceram. Soc.*. 44, 258-261 (1961).
- ¹⁸⁵ H. Cappelen, K. H. Johannsen, and K. Motzfeld. "Oxidation of Silicon Carbide in Oxygen and Water Vapor at 1500°C," *Acta Chem. Scand. A*, 35, 247-254 (1981).
- ¹⁸⁶ T Narushiina. T. Goto, Y. Iguchi, and T. Hirai, "High-Temperature Oxidation of Chemically Vapor-Deposited Silicon Carbide in Wet Oxygen at 1823 to 1923 K," *J. Am. Ceram. Soc.* 73, 1580-1584(1990).
- ¹⁸⁷ M. Maeda, K.Nakamura, and T. Ohkubo, "Oxidation of Silicon Carbide in a Wet Atmosphere," *J. Mater. Sci.* 23, 3933-3938 (1988).
- ¹⁸⁸ R. E. Tressler, J. A. Costello, and Z. Zheng. "Oxidation of Silicon Carbide Ceramics"; pp. 307-314 in *Industrial Heat Exchangers*. Edited by A. J. Haye, American Society of Metals, Warrendale, PA, 1985.
- ¹⁸⁹ E.L. Brady, "Chemical Nature of Silica Carried by Steam." *J. Phys. Chem.* 57, 706-710 (1953)

-
- ¹⁹⁰ C.S. Tedmon Jr. "The Effect of oxide volatilization on the Oxidation Kinetics of Cr and Fe-Cr Alloys," *J. Electrochem. Soc.* 113, 766-768 (1967).
- ¹⁹¹ G.H. Geiger and D. R. Poirier, *Transport Phenomena in Metallurgy*: P464, Addison-Wesley, Reading MA, 1973
- ¹⁹² R.A. Svehla, "Estimated Viscosities and Thermal Conductivities of Gases at High Temperatures," NASA Technical Report R 132.
- ¹⁹³ A. Hashimoto, "the Effect of H₂O Gas on Volatilities of Planet-Forming Major Elements: I Experimental Determination of thermodynamic Properties of Ca-, Al-, and Si-Hydroxide Gas Molecules and Its Application to the Solar Nebula," *Geochim. Cosmochim. Acta* 56, 511-532 (1992)
- ¹⁹⁴ O.H. Kirkorian, "Thermodynamics of Silica-Steam System": p.481 in *Symposium on Engineering with Nuclear Explosives*. Vol.1 Las Vegas, NV. Jan. 14-16, 1970
- ¹⁹⁵ M.D. Allendorf, C. F. Melius, P. Ho, and M. R. Zachariah, "Theoretical Study of the Thermochemistry of Molecules in the Si-O-H System." *J. Phys. Chem.* 99, 15285-1593 (1995)
- ¹⁹⁶ EJ Opila, R.C. Robinson, D.S. Fox, R.A. Wenglarz, and M.K. Ferber, "Additive effects on Si₃N₄ Oxidation/ Volatilization in Water Vapor," *J. Am. Ceram. Soc.* 86, 1262-71 (2003)
- ¹⁹⁷ <http://www.ceraset.com/>
- ¹⁹⁸ Y. Li, E. Kroke, R. Riedel, C. Fasel, C. Gervais and F. Babonneau , "Thermal cross-linking and pyrolytic conversion of poly(ureamethylvinyl)silazanes to silicon-based ceramics," *Appl. Organometal. Chem.* 15, 820-832 (2001).
- ¹⁹⁹ A. Dhamme, MS thesis, University of Central Florida, 2003.

-
- ²⁰⁰ F. Berger, M. Weinmann, F. Aldinger and K. Muller, "Solid-state NMR Studies of the Preparation of Si-Al-C-N Ceramics from Aluminum-modified Polysilazanes and Polysilycarbodiimides," *Chem. Mater.* *16*, 919-929 (2004)
- ²⁰¹ K.J.D. Mackenzie and M.E. Smith *Multinuclear Solid-State NMR of Inorganic Materials*, Pergamon, 2002.
- ²⁰² N.S.C.K.Yive, R. Corriu, D. Leclercq, P.H. Mutin, and A. Vioux, "Polyvinylsilazane- a Novel Precursor to Silicon Carbonitride," *New J. Chem.*, *15*, 85-92 (1991).
- ²⁰³ J. Haug, P. Lamparter, M. Weinmann, and F. "Diffraction Study on the Atomic Structure and Phase Separation of Amorphous Ceramics in the Si-(B)-C-N system. 1. Si-C-N Ceramics," Aldinger *Chem. Mater.* *16*, 72-82 (2004).
- ²⁰⁴ S. Trassl; H.J. Kleebe, H. Stormer, G. Motz, E. Rossler, and G. Ziegler "Characterization of the Free-carbon Phase in Si-C-N Ceramics: Part II, Comparison of Different Polysilazane Precursors," *J. Am. Ceram. Soc.* *85*, 1268-1274 (2002).
- ²⁰⁵ S. Trassl, G. Motz, E. Rossler, G. J. Ziegler, "Characterisation of the Free-carbon Phase in Precursor-derived SiCN Ceramics," *Non-cryst. Solids* *293*, 261-267(2001).
- ²⁰⁶ M.A. Munoz-Hernandez, T.S. Keizer, P. R. Wei, S. Parkin, and D.A. Atwood, "Reactivity and Derivatization of Five-coordinate, Chelated Aluminum," *Inorg. Chem.* *40*, 6782-6787 (2001).
- ²⁰⁷ D. Hardie, and K. H. Jack, "Crystal Structures of Silicon Nitride," *Nature* *180*, 332-333(1957).
- ²⁰⁸ S.N. Ruddlesden, and P. Popper, "Crystal Structures of the Nitrides of Silicon and Germanium," *Acta Crystallogr.* *11*, 465-468(1958).

-
- ²⁰⁹ R. Grun, "Crystal-structure of Beta-Si₃N₄-Structure and Stability Considerations between Alpha-Si₃N₄ and Beta-Si₃N₄," *Acta Crystallogr. B35*, 800-804 (1979)
- ²¹⁰ K.H. Jack, *Progress in Nitrogen Ceramics*, Martinus Nijhoff, The Hague, 1983
- ²¹¹ A.J. Moulson, "Reaction-bonded Silicon-nitride –Its Formation and Properties," *J. Mater. Sci. 14*, 1017-1050(1979)
- ²¹² Y. Iwamoto, W. Volger, E. Kroke, R. Riedel, T. Saitou, and K. Matsunaga, "Crystallization Behavior of Amorphous Silicon Carbonitride Ceramics Derived from Organometallic Precursors," *J. Am. Ceram. Soc. 84*, 2170-78 (2001).
- ²¹³ RM. Laine, F. Babonneau, K.Y. Blowhowiak, R.A. Kennish, J.A. Rahn, G. J. Exarhos, and K. Waldner, "The Evolutionary Process During Pyrolytic Transformation of Poly(N-methylsilazane) from a Preceramic Polymer into an Amorphous-silicon Nitride Carbon composite," *J. Am. Ceram. Soc.*, 78, 137-145 (1995)
- ²¹⁴ T. Yamada, T. Kawahito, T. Iwai, "Crystallization of Amorphous Si₃N₄ Prepared by the Thermal-decomposition of Si(NH)₂," *J. Mater. Sci. Lett.*, 2, 275-278(1983)
- ²¹⁵ Y. Goto and G. Thomas, "Phase-transformation and Microstructural Changes of Si₃N₄ During Sintering," *J. Mater. Sci. 30*, 2194-2200(1995).
- ²¹⁶ R.E. Tressler, "Theory and Experiment in Corrosion of Advanced Ceramics," pp3-22 in *Corrosion of Advanced Ceramics*. Edited by K.G. Nickel, 1994.
- ²¹⁷ K.J.D. Mackenzie and M.E. Smith, "²⁹Si NMR," pp205-214 in *Multinuclear Solid-state NMR of Inorganic Materials*, Pergamon, 2002.

-
- ²¹⁸ M. Schmucker, K.J.D. MacKenzie, H. Schneider H, and R. Meinhold, "NMR Studies on Rapidly Solidified SiO₂-Al₂O₃ and SiO₂-Al₂O₃-Na₂O-glasses," *J. Non-cryst. Solids* 217, 99-105 (1997).
- ²¹⁹ ZH Luan, CF Cheng, WZ Zhou, and J. Klinowski, "Mesopore Molecular Sieve MCM-41 Containing Framework Aluminum," *J. Phy. Chem.* 99, 1018-1024 (1995)
- ²²⁰ L.U.J.T. Ogbuji, "Role of Si₂N₂O in the Passive Oxidation of Chemically-Vapor-Deposited Si₃N₄," *J. Am. Ceram. Soc.* 75, 2995-3000 (1992)
- ²²¹ S.V. King, "Ring Configurations in a Random Network Model of Vitreous Silica," *Nature* 213, 1112-3 (1967).
- ²²² P. Umari and A. Pasquarello, "Modeling of the Raman Spectrum of Vitreous Silica: Concentration of Small Ring Structures," *Physica B.* 316-317, 572-574 (2002).
- ²²³ J.P. Rino, I. Ebbsjö, R.K. Kalia, A. Nakano and P. Vashishta, "Structure of Rings in Vitreous SiO₂," *Phys. Rev. B* 47, 3053-3062 (1993).
- ²²⁴ K. Vollmayr, W. Kob and K. Binder, "Cooling-rate Effects in Amorphous Silica: A Computer-simulation Study," *Phys. Rev. B* 54, 15808-15827 (1996).
- ²²⁵ T. Bakos, S.N. Rashkeev and S.T. Pantelides, "Reactions and Diffusion of Water and Oxygen Molecules in Amorphous SiO₂," *Phys. Rev. Lett.* 88, 055508 (2002).
- ²²⁶ M.P. Brady, B.A. Pint, P.F. Tortorelli, I.G. Wright and R.J. Hanrahan, Jr, "High-Temperature Oxidation and Corrosion of Intermetallics," *Mat. Sci. Tech.*, 229-325 (2000).
- ²²⁷ T. Ekström and M. Nygren, "SiAlON Ceramics," *J. Am. Ceram. Soc.* 75, 259-276 (1992).

-
- ²²⁸ A Müller, P. Gerstel, E. Butchereit, K.G. Nickel and F. Aldinger, "Si/B/C/N/Al Precursor-Derived Ceramics: Synthesis, High Temperature Behavior and Oxidation Resistance," *J. Euro. Ceram. Soc.* 24, 3409-17 (2004).
- ²²⁹ E. Butchereit and K.G. Nickel, "Beneficial Effect of Aluminum on the Oxidation Behavior of Precursor-Derived Ceramics," pp325-338 in *High Temperature Corrosion and Materials Chemistry IV*, Edited by E. Opila, et al., The Electrochemical Society: Washington, 2003.
- ²³⁰ C.E. Ramberg, G. Cruciani, K.E. Spear, R.E. Tressler and C. F. Ramberg, "Passive-oxidation kinetics of high-purity silicon carbide from 800 degrees to 1100 degrees C," *J. Am. Ceram. Soc.* 79, 2897-2911 (1996).
- ²³¹ R.C.A. Harris, "Oxidation of 6H-a Silicon Carbide Platelets," *J. Am. Ceram. Soc.* 58, 7-9 (1975).
- ²³² L. Filipuzzi, R. Naslain and C. Jaussaud, "Oxidation Kinetics of SiC Deposited from CH₃SiCl₃/H₂ under CVI Conditions," *J. Mater. Sci.*, 27, 3330-34 (1992).
- ²³³ J.D. Kalen, R.S. Boyce, and J.D. Cawley, "Oxygen Tracer Diffusion in Vitreous Silica," *J. Am. Ceram. Soc.* 74, 203-09 (1991)
- ²³⁴ J. D. Cawley and R. S. Boyce, "Solution to the Diffusion Equation for the Double Oxidation in Dry Oxygen Including Lazy Exchange between Network and nterstitial Oxygen," *Philos. Mag. B.* 58, 589 (1988).
- ²³⁵ J. Rodríguez-Viejo, F. Sibieude, M.T. Clavaguera-Mora and C. Monty, "O-18 Diffusion Through Amorphous SiO₂ and Cristobalite," *Appl. Phys. Letter.* 63, 1906-1908 (1993).
- ²³⁶ H. Rawson, *Properties and Applications of Glass, Glass Science and Technology*, 1980

-
- ²³⁷ E. J. Opila, J. L. Smialek, R. C. Robinson, D. S. Fox, and N. S. Jacobson, "SiC Recession Caused by SiO₂ Scale Volatility under Combustion Conditions: II, Thermodynamics and Gaseous-diffusion Model," *J. Am. Ceram. Soc.* 82, 1826-1834(1999)
- ²³⁸ E. J. Opila, "Oxidation and Volatilization of Silica Formers in Water Vapor," *J. Am. Ceram. Soc.* 86, 1238-1248 (2003).
- ²³⁹ D.S. Fox, E. J. Opila, Q.N. Nguyen, D. L. Humphrey, and S.M. Lewton, "Paralinear Oxidation of Silicon Nitride in a Water-Vapor/Oxygen Environment," *J. Am. Ceram. Soc.* 86, 1256-1261 (2003).
- ²⁴⁰ E. A. Gulbransen and S. A. Jansson, "High-temperature Oxidation, Reduction, and Volatilization Reactions of Silicon and Silicon Carbide," 181-183(1972)
- ²⁴¹ E. J. Opila and R. E. Hann, "Paralinear Oxidation of CVD SiC in Water Vapor ," *J. Am. Ceram. Soc.* 80, 197-205(1997).
- ²⁴² P.F. Tortorelli and K. L. More, "Effects of High Water-Vapor Pressure on Oxidation of Silicon Carbide at 1200°C," *J. Am. Ceram. Soc.* 86, 1249-55 (2003).
- ²⁴³ K. G. Ahari, K.S. Coley, and J.R. Nicholls, "Statistical Evaluation of Corrosion of Sialon in Burner Rig Simulated Combustion Atmospheres," *J. Euro. Ceram. Soc.* 17, 681-88 (1997).
- ²⁴⁴ A. Dhima, B. Stafa, and M. Allibert, "Activity Measurement in Steel-Making-Related Oxides Melts by Differential Mass Spectrometry," *High Temperature Science* 21, 143-159(1986).
- ²⁴⁵ L. An, R. Riedel, C. Konetschny, H-J. Kleebe, and R. Raj, "Newtonian Viscosity of Amorphous Silicon Carbonitride at high temperature", *J. Am. Ceram. Soc.* 81, 1349-52 (1998).

-
- ²⁴⁶ H.E. Harry and G.D. Linsey, “Accelerated oxidation of SiC CMC's by water vapor and protection via environmental barrier coating approach,” *J. Euro. Ceram. Soc.* 22, 2741-47 (2002).
- ²⁴⁷ W.D. Kingery, H. K. Bowen, and D. R. Uhlmann, *Introduction to Ceramics*, 2nd ed. 1975.
- ²⁴⁸ Y.S. Cheong, P. Mukundhan, H. Du, S.P. Withrow, “Improved Oxidation Resistance of Silicon Nitride by Aluminum Implantation: I, Kinetics and Oxide Characteristics,” *J. Am. Ceram. Soc.* 83, 154-160 (2000)